Verification, Validation and Application of the NorSand Constitutive Model in PLAXIS

Single-stress point analyses of experimental lab test data and finite element analyses of a submerged landslide

by

L.J. Woudstra

in fulfilment of the requirements for the degree of
Master of Science
at the Delft University of Technology,
to be defended publicly on 10-09-2021

Student number:	4310837	
Project duration:	October, 2020 - September, 2021	
Thesis Committee:	Dr. ir. R.B.J. (Ronald) Brinkgreve	TU Delft, Geo-engineering
	Prof. Dr. ir. M.A. (Michael) Hicks	TU Delft, Geo-engineering
	Dr. ir. A.P. (Bram) van den Eijnden	TU Delft, Geo-engineering
	ir. C. (Cor) Kasbergen	TU Delft, Structural Mechanics
	Dr. ir. F. (Nando) Marinelli	Bentley Systems, PLAXIS

Delft University of Technology
Faculty of Civil Engineering and Geo-Sciences
Master Applied Earth Sciences

TU Delft | Delft University of Technology | Faculty of Civil Engineering and Geo-Sciences | Master Track Geo-Engineering

Bentley Advancing Infrastructure

PLAXIS

Preface

This thesis serves the purpose of outlining research and analysis carried out by a student from Delft University of Technology. The document before you is written in fulfilment of the requirements for the degree of Master of Science in Geo-technical Engineering at the faculty of Civil Engineering and Geo-sciences. The conducted research is supported by Delft University of Technology and Bentley Systems, PLAXIS. The main focus of this thesis is the research in the behaviour of the newly PLAXIS implemented constitutive model NorSand. This research is carried out to have an understanding of its capability to approximate the behaviour of particulate materials in various loading paths. Doing so gives further insight on its potential to model and predict geo-technical structures that consist of, or interact with, said particulate material, such that their integrity can be maintained and potential failures can be mitigated. For this purpose, the model is verified and validated by comparing it to various experimental lab tests and other methods. Additionally, NorSand is applied on a finite element model of an underwater slope, which is in undrained plain strain conditions, to determine the structural response. For more details on the conducted analysis, refer to the final chapter and appendices of this report. Those interested in obtaining further information may contact the author and the corresponding supervisors.

Delft, September 2021

Acknowledgements

This report is the final product of 9 months of research and analysis as part of graduation work carried out with Bentley Systems and Delft University of Technology. The formulation of this document would not have been possible without the supervision and support of my graduation committee. I would like to thank my direct supervisor at Bentley Systems, Ferdinando Marinelli, for his guidance, willingness to answer numerous questions and incredibly valuable knowledge that he has passed on to me. I would also like to express my gratitude to Ronald Brinkgreve for his constructive feedback and guidance throughout the entire project. Furthermore, I would like to thank Sandro Brasille for involving me in the biweekly team meetings - even though I had worked from home throughout the entire project due to the global pandemic, I was still able to get a feel of the working environment I was eager to experience.

Finally, I would like to express my appreciation to my parents and sister, Jamila, Loek and Dinah, for their never-ending support and for always driving me forward to learn, achieve more and believe in myself. I would also like to thank Amilia for her support and patience. Many thanks to my great friends, known collectively as the APS, for their additional support. Last but not least, I am grateful for the support and motivation I have received from my friends and colleagues at the university and Bentley Systems.

L.J. Woudstra

Delft, September 2021

Abstract

As the construction of sub-aerial and submarine geotechnical structures increase in amount, rate and size, so do their associated risks. Often, with use constitutive models, finite element analyses (FEAs) are performed in order to identify and mitigate these risks. NorSand, which is a constitutive model based on critical state soil mechanics for particulate materials (e.g., sand), is one of the first models to integrate the state parameter ψ into its constitutive framework to model dense and loose sands material with the same parameter set. Importantly, it is able to identify the liquefaction potential as it can simulate softening behaviour due to pore pressure increase of loose soils in undrained conditions. Since NorSand has recently been implement into PLAXIS, a geotechnical analysis software capable of performing FEAs, it must be verified, validated and applied with the software, which is done in this report.

First, stress-path and parametric analyses were conducted at single stress points. The stress-path analyses show how the state variables evolve for different triaxial conditions. Systematically changing the input parameters to extremes found in literature helped determine their influence on the evolution of stresses and strains. The resulting figures can be used to help future calibrations to experimental lab test data.

The PLAXIS implemented NorSand (PLAXIS NorSand) was verified by comparing it with an implementation written in Visual Basic for Applications (VBA NorSand) by the authors of the model Jefferies and Been. Verification in this context means determining if PLAXIS NorSand is able to produce outputs as intended by the authors. Various testing conditions, both triaxial and direct simple shear, showed overlap and agreement between the outputs of both implementations, verifying PLAXIS NorSand.

Then, the model was compared to, albeit not in a traditional sense, an 'analytical solution', which is the relationship between the mobilized friction ratio M_i and state parameter ψ in its simplest form. The mobilized friction ratio and stress ratio at peak strength of PLAXIS NorSand and the 'analytical solution' were compared. The values between both showed less than 3% difference, further verifying PLAXIS NorSand.

The constitutive model was then validated - i.e., established that PLAXIS NorSand is able to approximate soil behaviour as intended. First, by using the soil parameter set that had been derived from lab tests of Erksak sand as a baseline, the input parameters were varied until PLAXIS NorSand was calibrated to individual triaxial tests as best as possible. Then, triaxial tests of Erksak, Nerlerk and Ticino sand were approximated with PLAXIS NorSand without changing the soil parameters determined from lab test data.

PLAXIS NorSand is able to follow lab test data decently well with one parameter set. And if one decides to take the time and calibrate individual lab tests, and deviate from soil parameters determined from a set of lab tests, they can be matched even better. Additionally, it showed a consistent need for activation of the softening flag ($S = 1$) in order to appropriately model loose soils in undrained conditions. Furthermore, NorSand exhibits indefinite hardening in dense soils during undrained loading, which can be avoided by employing a 'cavitation cut-off'.

The last part of this report tested PLAXIS NorSand by applying it in FEAs of a simplified submerged landslide, which was subjected to 20 centimeters of displacement at the crest through a rigid slab in undrained conditions. First, the difference in slope behaviour due to change in soil density within NorSand was determined: dense soil resulted in the slope to be able to bear the full 20 centimeter displacement, whereas increasing the void ratio (i.e., increasing the positive value for the state parameter) gave the effect of even quicker slope collapse and a lower bearing capacity. In other words, when using NorSand, the looser soil the further the failure surface moves up and the quicker the structure fails to maintain equilibrium.

Lastly, NorSand was compared to Modified Cam-Clay and Mohr-Coulomb to highlight the

differences in their ability to model static liquefaction, while being triggered by unrealistic loading conditions. Even though none of the FEAs showed actual liquefaction, since it is accompanied with the fluidization and loss of structure, they still gave in indication of the liquefaction potential. NorSand, contrary to the other constitutive models, showed the expected high sensitivity to forced displacement resulting in clear shear bands resembling Prandtl-type failure mechanism and early onset soil body collapse.

List of Figures

List of Tables

List of Symbols

Symbol	Description	Unit
u	Pore pressure	kPa
σ	Total stress	kPa
σ'	Effective stress	kPa
σ_1	Major principle stress	kPa
σ_2	Middle principle stress	kPa
σ_3	Minor principle stress	kPa
θ	Lode angle	$^\circ$
$\dot{x}$	Differential with respect to time	-/t
p	Triaxial isotropic (mean) stress invariant	kPa
p_0	Pre-consolidation stress	kPa
p_c	Critical mean effective stress	kPa
p_i	Mean effective stress at image state	kPa
q	Triaxial deviatoric (shear) stress invariant	kPa
η	Stress ratio	-
η_{max}	Maximum stress ratio	-
M_{tc}	Critical friction ratio from triaxial compression tests	-
M_i	Mobilized friction ratio	-
ε	Total strain	-
ε^e	Elastic strain	-
ε^p	Plastic strain	-
ε^{ij}	Strain tensor	-
ε_1	Major principle strain	-
ε_2	Middle principle strain	-
ε_3	Minor principle strain	-
ε_q (or γ_s)	Total deviator strain	-
ε_q^p	Plastic deviator strain	-
ε_v	Total volumetric strain	-
ε_v^e	Elastic volumetric strain	-
ε_v^p	Plastic volumetric strain	-
D^p	Plastic dilatancy rate	-
D_{min}	Minimum dilatancy rate	-
e	Void ratio	-
e_c	Critical void ratio	-
ψ	State parameter	-
ψ_0	State parameter at initial conditions	-
ψ_i	State parameter at the image state	-
R	Over-consolidation ratio	-
λ	Slope of the normal consolidation line	-
κ	Slope of the un- and reloading line	-
Γ	Critical void ratio at $p = 1$ kPa	-
χ_{tc}	Slope of the linear relationship between D_{min} and ψ determined in triaxial compression	-
χ_i	Slope of the linear relationship between D_{min} and ψ_i	-
N	Volumetric coupling coefficient	-
ν	Poisson's ratio	-
K	Bulk modulus	MPa
G	Shear modulus	MPa
G_{ref}	Shear modulus at $p_{ref} = 100$ kPa	MPa
I_r	Shear rigidity	-
n_G	Exponent of the elasticity power-law	-
H	General hardening parameter	-
H_0	Hardening parameter 1	-
$H\psi$	Hardening parameter 2	-
S_{soft}	Softening term	kPa
S	Softening flag	-
f	Yield function	kPa
g	Plastic potential function	kPa
Λ	Plastic multiplier	-

List of Abbreviations

Abbreviation	Description
NS	NorSand
MC	Mohr-Coulomb
OCC	Original Cam-Clay
MCC	Modified Cam-Clay
FEM	Finite Element Method
FEA	Finite Element Analysis
PLX	PLAXIS
VBA	Visual Basic Application
TXU	Undrained Triaxial Compression
TXD	Drain Triaxial Compression
DSSU	Undrained Direct Simple Shear

Contents

1 Introduction

1.1 Problem description

Geo-technical problems often involve large structures that interact with soil or are made out of soil. These structures can be sub-aerial, such as tailings dams, which are massive sand dikes that contain rejected soil from mining operations and belong to the largest man-made structures in the world, as they can be more than 100 m high and in some cases several kilometers wide. Or submarine structures, such as large natural or man-made slopes under water, which are one of the main threats to offshore assets. Liquefied submerged slopes or embankments are often characterized by relatively small failure angle, sudden failure, a considerable amount of released soil mass and large influencing areas. These make static liquefaction to be one of the most catastrophic mechanisms of under-water slope failures. Instability of these slopes can be triggered by static loads, such as sediments deposition, toe erosion, rising of an embankment height, scours near a structure or dredging activities (W. Zhang and Askarinejad, 2019). Collapse of these sub-aeral and submarine structures can result in massive economical and environmental impact.

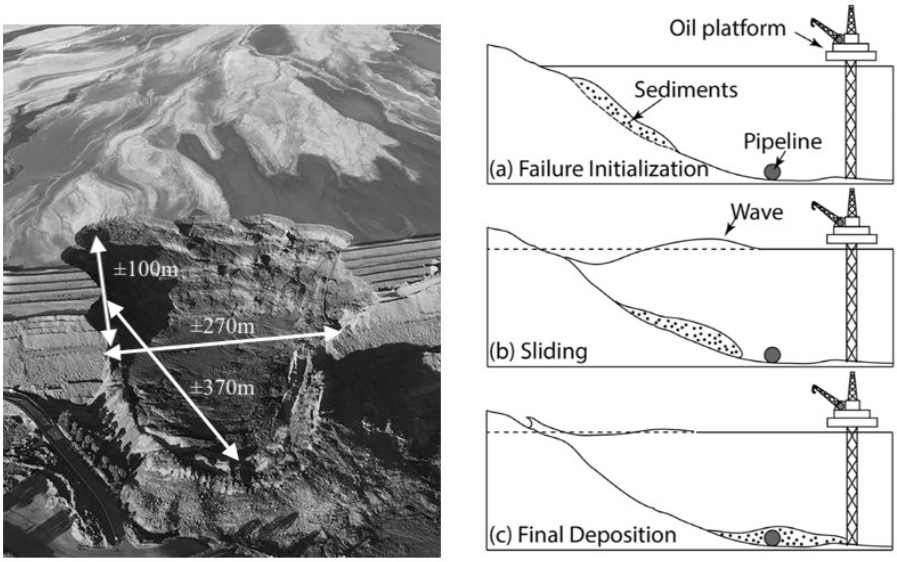

Left: Newcrest Cadia tailings dam failure Right: Illustration of a submarine landslide

Figure 1.1: Left: Newcrest Cadia tailings dam failure. Right: illustration of a submarine landslide affecting underwater infrastructure (taken from X. Zhang et al., 2019).

1.2 Project background

For these reasons, it is crucial analyze the stability of these sensitive structures with the use of numerical methods (e.g., FEM) with advanced constitutive models that can simulate the mechanical behaviour of tailings materials and identify and prevent potential failure mechanisms (e.g., liquefaction) from different hydro-mechanical conditions. In this study, the constitutive model formulated by Jefferies and Been (1993), known as NorSand, will be used to analyze the performance of underwater slopes through numerical simulations performed with PLAXIS 2D. Based on fundamental principles of the critical state theory, NorSand can capture the porosity dependency of granular materials to simulate the compaction of loose soils as well as the tendency of dilating characterizing dense material through normality and limit hardening.

1.3 Objectives

The objectives of this thesis are threefold. First, it is to analyze the model behaviour. Then, it is to verify and validate the NorSand constitutive model as it has only recently been integrated into PLAXIS. Finally, NorSand is applied to established how well the constitutive model is able to simulate the behaviour of underwater slopes - in particular their failures. To achieve these objectives, many questions have to answered:

- What is NorSand?
  - What is the difference between NorSand and other constitutive models?
  - What is the physical meaning behind all the components of NorSand?
- How does NorSand perform in PLAXIS?
  - What are the mechanics of the model during various stress paths in single stress point analyses?
  - What are the influences of individual model parameters?
  - How close is the PLAXIS integrated NorSand to the original model?
  - How well does the model agree with the 'analytical solution'?
- How well does NorSand model sand behaviour?
- How does NorSand simulate failure in underwater slopes?
  - Are there well-documented case studies of flow liquefaction failures of underwater slopes?
  - What are underwater slopes and what are the mechanics behind flow liquefaction within these structures?
  - What data and which parameters are important in order to make realistic models?
  - What can be assumed, to which extent can one simplify the problem and what are the resulting boundary conditions?
  - How does soil density influence the FEA?
  - What are the differences in behaviour of FEM models with different constitutive models?

1.4 Methodology

Answering the aforementioned questions can be made easier if one establishes a framework:

- Literature review. This entails an in-depth study on constitutive models in general and the inner workings of the NorSand model itself, structures at which liquefaction can occur, and previous case studies.
- Model behaviour Analyses.
  - The constitutive framework will be used to investigate the performance of the model through parametric analyses to explore the effect of each parameter on the soil response.
  - Employing a stress-path analysis to check the evolution of certain state variables though various loading conditions.
- Verification and Validation. Demonstrating that the newly PLAXIS implemented NorSand is the same as the original model developed by the authors verifies NorSand. Determine that PLAXIS NorSand behaves as expected, validates the model.

  - Comparison between the PLAXIS integrated-NorSand (PLAXIS NorSand) versus the original NorSand that is written in excel through VBA (VBA NorSand).
  - Comparison of PLAXIS NorSand to the theoretical formulation on which it is based on.
  - Comparison of PLAXIS NorSand to the stress-strain response of experimental lab test data by performing single stress-point analyses.

- Application. Use the constitutive model in conjunction with finite element models.
  - Compare NorSand to different constitutive models through FEA of a simplified underwater slope.
  - Pre-processing and preparation of data for the creation of numerical models.
  - Running and re-running the simulations.
  - Post-processing of results.

- Conclusion. Conclusions, capabilities, limitations and recommendations on the use of the NorSand model for applications involving liquefiable structures will be provided.

1.5 Outline

The structure of this report goes as follows. Chapter 2 lays down the general framework on concepts that are repeated in other chapters. This includes what liquefaction entails; the use and benefits of triaxial tests; typical stress-strain behaviour of sand; and the over-consolidation ratio.

Before the actual modeling can be expounded, the general concepts of constitutive models must be explained, which is done in chapter 3. A few models will be shown, which are in a sense the stepping stones on which the NorSand model has been built on. Then, NorSand itself is explained in-depth. This includes the reasoning and logic behind its various components.

Chapter 4 goes through parametric and stress-path analyses to go deeper into the model behaviour.

The next chapter checks if the newly implemented constitutive model within PLAXIS is actually the model that was created by the authors through verification. This is followed by validation, which explores the constitutive model behaviour en determines if it behaves as intended.

Chapter 6 goes into the application of PLAXIS NorSand by modeling of an underwater slope. It first explains the general structure of these entities and how they are approached within models. Then a simplified finite element model of an underwater slope is introduced, which is then analyzed by simulating deformation with different constitutive models, i.e., Mohr-Coulomb, Modified Cam-Clay, and NorSand, to determine the differences, benefits and drawbacks of each model. It will also research the effects of different densities on the FEA.

The last chapter will conclude this report by summarizing the results and related discussions, followed by giving recommendations.

2 General Framework

Behaviour of soil depends on many factors, such as effective stress regime, void ratio, fabric, etc. Constitutive models aim to capture the effects of these factors on soil behaviour, and in turn predict their behaviour for engineering problems as close as possible. One must not forget that constitutive models are based on idealizations after all.

This chapter lays establishes a general framework for understanding soils. First, the concept of liquefaction is explained. Then, a quick rundown on common lab-tests within the field of Geo-technical engineering are illustrated. Lastly, the typical stress-strain behaviour of sand is introduced.

2.1 Liquefaction

When a unit of granular material, such as soil, sediments and wastes in tailings dams, is subjected to stresses, part of it is carried by the soil skeleton as effective stresses (σ') and, if saturated, part of it by the water inside the pores as pore water pressure (u). This is can be summed up with Terzaghi's Principle:

$$\sigma = \sigma' + u \tag{2.1}$$

The strength of granular material is given by the magnitude of effective stress, and the deformation of the material is due to the change in effective stress. Loading these materials will increase the total stress, but if the pore water has no time to drain (i.e., undrained loading conditions) the water will take the stress instead of the soil skeleton ($\sigma = u$). Particulate material will liquefy when it is contractive, saturated and the effective stress is zero - it will lose its strength and stiffness and start behaving like a fluid. After liquefaction, the excess pore pressure will dissipate and the soil will consolidate again (Figure 2.1). Liquefaction comes in two flavours: static liquefaction (e.g., due to monotonic loading when increasing the embankment height) and cyclic liquefaction (e.g., due to earthquakes). This report will focus on the mechanisms of static liquefaction.

Figure 2.1: Sunken car stuck in densified soil after an liquefaction due to an earthquake.

2.2 Triaxial test

Lab testing is the primary source for our understanding of soil behaviour. Control of initial conditions and stress paths are huge advantages of these tests. Different tests approach (read: do not simulate, but at best somewhat approximate) different real-life failure mechanisms.

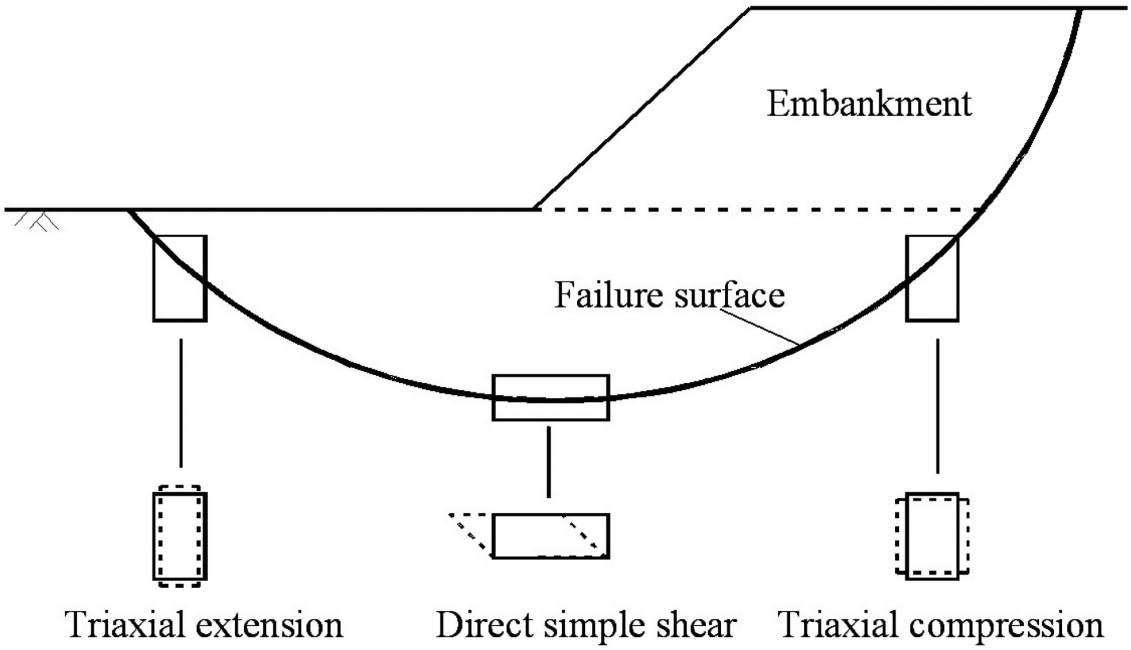

Figure 2.2: Different tests used for different parts of a failure mechanism. Taken from Wang, Shen, and Ye, 2008.

The triaxial test (Figure 2.3) in particular is used both in the industry and research. In short, the test involves consolidating a cylindrical soil specimen under confining pressure (σ_3, which is assumed hydrostatic for convenience. A deviator stress $\Delta\sigma$ is then applied in the vertical direction, such that the total stress in the vertical direction is $\sigma_1 = \sigma_3 + \Delta\sigma$. As all principal stresses (section 3.1.2) are known and controlled during a triaxial test no stresses or strains are inferred when used as part of a constitutive model. This way no stress conditions have to be assumed, otherwise resulting in uncertainty in a model that already approximates behaviour. The steps during a triaxial test are described in more detail in Appendix A.

During testing, the soil is either compressed or 'extended'. True extension is not possible since many soils do not have strong cohesion like intact rocks. Therefore, soil samples are compressed such that cell pressure is larger than the axial load, simulating extension as a result. This report focuses on triaxial compression.

A typical set-up of triaxial testing hardware is illustrated in Figure 2.4. Axial load, resulting in deviatoric stress, is applied with use of a drive unit capable of delivering different strain rates. The applied load is measured by a load cell. The axial displacement is measured using a linear displacement transducer (LVDT). The triaxial cell is filled with de-aired water exerting cell pressure on the sample. The soil sample has two porous discs at the sample bottom and top for possible drainage, and is surrounded laterally by a rubber membrane. The top and bottom porous discs are attached to the upper and lower platens, respectively. There are three pressure connections to the system that are used to measure the pore pressure or volume changes and apply back pressure and cell pressure. The typical size of the cylindrical soil specimen is 36mm in diameter and 76mm in length.

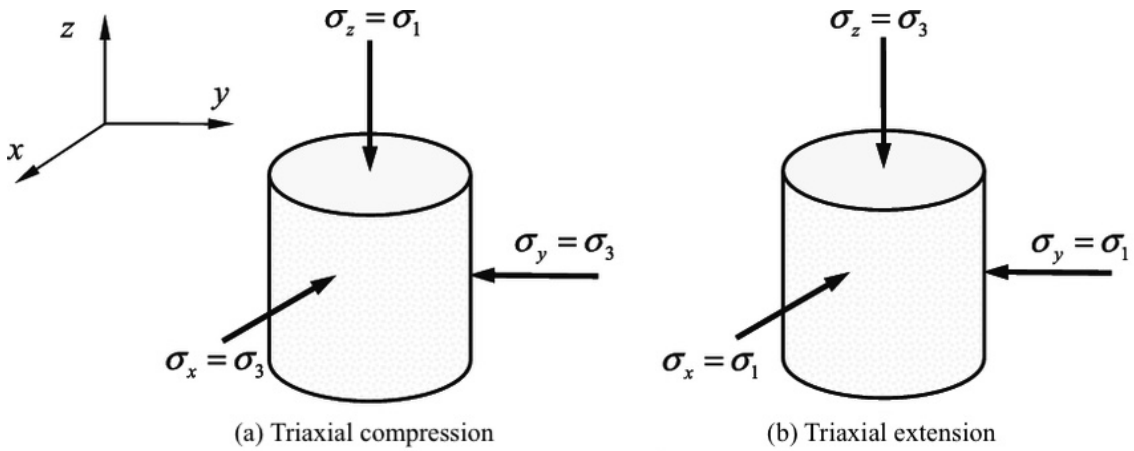

Figure 2.3: Schematic representation of triaxial compression and extension during phase 2. Altered from Gao and Zhao, 2013.

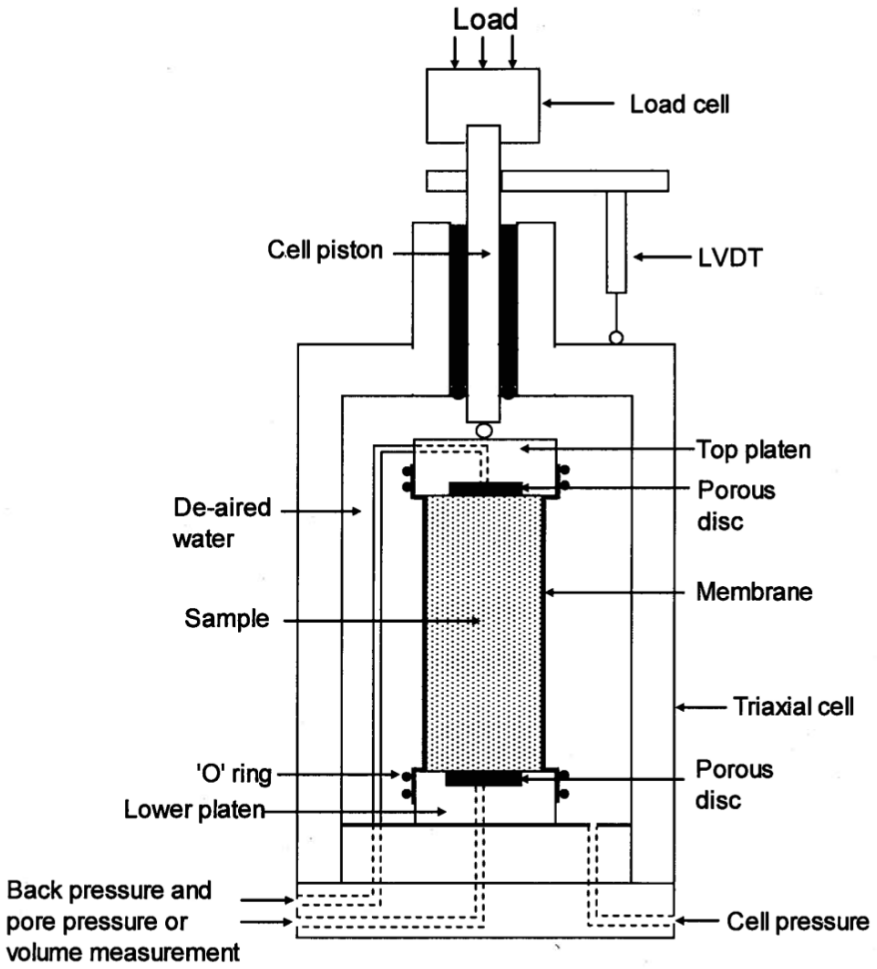

Figure 2.4: Schematic representation of the triaxial apparatus. Taken from Dabeet, 2005.

2.3 Typical stress-strain behaviour of sand

From strain-controlled triaxial lab tests in compression, typical schematics of stress-strain curves for dense and loose sand in drained and undrained condition can be made. It is important to keep in mind that behaviour that is shown in drained conditions is an indication how the soil will behave in undrained conditions. Undrained behaviour arises due to boundary conditions, and is not in itself fundamental soil behaviour, which is the case for drained behaviour. Therefore, understanding and modeling drained behaviour is key for approaching soil behaviour in general.

Consolidation due to isotropic compression is well known. Another important characteristic of particulate material is its ability to contract or dilate upon shearing. When the material is loosely packed the material can further densify by moving into its pore space when sheared (Figure 2.5a). Dense material, however, cannot further densify when sheared. Hence, it must roll over itself during deformation, increasing its pore space with dilation as a result (Figure 2.5b).

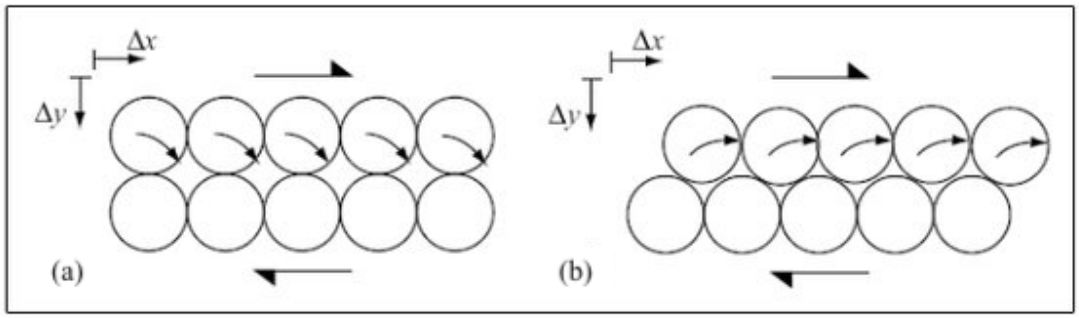

Figure 2.5: (a) Illustration of densification of loose material upon shearing. (b) Illustration of dilation of dense material upon shearing. Altered from Elbadawy, 2014.

It is important to differentiate between the definition of dilation in the absolute sense or that of rate (Figure 2.6b). In short, the first definition is simply the integral of the latter over the particular stress path imposed on the soil. In many cases, the absolute volume change may be contractive after a particular shear strain, even though the material is dilating in terms of rate. If the soil dilates according to the absolute definition, then the undrained strength will be greater than the drained (Figure 2.7a), and hence, liquefaction becomes impossible (as long as the situation was originally statically stable). This report uses the rate definition of dilation. This definition is preferred because it is an expression of the work flow in the soil, which is fundamental to plasticity-based constitutive models.

Figure 2.6 shows the typical behaviour of dense and loose sand in drained conditions, starting from the same initial stress conditions (i.e., same mean effective stress p'). Both axial (ε_1) and deviator (ε_q) strains are used in literature as they both give similar trends (strains are explained in section 3.1.3). From Figure 2.6a it can be seen that dense sand shows a peak deviator stress and softens to a residual value at larger strains. Loose sand, however, does not peak and instead reaches its residual strength directly. Figure 2.6b illustrates that in dense sand, after some contraction, the soil turns dilative (i.e., the soil volume increases as its pore size increase). Loose sand remains fully contractive. After large axial strain both soils reach critical state and stop changing in volume. When shearing is continued they simply further deform without volumetric strain - this behaviour occurs when a soil is at critical state.

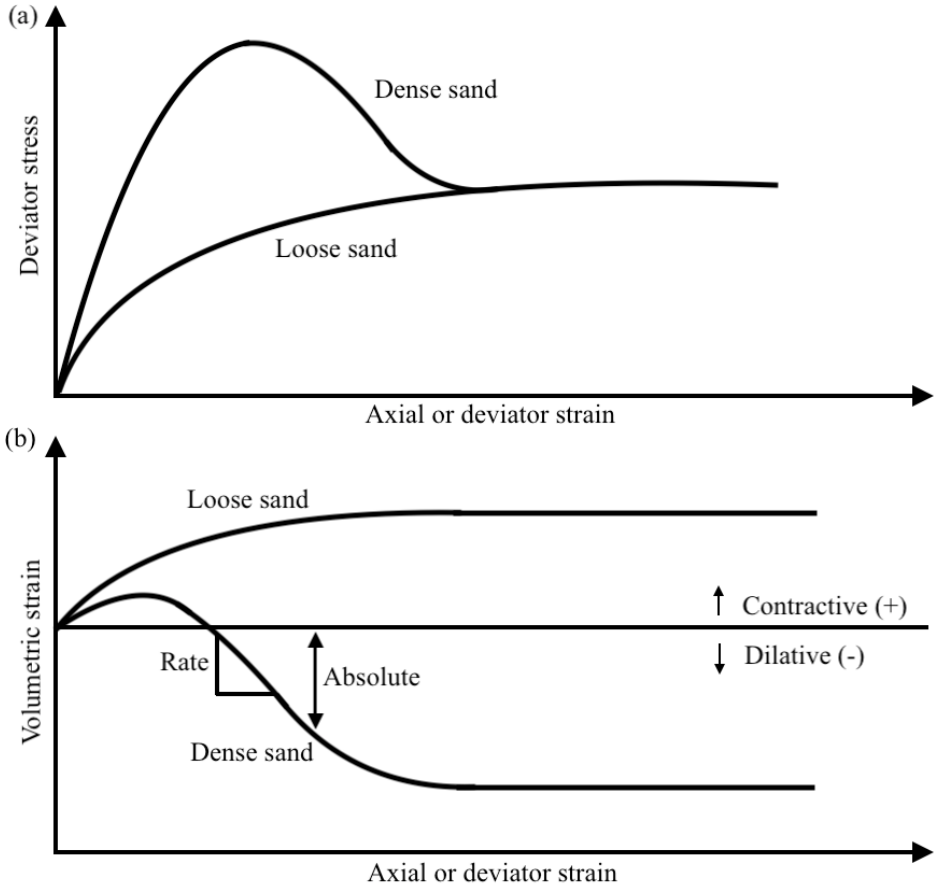

Figure 2.6: Typical drained behaviour of dense and loose sand. (a) Deviator stress q vs. axial ε_1 or deviator ε_q strain. (b) Volumetric strain ε_v vs. axial ε_1 or deviator ε_q strain.

Undrained behaviour is a boundary condition which indicates the inability of pore water to properly dissipate during loading. As fluids can generally be assumed infinitely stiff, volume change of the soil as a whole is inhibited during loading (i.e., Poisson's ratio $\nu = 0.5$).

Since loose soil contracts during drained loading, it will also have the tendency to contract during undrained loading. However, pore water is occupying the pore space and cannot move. Therefore, the grains will push into the pore water, increasing the water pressure (Figure 2.7b). Recalling Terzaghi's Principle (equation 2.1), one can deduce that the initial effective stress is reduced by the current increase of pore pressure, where the pore pressure is equal to the applied axial stress. In other words, the loose soil softens until it reaches critical state and the soil stops its tendency to change in volume (Figure 2.7a). Loose soil can liquefy in undrained conditions if it softens sufficiently and its effective stress is reduced to zero.

Undrained conditions have the opposite effect on dense sands. Whereas loose soil contracts upon shearing, dense soils dilate. But again, due to undrained conditions, the pore water is trapped and is unable to move. The grains start 'pulling' on the pore water resulting in negative pore pressures. This in turn increases the effective stress of the sand and it starts hardening - the soil will not liquefy. Keep in mind that there is a physical limit to how low the water pressure can go (about -100 kPa i.e., absolute vacuum), before the water vaporises due to cavitation.

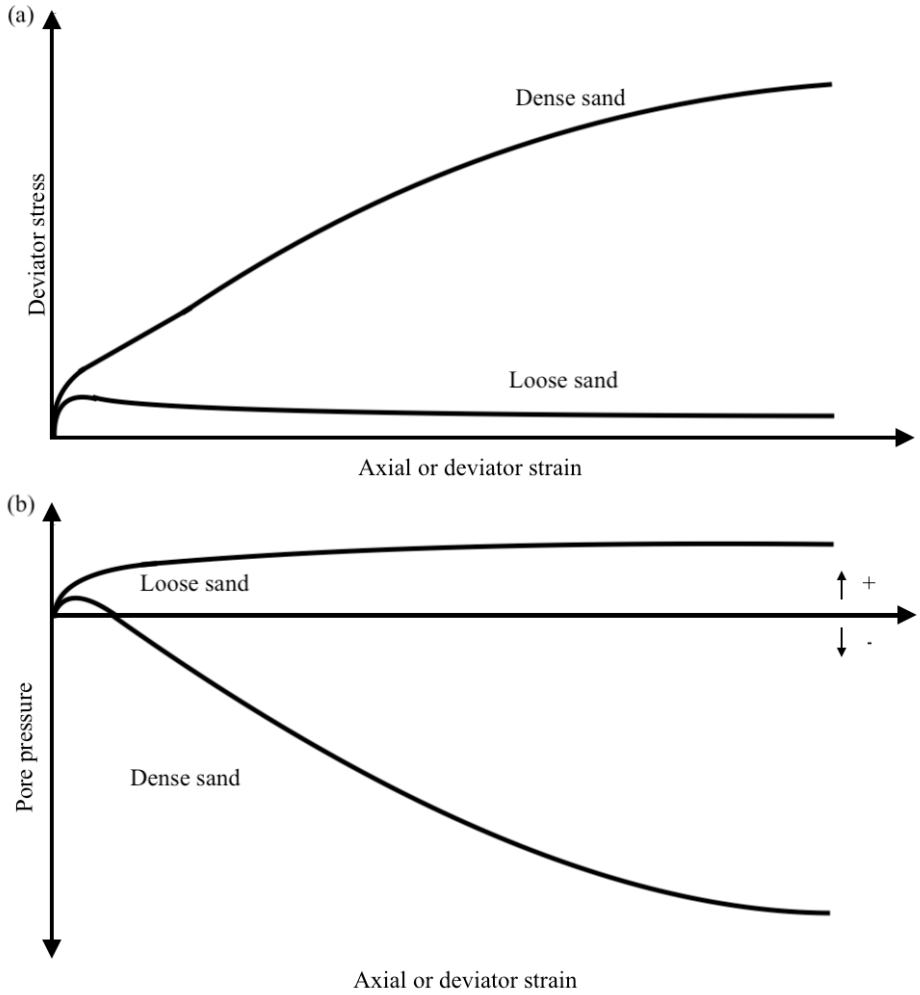

Figure 2.7: Typical undrained behaviour of dense and loose sand. (a) Deviator stress (q) vs. axial (ε_1) or deviator (ε_q) strain. (b) Pore pressure (u) vs. axial (ε_1) or deviator (ε_q) strain.

Soil strength is directly related to mean effective stress. For higher mean effective stresses soil has a stiffer response and higher strength. Figure 2.8 is a schematic demonstrating the effect of mean effective stress on stress-strain curves. The three plots have identical initial void ratios and preparation methods.

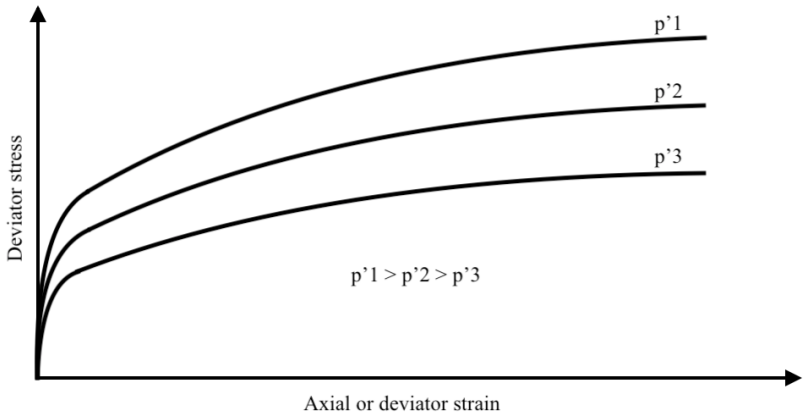

Figure 2.8: Typical drained behaviour of sand with different consolidation pressures.

Although the behaviours described in Figures 2.6, 2.7 and 2.8 are generally applicable, differences in soil behaviour are observed for different soils, and also for the same soil using different preparation methods. This is due to different sample preparation methods resulting in different initial fabric, where fabric refers to "the arrangement of particles, particle groups, and pore spaces in a soil" (Mitchell and Soga, 2005 as cited in Dabeet, 2005). The effect of different fabric is illustrated in Figure 2.9. One of the samples was prepared by moist tamping and the other sample was prepared by wet pluviation, with the former showing stiffer behaviour than the latter. This demonstrates that fabric, or anisotropy, is of equal importance for the behaviour of sands. This is an inconvenience, given that there is no easy and standard method for measuring fabric. Promising research is done to quantify inter-particle contact orientations and forces in the constitutive behaviour and represent it as an equivalent state parameter (section (3.3.3) as a scalar description of packing density. For now, it is best to recognize its effects and be conservative in how the effects are included in engineering design and assessment.

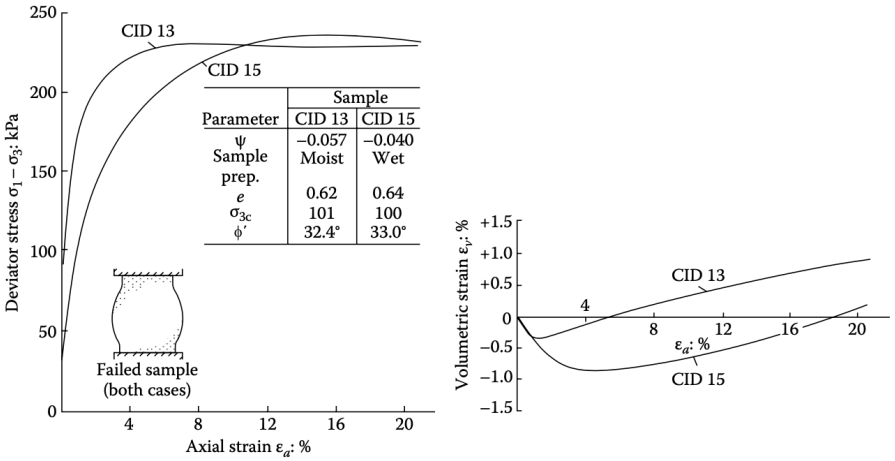

Figure 2.9: Effect of sample preparation on the behaviour of Kogyuk sand. Taken from Been and M. Jefferies, 2015.

3 NorSand elasto-plastic model

In this chapter, the NorSand model is explained in detail. First, the concept and basics of constitutive models are explained. Then, Cam-Clay, which can be seen as the stepping stone leading up to NorSand, is illustrated. Other models, such as Mohr-Coulomb, which are important in their own right and may give a better understanding of constitutive models, are explained in Appendix B. The last section gives the model formulation of NorSand, explaining the ideas and experimental justification behind the parameters.

3.1 Constitutive models

Soil constitutive modelling provides qualitative and quantitative understanding of soil behaviour, which are derived from mechanics. The need for proper models are in high demand as computers are able to handle increasingly complex numerical analysis, which are becoming standard procedure.

Soil behaviour depends on many factors including stress level and void ratio. Even though tests give great insights to behaviour of a soil in question, they by no means describe other possible combination of stress levels. And performing numerous tests at every possible combination of stress level and void ratio is impractical. Useful constitutive models allow for quick, cheap and sufficiently accurate prediction in strength change and deformation characteristics for the full range of applicable combinations of stress level and void ratio.

This section briefly describes elasto-plastic soil modelling. This is followed by an explanation on stress invariants, followed by strain elasticity and plasticity. Finally, an overview of commonly used soil models is given, ending at NorSand.

3.1.1 Elasto-plastic modelling

Soil is an elasto-plastic material, meaning it exhibits both elasticity and plasticity. A typical elasto-plastic model is comprised out of elasticity and plasticity, a yield surface, a flow rule, and a hardening/softening rule.

- Elasticity is associated with recoverable strains, and purely elastic behaviour is usually only observed in soil at very small strains. The direction of an elastic strain increment is the same as its related stress.
- Plasticity is associated with irrecoverable strains. These can occur alongside elasticity or without (e.g., at peak dilation).
- The yield surface, commonly denoted as function $f = 0$, is the boundary between elastic and plastic strains (Figure 3.1). A change in stress state inside the yield surface (i.e., where $f < 0$) causes elastic strains while stress states that want to evolve beyond the original yield surface (i.e., where $f = 0$ and $\dot{f} \neq 0$, will push the boundary until the yield surface arrives at that state, causing plastic strains (the soil yields).
- A flow rule controls the direction and relative magnitude of the plastic strain increments due to yielding (i.e., change in yield surface size). When a soil is sheared its volume changes according to this flow rule, which is the stress-dilatancy relation.

  Flow rules can be associated or non-associated, meaning the plastic strain increment ratio is normal or not normal to the yield surface, respectively. Associated flow (i.e., normality) rules have been used in original soil constitutive models as these models do not violate Drucker's postulate (Drucker, 1951 as cited in Been and M. Jefferies, 2015), with convex yield surfaces and plastic strain increment vectors that are normal to those surfaces as a result (Figure 3.1). Normality greatly simplifies models since flow rules are automatically defined if the yield surfaces are defined (Figure 3.1).

- Hardening/softening rules describe the amount of plastic strains and movement of the yield surface itself during yielding: they increase in size during hardening and decrease during softening. Since stress states cannot lie outside the yield surface, they stay on it as the surface changes in size due to the consistency condition (Figure 3.2).

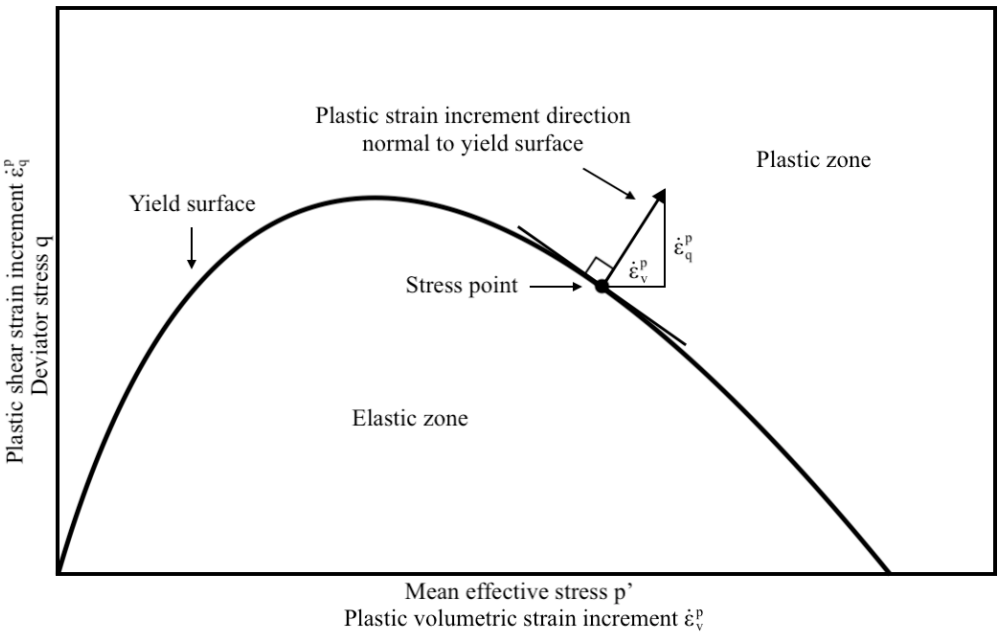

Figure 3.1: An example of a yield surface and depiction of normality.

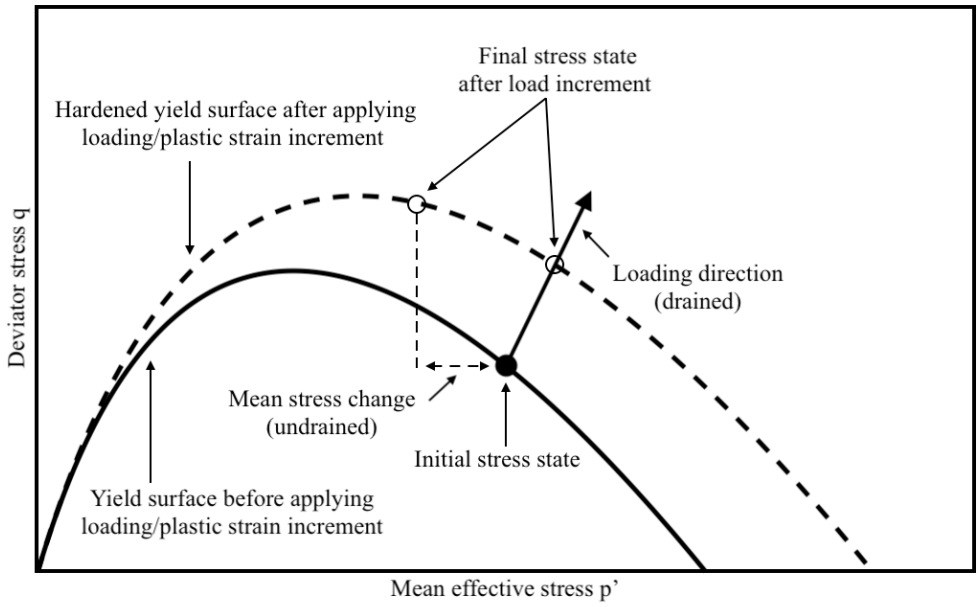

Figure 3.2: Illustration of change in yield surface size (hardening) and the consistency condition. Altered from Been and M. Jefferies, 2015.

3.1.2 Stress invariants

Imagine an infinitesimally small unit volume and its related coordinate system within a stress state. The normal and shear stresses acting on that volume can be summarized in stress tensor σ shown in Figure 3.3a:

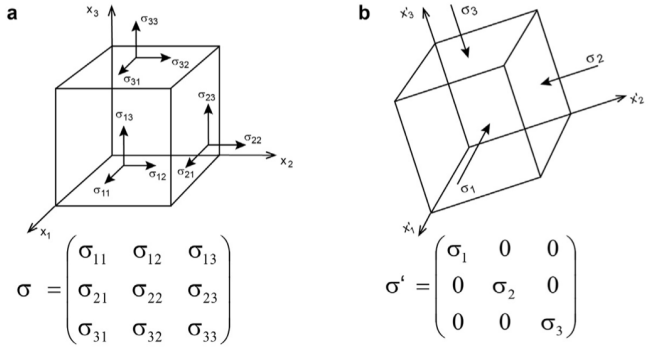

Figure 3.3: (a) A representation of the stress state, (b) A Representation of the orientation of the principal stresses for that same stress state, where σ_1 is the major, σ_2 the intermediate and σ_3 the minor principal stress. Taken from Heidbach et al., 2018.

When a body subjected to a stress tensor, it can change both in size and shape, which is done by the hydrostatic and deviatoric part of the stress tensor, respectively. As such, written in index notation, the stress tensor can be decomposed into:

$$\sigma_{ij} = s_{ij} + p\delta_{ij} \tag{3.1}$$

where δ_{ij} is the Kronecker delta (with $\delta_{ij} = 1$ if $i = j$ and $\delta_{ij} = 0$ if $i/ = j$), p is the mean stress given by:

$$p = \frac{1}{3}\sigma_{kk} \tag{3.2}$$

The product $p\delta_{ij}$ is the hydrostatic, or isotropic, stress tensor and contains only normal stresses. The deviatoric stress tensor can be obtained by subtracting the isotropic stress tensor from the stress tensor:

$$s_{ij} = \sigma_{ij} - p\delta_{ij} \tag{3.3}$$

If one changes, i.e., transforms, the orientation of that volume and its coordinate system, different forces of that stress state act upon that volume. Due to the conservation of momentum the stress tensor has to be symmetric. This implies that a coordinate system exists where shear stresses vanish along the faces of the volume, leaving only the normally acting principal stresses (figure 3.3 b). σ_1 is the major principal stress, σ_2 the intermediate and σ_3 the minor (i.e., $\sigma_1 \geq \sigma_2 \geq \sigma_3$). Therefore, alternatively, if one applies only the normally acting principal stresses (where $\sigma_1 > \sigma_3$) shear stresses do develop on other planes. The magnitude and direction of the principal stresses can be found by determining the eigenvalues and eigenvectors of the stress tensor σ leading to the characteristic equation:

$$\sigma^3 - \sigma^2 I_1 + \sigma I_2 - I_3 = 0 \tag{3.4}$$

where coefficients I_1, I_2 and I_3 are called the first, second and third stress invariant, respectively, since they do not vary depending on orientation and are thus constant for a giving stress state. This same concept can be applied to the deviatoric stress tensor, giving rise to the deviatoric stress invariants J_1, J_2 and J_3.

As one seeks to generalize constitutive models such they can be applied in numerical models while not having to rely on friction angles (measure of strength, explained in Appendix B) or worry about which orientation the problem is looked at, stress invariants σ'_m and σ'_q, which are the isotropic (mean) and deviatoric (shear) stresses, are used (equations 3.5 and 3.6, respectively). The apostrophe next to the letters indicate effective stresses.

$$\sigma'_m = \frac{1}{3}I_1 = \frac{1}{3}(\sigma'_{11} + \sigma'_{22} + \sigma'_{33}) = \frac{1}{3}(\sigma'_1 + \sigma'_2 + \sigma'_3) \tag{3.5}$$

$$\begin{aligned}\sigma'_q = \sqrt{3J_2} &= \sqrt{3(\frac{1}{6}[(\sigma'_{11} - \sigma'_{22})^2 + (\sigma'_{22} - \sigma'_{33})^2 + (\sigma'_{33} - \sigma'_{11})^2] + \sigma'^2_{12} + \sigma'^2_{23} + \sigma'^2_{31})} \\ &= \sqrt{\frac{1}{2}[(\sigma'_1 - \sigma'_2)^2 + (\sigma'_2 - \sigma'_3)^2 + (\sigma'_3 - \sigma'_1)^2]}\end{aligned} \tag{3.6}$$

However, a third invariant is needed if three principal stresses are reduced to two without losing information. This invariant is called the Lode angle, θ (equation 3.7). Figure 3.4 shows how the three stress invariants work in conjunction. The Lode is the angle between point p and the pure shear line, and depends on σ_2 (table 3.1)

$$\theta = \frac{1}{3}arcsin(\frac{13.5 s_1 s_2 s_3}{\sigma'^3_q}),\ with\ s_1 = \frac{(2\sigma'_1 - \sigma'_2 - \sigma'_3)}{3},\ etc. \tag{3.7}$$

Table 3.1: Lode angles (TX = triaxial).

	TX Compression ($\sigma_2 = \sigma_3$)	**TX Extension ($\sigma_2 = \sigma_1$)**	**Plane-strain (σ_2 varies)**
θ	30°	-30°	-30°$\leq \theta \leq$ 30°

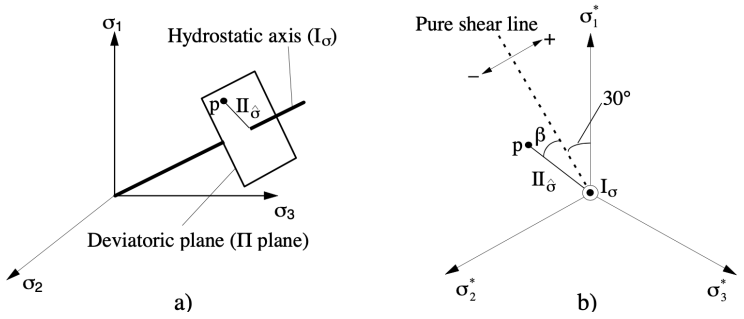

Figure 3.4: (a) Representation of the principal stress space, (b) Deviatoric plane. Taken from Barnichon, 1998.

Most ideas in soil mechanics have developed in the context of the triaxial test, and therefore the stress invariants are rewritten. Since in triaxial compression $\sigma'_2 = \sigma'_3$, the invariants σ'_m and σ'_q turn into p' and q, respectively:

$$p' = \frac{(\sigma'_1 + \sigma'_2 + \sigma'_3)}{3} \tag{3.8}$$

$$q = (\sigma'_1 - \sigma'_2) \tag{3.9}$$

Notice how the deviator stress invariant q does not contain a dash. This is because this invariant is inherently effective since the pore pressure is never included in its value, even if the total principal stresses are used. For the sake of ease, from now on effective stresses are written without apostrophes (e.g., p instead of p'), unless explicitly mentioned otherwise.

3.1.3 Elastic and plastic strains

Most soil models are based on plasticity, which is in itself a macro-scale abstraction of the underlying micro-mechanical reality of grain realignments and movements (Been and M. Jefferies, 2015). In spite of this abstraction, it reasonably captures the behaviour of soils in a computable way. An important behavioural aspect of soil is its the way it deforms, which is quantified by measuring strains ($\frac{\Delta L}{L}$). Analogous to stresses, similar quantities can be defined for the strain tensor ε_{ij}:

$$\varepsilon_{ij} = \begin{bmatrix} \varepsilon_{11} & \varepsilon_{12} & \varepsilon_{13} \\ \varepsilon_{21} & \varepsilon_{22} & \varepsilon_{23} \\ \varepsilon_{31} & \varepsilon_{32} & \varepsilon_{33} \end{bmatrix} = \varepsilon \tag{3.10}$$

The strains related to the isotropic σ'_m (equation 3.5) and deviatoric σ'_q (equation 3.6) stress invariants are the volumetric ε_v and deviatoric (shear) ε_q strains, respectively. ε_v, which is a measure of the relative change in size (and thus not shape), is defined as the sum of the principal strains:

$$\varepsilon_v = \varepsilon_{11} + \varepsilon_{22} + \varepsilon_{33} \tag{3.11}$$

ε_q, which is a measure shape deformation, is defined as:

$$\varepsilon_q = \sqrt{\frac{2}{3}(\varepsilon_{s_{ij}}\varepsilon_{s_{ij}})} = \sqrt{\frac{2}{3}}\|\varepsilon_s\| \tag{3.12}$$

where $\varepsilon_{s_{ij}}$ is the deviatoric strain tensor:

$$\varepsilon_{s_{ij}} = \varepsilon_{ij} - \frac{\varepsilon_v \delta_{ij}}{3} = \begin{bmatrix} \varepsilon_{11} - \frac{\varepsilon_v}{3} & \varepsilon_{12} & \varepsilon_{13} \\ \varepsilon_{21} & \varepsilon_{22} - \frac{\varepsilon_v}{3} & \varepsilon_{23} \\ \varepsilon_{31} & \varepsilon_{32} & \varepsilon_{33} - \frac{\varepsilon_v}{3} \end{bmatrix} \tag{3.13}$$

and the norm of that tensor is:

$$\|\varepsilon_s\| = \sqrt{(\varepsilon_{11} - \frac{\varepsilon_v}{3})^2 + (\varepsilon_{22} - \frac{\varepsilon_v}{3})^2 + (\varepsilon_{33} - \frac{\varepsilon_v}{3}) + 2(\varepsilon_{12}^2 + \varepsilon_{23}^2 + \varepsilon_{31}^2)} \tag{3.14}$$

Recall that σ_m and σ_q can be rewritten for triaxial conditions into p and q. The same can be done for the volumetric and deviatoric strains:

$$\varepsilon_v = \frac{(\varepsilon_{33} + 2\varepsilon_{11})}{3} \tag{3.15}$$

$$\varepsilon_q = \frac{2|\varepsilon_{33} - \varepsilon_{11}|}{3} \tag{3.16}$$

Within geo-technical engineering, and thus also this report, a compression positive notation is used (opposite to the convention within other engineering domains), such that positive volumetric strain ε_v is associated with void ratio reduction.

Strain can be recoverable (elastic) or irrecoverable (plastic). The boundary between recoverable and irrecoverable strains as a yield condition was first proposed by Tresca (1864). Before yielding only elastic strains occur. During yielding both elastic and plastic strains can occur. The total stress can then be decomposed into:

$$\varepsilon = \varepsilon^e + \varepsilon^p \tag{3.17}$$

where ε^e is the elastic recoverable strain and ε^p is the plastic irrecoverable strain, which is illustrated in Figure 3.5. The most important takeaway is that if stress is reduced before the soil yields, all deformations are recovered.

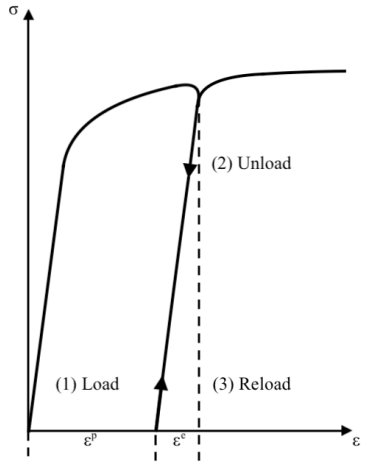

Figure 3.5: Simplified and idealized illustration of an unloading and reloading cycle on a soil. During unloading, the recovered elastic strain ε^e is identified as well as the permanent plastic strain ε^p.

Another important distinction between the two, is the treatment of strains. In elasticity, principal strain increments are in the same direction as principal stress increments. This creates the relationship between stress and elastic strains as:

$$\sigma_{ij} = C_{ijkl}\varepsilon^e_{kl} \tag{3.18}$$

where C_{ijkl} is the stiffness matrix containing Hooke's Law. With plasticity, plastic strain are directed normal to the stress defining the yield surface, and not the stress increments that initiates the yielding. This is called normality and it is essentially a way for a material to maximize the energy absorbed during yielding. Normality can be summarized in equation form:

$$\dot{\varepsilon}^p_{ij} = \Lambda\left(\frac{\partial g}{\partial \sigma_{ij}}\right) \tag{3.19}$$

where Λ is the plastic multiplier and g the plastic potential function, which in the case of normality is the same as the yield function (i.e., $g = f$). Using normality, the volumetric and deviatoric plastic strains are computed as:

$$\dot{\varepsilon}^p_v = \Lambda\left(\frac{\partial g}{\partial p}\right) \qquad \dot{\varepsilon}^p_q = \Lambda\left(\frac{\partial g}{\partial q}\right) \tag{3.20}$$

and the related plastic dilatancy function D^p is then computed as:

$$D^p = \frac{\frac{\partial g}{\partial p}}{\frac{\partial g}{\partial q}} = \frac{\dot{\varepsilon}^p_v}{\dot{\varepsilon}^p_q} \tag{3.21}$$

The state of the material is governed by the so-called Khun-Tucker conditions:

$$f \leq 0 \qquad \Lambda f = 0 \qquad \Lambda \geq 0 \tag{3.22}$$

If $f < 0$ then the material state is elastic (i.e., $\lambda = 0$), while if $f = 0$ the state of the material can be in plastic ($\Lambda > 0$) or neutral loading ($\Lambda = 0$). To characterize the state of the material the same logic can be used by considering further conditions, the so-called persistency conditions:

$$\dot{f} \leq 0 \qquad \Lambda \dot{f} = 0 \qquad \Lambda \geq 0 \tag{3.23}$$

where $\dot{f} < 0$ represents an elastic unloading, $\dot{f} = 0$ and $\Lambda > 0$ a plastic loading, and $\dot{f} = 0$ and $\Lambda = 0$ a neutral loading.

3.2 Cam-Clay

Cam-Clay is an associated flow constitutive model based on critical state soil mechanics (CSSM), and one of the earliest advanced constitutive models for soil. CSSM revolves around the concept that particulate materials tend to a final critical void ratio (Figure 3.8c) and residual strength (Figure 3.8b) after large shear strains. Cam-Clay exists in two main varieties: Original Cam-Clay (OCC) and Modified Cam-Clay (MCC). Even though OCC is not utilized in commercial software, it has been the stepping stone in the development of MCC, NorSand and other critical state soil models. MCC, however, is widely used in geotechnical analyses for normally consolidated clays.

Cam-Clay is a work dissipation model (Schofield and Wroth, 1968 as cited by Been and M. Jefferies, 2015). This means that an idealized dissipation of plastic work, done on an element of soil by the stresses acting on it, is assumed as the soil undergoes a strain increment. The rate of working on the soil skeleton by the external loads per unit volume is:

$$\dot{W} = q\dot{\varepsilon}_q + p\dot{\varepsilon}_v \tag{3.24}$$

During dissipation, only plastic strains are involved as elastic strains are recoverable. As such, equation 3.24 can be rewritten into:

$$\dot{W}^p = \dot{W} - \dot{W}^e = q\dot{\varepsilon}_q^p + p\dot{\varepsilon}_v^p \tag{3.25}$$

Dividing by p and $\dot{\varepsilon}_q^p$ gives:

$$\frac{\dot{W}^p}{p\dot{\varepsilon}_q^p} = D^p + \eta \tag{3.26}$$

which are the plastic dilatancy D^p and stress ratio η $(= \frac{q}{p})$, respectively, and together represent the dimensionless normalized dissipated plastic work. Cam-Clay is based on the assumption that the dissipation rate is constant throughout plastic shearing:

$$\frac{\dot{W}^p}{p\dot{\varepsilon}_q^p} = M \tag{3.27}$$

In other words, all the yield surfaces intersect the critical state line, illustrated in Figure 3.6. This due to the assumption of a single isotropic normal consolidation line (iso-NCL) which is parallel with the critical state line (CSL) in the e-p stress space, illustrated in Figure 3.7. Therefore, the mean effective stress at critical state p_c can be used as a reference parameter for calculating volumetric strains. Combining equations 3.26 and 3.27 gives a stress-dilatancy relationship (i.e., a flowrule):

$$D^p = M - \eta \tag{3.28}$$

which indicates that for critical state conditions ($D^p = 0$) it follows from equation 3.28 that:

$$\eta = M = \frac{q_c}{p_c} \tag{3.29}$$

The yield surface can be derived by assuming normality in q-p plane and the stress-dilatancy relationship of equation 3.28. As $q = \eta p$ by definition the differential is taken to define the change in shear stress as:

$$\dot{q} = p\dot{\eta} + \eta\dot{p} \tag{3.30}$$

Assuming the soil to be a work hardening plastic material from normality:

$$\frac{\dot{q}}{\dot{p}} = -\frac{\dot{\varepsilon}_v^p}{\dot{\varepsilon}_q^p} = -D^p \tag{3.31}$$

Rewriting gives:

$$\dot{q} = -D^p \dot{p} \tag{3.32}$$

Substituting equation 3.30 into 3.32 gives:

$$\frac{\dot{p}}{p} + \frac{\dot{\eta}}{D^p + \eta} = 0 \tag{3.33}$$

This identity of the normality condition is true regardless of the internal dissipation mechanisms of the soil, as long as perfect plasticity or work hardening holds. Substituting equation 3.28 into 3.33 and integrating with the integration coefficient as $ln(p_c)$ when $\eta = M$ (i.e., critical state and $p = p_c$), turns equation 3.33 into the yield surface:

$$f(p, q, p_c) = q - M \left[1 - \ln\left(\frac{p}{p_c}\right)\right] p \tag{3.34}$$

Imagine a soil on which primary loading, by means of isotropic compression (i.e., $q = 0$ and thus $\eta = 0$), is imposed. This would mean the yield surface is pushed outwards (i.e., hardens) at the bottom right of Figure 3.6. The critical mean effective stress is then determined by substituting $p = p_0$ and $\eta = 0$ into equation 3.34, giving $p_c = p_0/2.718$.

The essence of Cam-Clay is its hardening and softening mechanism. For now, drained triaxial conditions are assumed. When normally consolidated soils are sheared, stress states reach the yield surface at $\eta < M$ and the surface hardens, which is associated with contractive volumetric strains (Figure 3.8). Hardening continues until $\eta = M$ where the soil reaches the critical state and further shear strain increments do not cause any change in volume. Alternatively, when loading over-consolidated soils, the stress state reaches the surface at $\eta > M$ the surface softens, which is associated with dilation, until reaching the CSL.

The hardening rule, for OCC, is given in terms of increment of plastic volumetric strain in equation 3.35. Recall how p_c is used as a reference parameter for Cam-Clay as all the yield surfaces intersect the CSL. The CSL then becomes the hardening law for all stress paths. As such, the size of the yield surface can be linked to p_c.

$$\frac{\dot{p}_c}{p_c} = \frac{(1 + e)}{\lambda - \kappa} \dot{\varepsilon}_v^p \tag{3.35}$$

MCC differs from OCC in the shape of its yield surface. Looking at the surface of OCC (Figure 3.6), one can see that it predicts shear strains for hydrostatic loading - i.e., the strain increment vector is not horizontal at p_0 due normality. MCC solves this by introducing an elliptical yield surface (Figure 3.8b). Another important improvement is the inclusion of elastic shear in MCC, whereas OCC is rigid (meaning it is not accounted for) in elastic shear resulting in overestimation of strain increments at small strains.

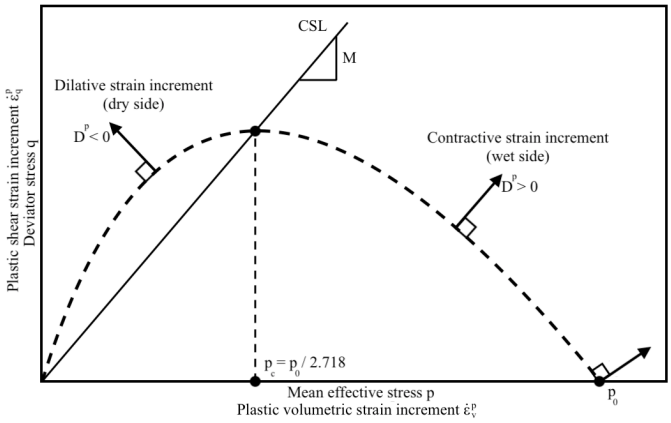

Figure 3.6: OCC yield surface where the dilatancy function D (i.e., dilation) is negative on the dry side and positive (i.e., contraction) on the wet side.

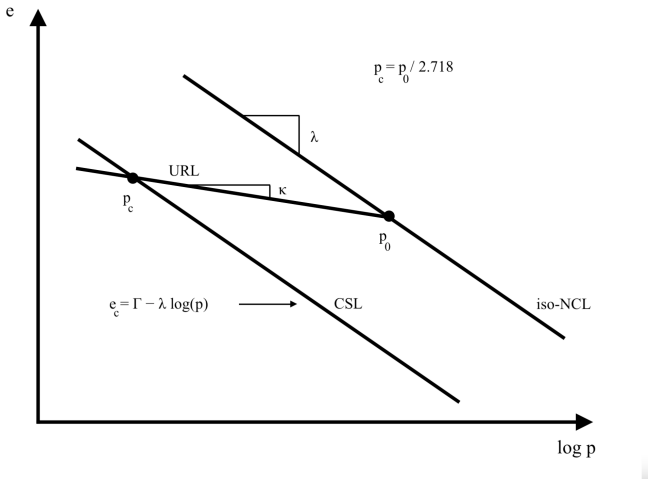

Figure 3.7: Parallel CSL and NCL with a URL intersecting both.

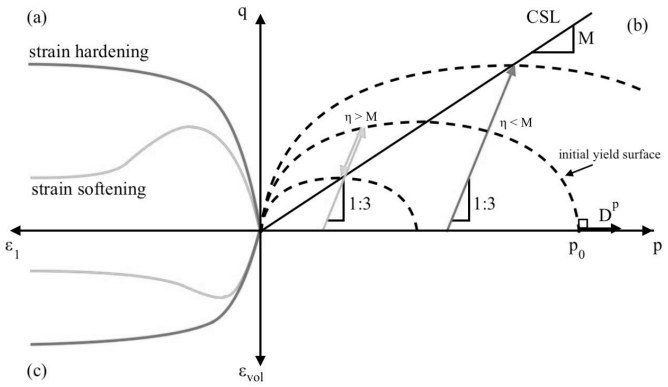

Figure 3.8: Hardening and softening behaviour until critical state. Behaviour is approached using the MCC constitutive model where a drained triaxial stress path is applied. Altered from Espinoza, 2019.

3.3 NorSand

This section goes into detail of the constitutive model that is NorSand. The reasoning behind using NorSand and the justifications and formulations of its components are explained.

3.3.1 Why NorSand?

CSSM explicitly recognizes that any particulate soil can exist over a spectrum of densities, and it quantifies the effect of void ratio (density) on soil behaviours, making it a powerful framework for predicting soil behaviour. Despite this, variants of OCC and MCC are avoided to model real sands as their behaviour, such as dilation and yielding, is represented poorly. This is due to the fact that soils that are denser than the CSL are treated as over-consolidated, resulting in unrealistic stiffness with heavily over-estimated strength. The math behind Cam-Clay models is not the cause of these unrealistic predictions, but the assumption is: all yield surfaces intersect the critical state line.

Instead of assuming a single iso-NCL, it must be recognized that granular soils exist in a spectrum of states - i.e., there exists an infinity of normal compression loci in the e-p plane, depending on the initial void ratio at deposition (which in general is arbitrary). The difference between the two is further illustrated in Figure 3.9. It may also become clear that instead of the singular NCL and CSL being parallel and offset by a 'spacing ratio', there exist infinite NCL that are not parallel to the CSL. The proof and in-depth explanation on the existence of infinite iso-NCLs is given in Appendix C.1.

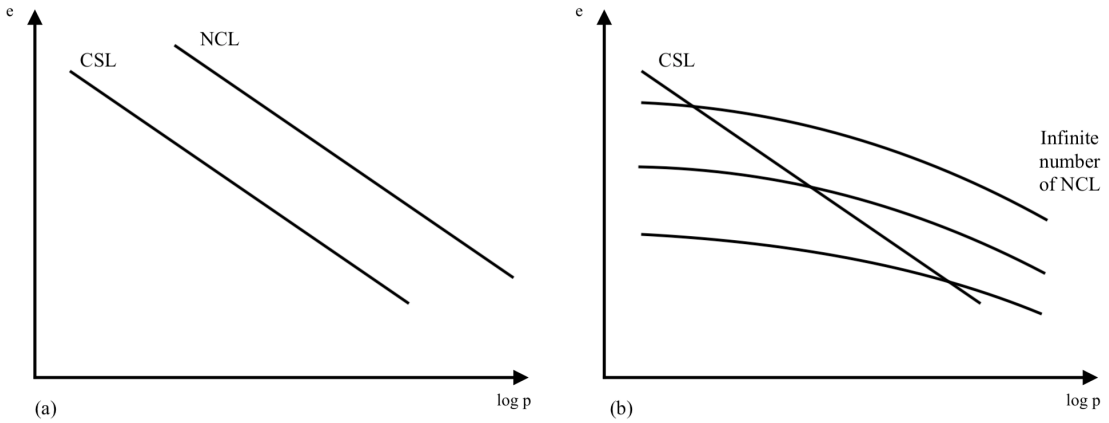

Figure 3.9: (a) Single NCL and (b) Infinite NCL. Altered from Been and M. Jefferies, 2015.

3.3.2 Critical state line

This section will explain the critical state theory. The history and in-depth explanation is given in C.2. Critical state theory is generalized using two axioms (M.G. Jefferies, 1993):

- Axiom 1. A unique locus, called the critical state locus (CSL), exists in q, p, e space such that soil can be deformed without limit at constant stress and constant void ratio.
- Axiom 2. The CSL forms the ultimate condition of all distortional processes in soil, so that all monotonic distortional stress state paths tend to this locus.

In other words, the critical state is taken to be the ultimate state the soil reaches if it is continuously deformed (sheared), defined as Axiom 2. Note that there are two conditions in the definition:

- (1) The soil is at constant void ratio.

- (2) It has no propensity to change from this constant void ratio condition.

Incorrect assessments and confusion arises if condition (2) is ignored, which is explored in section 3.3.5. The relationship between critical void ratio and mean effective stress is called the critical state locus:

$$e_c = \Gamma - \lambda ln(p_c) \tag{3.36}$$

where Γ and λ are intrinsic soil properties, meaning that they are not affected by fabric, stress history, density, etc. The subscript 'c' denotes critical state conditions. Caution is needed when looking at quoted values of λ as both log base 10 and natural logarithms are used. Natural logarithms are more convenient for constitutive modelling, whereas base 10 logarithms arise when plotting experimental data: the notations λ (or λ_e where emphasis is needed) and λ_{10} ($= 2.303\lambda$) are used, respectively. The parameter Γ also has an associated stress level, which is $p = 1$ kPa by convention.

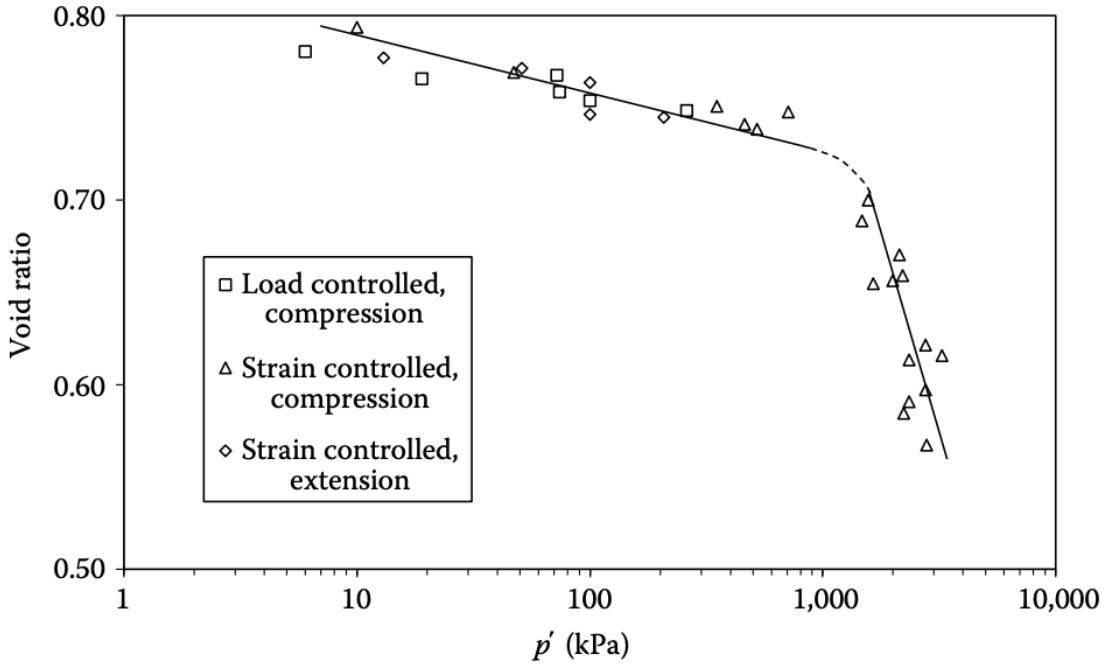

Figure 3.10: Critical state line for Erksak 330/0.7 sand from undrained tests that reached a distinct critical (steady) state. Taken from Been and M. Jefferies, 2015.

3.3.3 State parameter

As soils exist within a spectrum of states, it is important to measure that state against a reference point to predict and explain behaviour. A concept for such a reference has been established in section 3.3.2 as the CSL, which is unique for each soil. And since there exists an infinite amount of NCLs, there is no set distance from the CSL during primary loading like in Figure 3.9a. The distance of the soils void ratio from the reference state in void ratio-stress space is a first-order measure: soils not at the critical state must change volume as they are sheared since it is a basic postulate that the critical state represents the ultimate condition which is reached after sufficient shear. And the further a soils state deviates from the final critical state, the faster dilation or contraction happens. The state parameter ψ is illustrated in Figure 3.11a, and is defined as the measure of this deviation:

$$\psi = e - e_c \tag{3.37}$$

where e is the current void ratio of the soil and e_c is the void ratio of the critical state at the current mean stress.

Since the critical void ratio is dependent on mean effective stress, so is the state parameter. Soils can now be defined loose or dense in a more quantitative sense: a soil with a negative state parameter can be classified as a dense soil, whereas one with a positive state parameter is loose. This concept gives insight to how dilatancy in sands with a high relative density (i.e., low void ratio) is suppressed and can contract under high confining stress levels (i.e., high mean effective stress). It is the magnitude of dilation that determines strength, not the void ratio or density at which dilation occurs, which is Rowe's stress–dilatancy concept rephrased (chapter 3.3.5).

Figure 3.11a illustrates the meaning of the state parameter, where the CSL is simplified and the bend is left out as engineering practices rarely exceed isotropic stress states of 1000 kPa. Additionally, it shows how expected state paths of sheared soils can approximated as straight lines. In reality, if starting from isotropic conditions, there will be an initial contraction before dilation sets in, but this is a detail on the basic state path vector and can be ignored for simplicity. Alternatively, these paths can be illustrated in the $p' - q$ space (Figure 3.11b).

It is convenient to use conditions at the start of a test when reducing laboratory data to develop soil properties, as that requires the least effort. However, working in terms of initial conditions unnecessarily complicates things when moving from practical engineering to doing the math and putting things in a formal framework – the math is simpler if expressed in terms of current values. As each approach has its own application, both are defined as:

- ψ_0 = state parameter as measured at the start of the loading path using initial void ratio and critical void ratio at initial mean effective stress: $\psi_0 = e_0 - e_c$ (at p_0)
- ψ = state parameter measured using current void ratio and critical void ratio at the current mean effective stress: $\psi = e - e_c$

Finally, instead of taking the theory at face value, it can be substantiated with experimental data. Figure 3.12 shows minimum dilation versus the state parameter for 20 different soils, presented in the form of D_{min} against ψ_0 as explained earlier. The data plotted on this figure range from clean quartz sands through to silty sands and the mean effective confining stress from 19 to 1200 kPa. The overall trend shows that for a negative initial state parameter, the soil shows a peak dilation rate, which coincides with a dense soil. From this point onward, the current value of the state parameter is used.

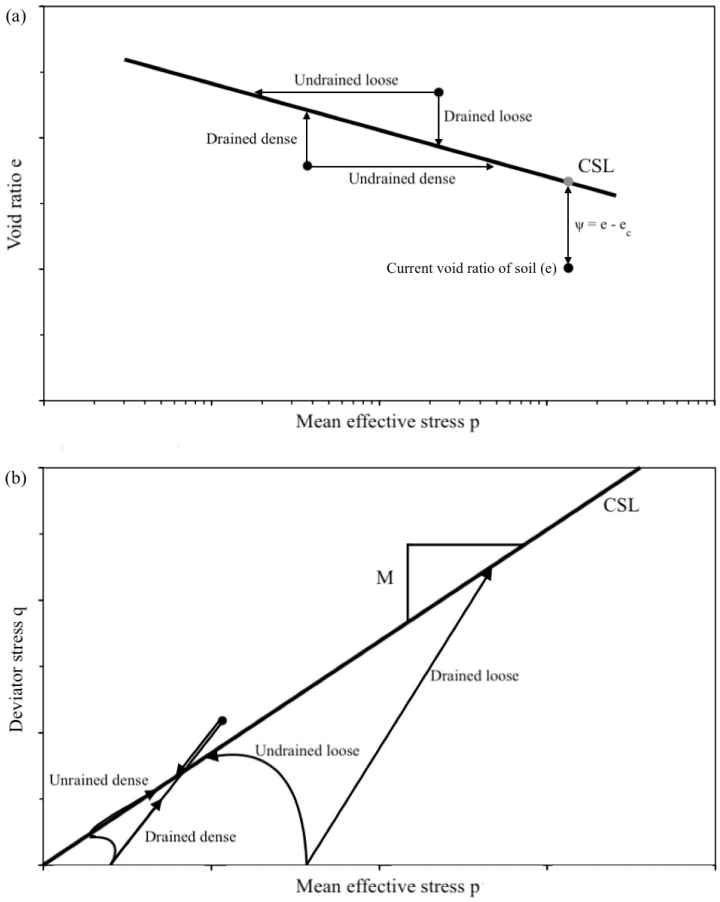

Figure 3.11: Projection of the critical state line in (a) $e - p'$ space and (b) $q - p'$ space. The CSL in this space has the slope $M = \frac{q_c}{p_c}$, which are the deviator and mean effective stress at critical state.

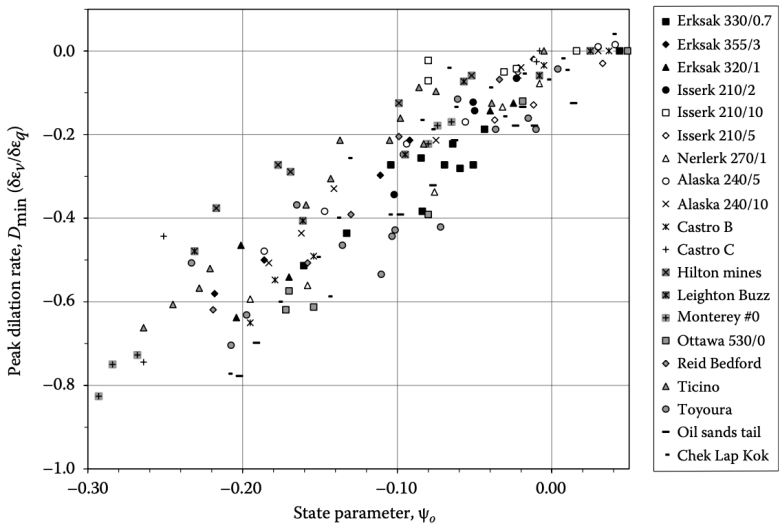

Figure 3.12: Maximum dilatancy D_{min} of 20 soils in standard drained triaxial compression. Taken from Been and M. Jefferies, 2015.

3.3.4 State-dilatancy

As mentioned in section 3.3.1, dense soils exhibit a maximum dilatancy for a given state. Figure 3.12 in section 3.3.3 showed a relation between the state parameter and dilatancy. Realizing that the trend between D_{min} and ψ_0 was unique depending on the fines content of a soil (hinted by the large scatter in Figure 3.12) gave an indication that there exists a soil property involved in relating state parameter to maximum dilatancy:

$$D_{min} = \chi_{tc}\psi \tag{3.38}$$

where χ_{tc} is a soil property defined under drained triaxial compression. Importantly, note that ψ is defined as its current, not initial, value and D_{min} generally occurs at the peak stress ratio. D_{min} is preferred to strength (i.e., η_{max}) to quantify the effect of state as D_{min} is related to the change in void ratio and ψ has void ratio as its input – essentially, the same quantity is used on both sides of equation (3.38). As the current definition of ψ is used, that means that for the condition of $\psi = 0$ naturally gives $D_{min} = 0$, which is the critical state. Figure 3.13 shows several examples of D_{min} versus ψ from drained triaxial tests from which the values of χ_{tc} were determined. Then, if the data in Figure 3.12 is re-plotted using D_{min}/χ_{tc}, there is a notable reduction in scatter of the data set as shown in Figure 3.14. Finally, as elastic strains are negligible at peak conditions, equation (3.38) can be rewritten as:

$$D^p_{min} = \chi_{tc}\psi \tag{3.39}$$

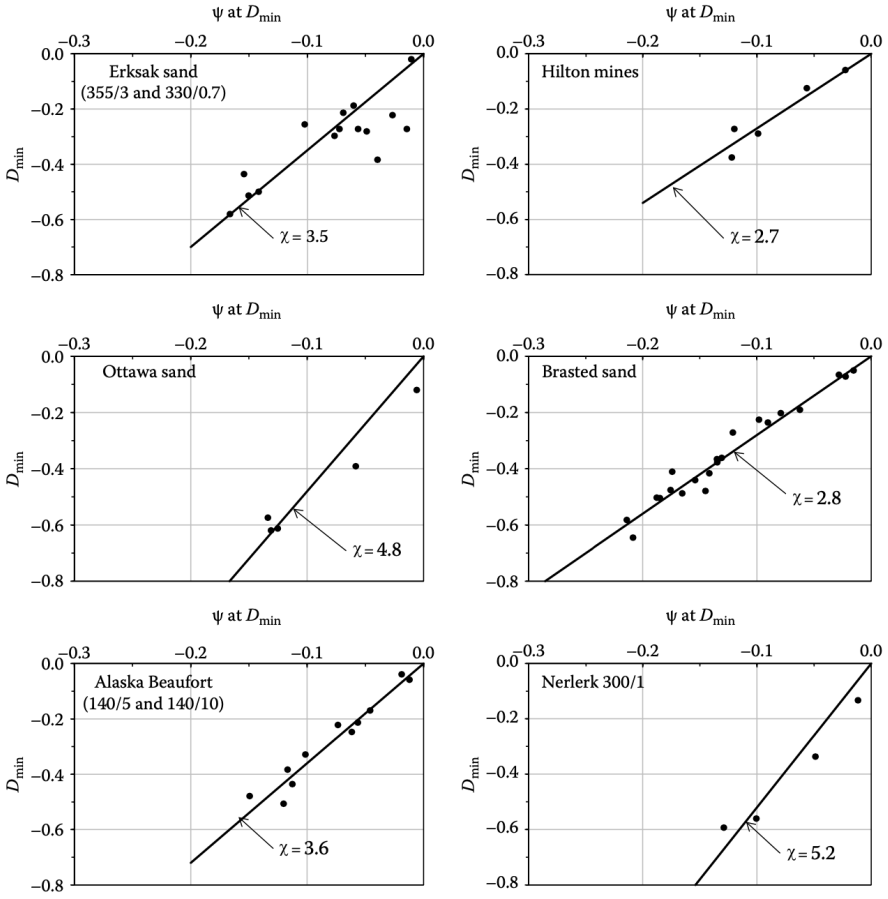

Figure 3.13: Derivation of χ for selected sands (χ is a material property relating maximum dilatancy to the state parameter for each sand). Taken from Been and M. Jefferies, 2015.

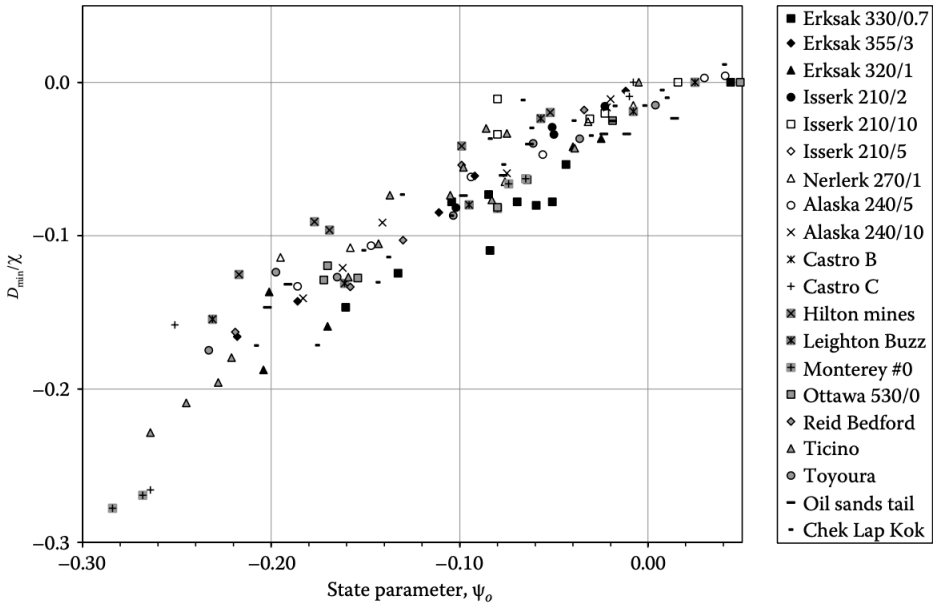

Figure 3.14: Maximum dilatancy D_{min}/χ of 20 soils in standard drained triaxial compression. Notice the improvement normalizing D_{min} by χ compared to figure 3.12. Taken from Been and M. Jefferies, 2015.

3.3.5 Stress-dilatancy

Analogous to state-dilatancy, so too can dilatancy be related to stress. The history and logic behind stress-dilatancy is given in C.3. Dense granular material exhibit a momentary 'image condition' (Figure 3.15), as in the image of the critical state, which indicates the change in volumetric strain rate from contraction to dilation. The stress-dilatancy relationship in NorSand is:

$$D^p = M_i - \eta \tag{3.40}$$

which is similar to the stress-dilatancy relationship in Cam-Clay (equation 3.28) but now with M_i, where subscript i denotes the current image condition (Figure 3.15). M_i is used in lieu of M_f (C.3), where Li and Dafalias (2000) suggested that the requirement becomes that M_i must approach M as the state parameter ψ goes to 0 - i.e., $M_i = f(\psi)$. It is easy to define the nature of M_i for dense soils ($\psi < 0$) as they display a peak strength that fits Nova's flowrule (Figure 3.17):

$$\eta_{max} = M_{tc} - (1 - N)D_{min} \tag{3.41}$$

where M is the friction ratio at critical state, and N the soil property that represents the volumetric coupling between the mean and distortional strains, and comes from Nova's flowrule at peak strength. In the OCC flowrule $N = 0$. An equally valid equation for peak strength is (i.e., simply equation 3.40 rewritten for peak strength):

$$\eta_{max} = M_i - D_{min} \tag{3.42}$$

Equivalencing equations 3.41 and 3.42 gives a more direct relationship between M_i and the state parameter:

$$M_i = M + ND_{min} = M + N(\chi\psi) \tag{3.43}$$

where D_{min} can be determined with equation 3.38.

Loose soil ($\psi > 0$) is more challenging to determine the nature of M_i as the limiting D_{min} in drained compression is at large strain as the soil gets to the critical state - there are no equivalent plots for loose soils as those produced with dense soils. Presently, two options are considered to tackle this issue (Figure 3.16):

- Modified Bishop, which links Bishop's (Skempton and Bishop, 1950 as cited by Been and M. Jefferies, 2015) observation on near constant friction in loose soils as they were sheared.
- Extended Dafalias, which makes equation 3.43 symmetric

Generally, the Extended Dafalias idealization is used to model loose sands. One reason is that peak strength develops at low strain in undrained conditions, and $M_i < M$ in order to achieve this.

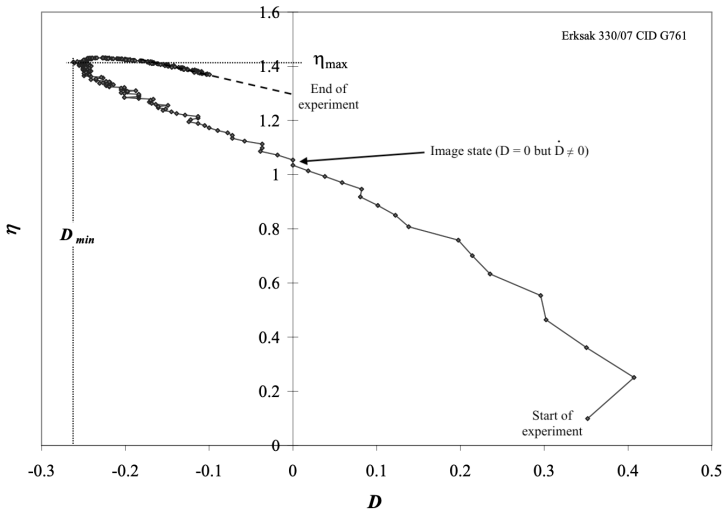

Figure 3.15: Plot of single drained triaxial test on dense Erksak sand reduced to stress-dilatancy form. Altered from Shuttle and M. Jefferies, 2010.

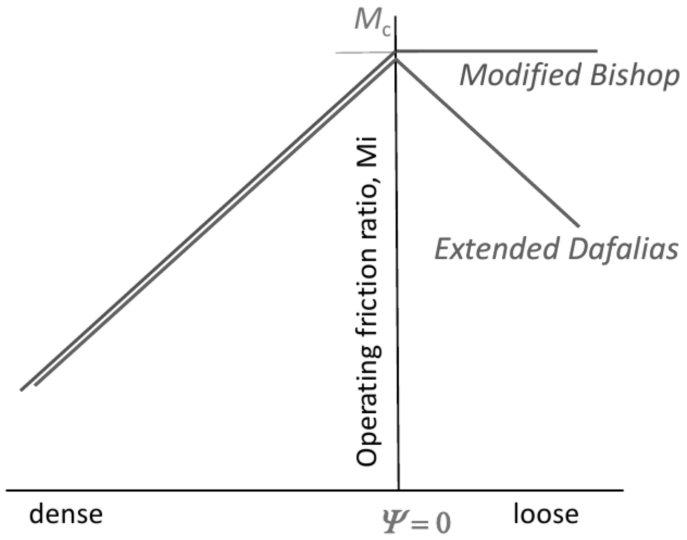

Figure 3.16: Formulation of friction ratio M_i according to Li and Dafalias, 2000 and Skempton and Bishop, 1950.

There is however an issue with defining the mobilized friction ratio as a function of ψ: during neutral loading, where the stress-state goes around the yield surface without any yielding (i.e., no plastic strains), the change in the mean stress will cause ψ to vary. But, a change in ψ means the soil is yielding, which contradicts the concept of neutral loading. To resolve this issue, the limiting dilation is defined in terms of ψ_i, which is the state parameter at the image condition. As a result, since there is only one image state per yield surface, ψ_i does not change during neutral loading and there is no unwanted yielding.

The next step is to define a new hardening limit as equation 3.38 cannot directly be used anymore. To ensure peak stress still occurs while using the calibration data, the following equivalency can be set up:

$$\chi_i \psi_i = \chi \psi \tag{3.44}$$

After some re-writing, the new hardening limit is found to be:

$$D_{min} = \chi_i \psi_i \tag{3.45}$$

with

$$\chi_i = \frac{\chi_{tc}}{(1 - \chi_{tc}\lambda / M_{tc})} \tag{3.46}$$

and

$$\psi_i = e - e_i = \psi + \lambda ln\left(\frac{p_i}{p}\right) \tag{3.47}$$

The relationship for M_i suggested by Jefferies and Shuttle, which is simply an expanded and more general version of equation 3.43, is given as:

$$M_i = M(\theta)\left(1 - \frac{N D^p_{min}}{M_{tc}}\right) = M(\theta)\left(1 - \frac{N \chi_i |\psi_i|}{M_{tc}}\right) \tag{3.48}$$

$M(\theta)$, previously written simply as M, is the general critical friction ratio and depends on the lode angle (expressed in radians):

$$M(\theta) = M_{tc} - \frac{M^2_{tc}}{3 + M_{tc}} cos\left(\frac{3\theta}{2} + \frac{\pi}{4}\right) \tag{3.49}$$

M_{tc} is the critical friction ratio at triaxial conditions, i.e., $M(\theta) = M_{tc}$ at $\theta = \frac{\pi}{6}$, and is used as a reference parameter. Soil property M_{tc} is generally found by doing multiple drained triaxial compression tests on sample of various densities. Each test is reduced to a value of peak measured dilatancy D_{min} at peak strength η_{max} (peak dilatancy should occur at the same point in the test as peak strength, see Figure 3.15). Fitting lines through the scatter and extrapolating, one can find η_{max} at $D_{min} = 0$, corresponding to the true critical state (Figure 3.17). In practice, elastic property data may not not be available. Hence, total strain (D instead of D^p) is used and reducing test data to η and D should give insight to soil behaviour.

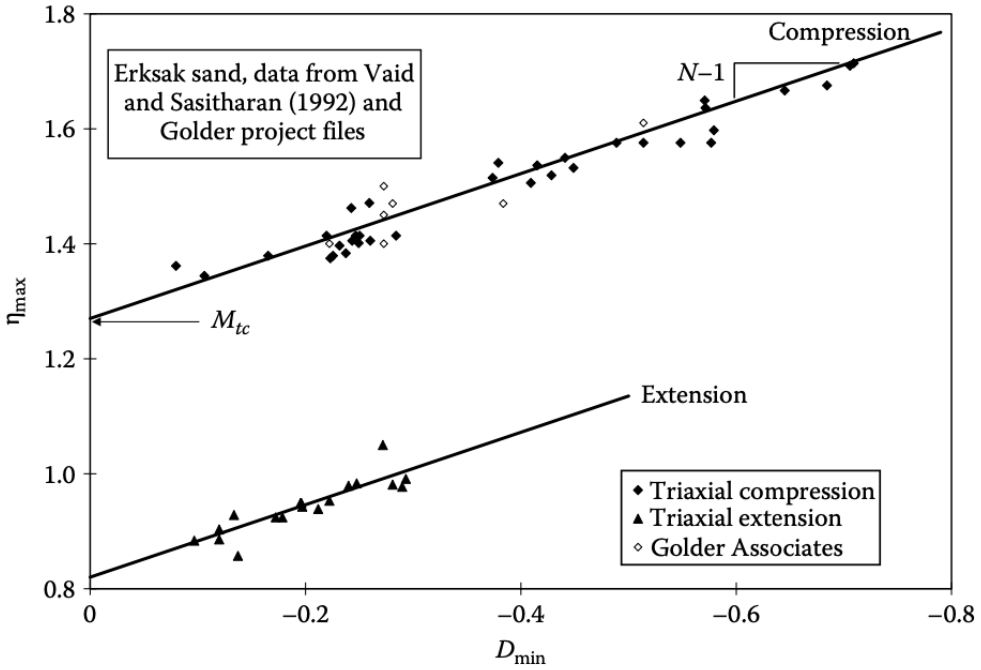

Figure 3.17: Experimental data for relation between peak strength and peak dilatancy for Erksak sand in triaxial compression and extension. Taken from Been and M. Jefferies, 2015.

3.3.6 Yield surface and Hardening

To quickly reiterate, NorSand adopts a Cam-Clay like stress-dilatancy relationship:

$$D^p = M_i - \eta \tag{3.50}$$

where M_i is the image stress ratio, which tends to critical state M with shear strain, and is equal to:

$$M_i = M(\theta)\left(1 - \frac{N\chi_i|\psi_i|}{M_{tc}}\right) \tag{3.51}$$

Determining the yield surface for NorSand follows the same route as done in Cam-Clay. Using the equation for a general yield surface:

$$\frac{\dot{p}}{p} + \frac{\dot{\eta}}{D^p + \eta} = 0 \tag{3.52}$$

and putting in the revised stress-dilatancy (equation 3.50) gives the NorSand yield surface:

$$f(q, p, p_i) = q - M_i\left[1 - ln\left(\frac{p}{p_i}\right)\right]p \tag{3.53}$$

Analogous to Cam-Clay, where the hardening parameter controlling the size of the yield surface is p_c, the hardening parameter in NorSand is p_i. A hardening law, which follow the Second Axiom, can be written as:

$$\dot{p}_i = \left[H\frac{p}{p_i}\left(\frac{M_i}{M_{tc}}\right)(p_{i,max} - p_i) - S_{soft}\right]\dot{\varepsilon}_q \tag{3.54}$$

where $p_{i,max}$, which is found by defining the yield surface at maximum dilation, is defined as:

$$p_{i,max} = p\ exp\left(-\frac{D^p_{min}}{M_{tc}}\right) = p\ exp\left(-\frac{\chi_i\psi_i}{M_{tc}}\right) \tag{3.55}$$

$p_{i,max}$ is not the true maximum but the maximum allowed p_i for that current state. It limits the evolution of p_i, and thus hardening, with respect to the current stresses in turn allowing to control dilatancy through normality. This hardening limit results in an internal cap to the yield surface (Figure 3.18). The hardening parameter H is a model soil property, and is a substitute for λ as it can no longer function as the plastic compliance since the yield surface and the CSL are decoupled. S_{soft} is the softening flag, which is defined as:

$$S_{soft} = S\omega \left(\frac{\eta}{M_i}\right)\left(\frac{K}{p}\right) D^p p_i \qquad \omega = 1 - \lambda\chi_{tc}/M_{tc} \tag{3.56}$$

The softening flag can be turned off ($S = 0$) for drained conditions and on ($S = 1$) for undrained conditions. At variance with drained loading, for which the evolution of p_i is governed by the smooth change enforced through the first-order hardening law, during undrained loading, the rate of change of p can easily become faster than the basic hardening law, thus leading to $p_i > p_{i,max}$. For this reason, a softening term S_{soft} is added to the hardening law resulting to a further decrease of the image stress p_i during undrained conditions to match the increased rate of change of p (Figure 3.19).

Yielding during unloading is another possible feature of NorSand, but is not implemented in PLAXIS as of yet. Even though no further time will be spent on this feature, it is still interesting to get a feeling of it and can therefore be read upon in Appendix C.4.

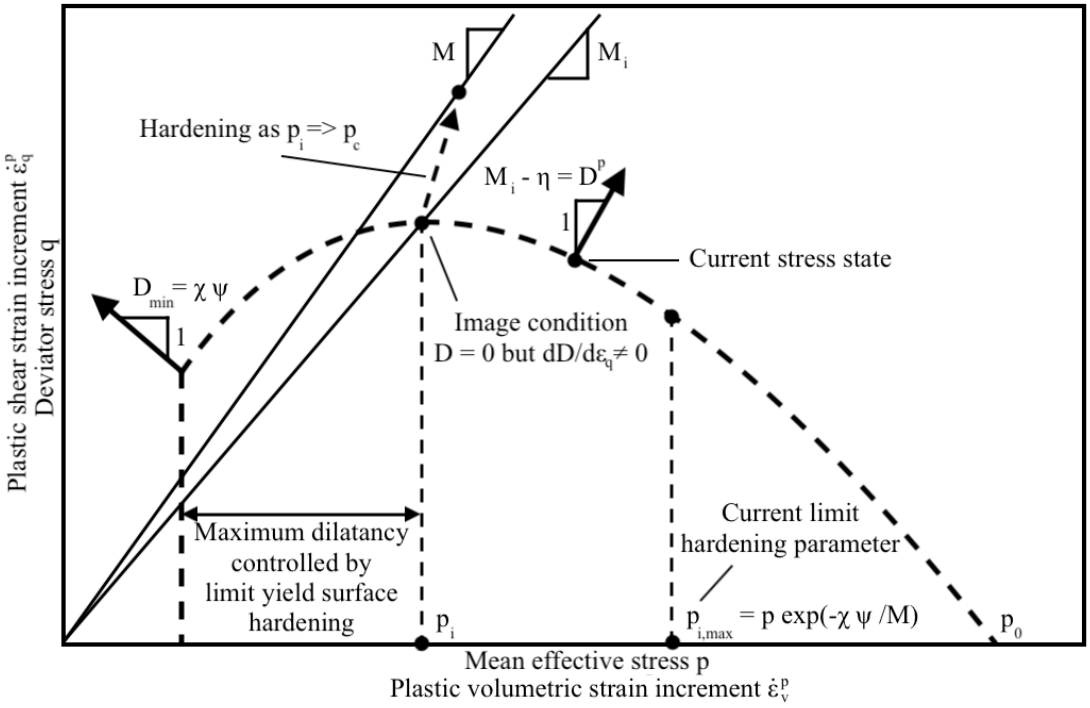

Figure 3.18: NorSand yield surface and internal cap due to limiting stress ratio η_L from the limit on hardening.

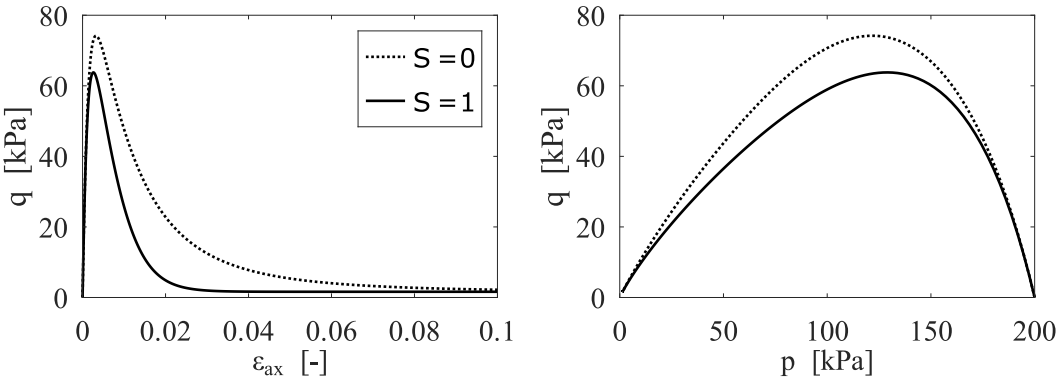

Figure 3.19: Effect of activating the softening flag ($S = 1$) on a loose soil in undrained triaxial conditions.

3.3.7 Elasticity

Even though real soil behaves cross-anisotropic, isotropic plasticity is adopted in NorSand on the grounds that it approached the behaviour adequately, requires few parameters, and it is difficult enough to determine those parameters. For now, anisotropy remains highly academic and theoretical, and is therefore not considered in this model. The dimensionless shear and bulk (equation 3.57) modulus are written as

$$I_r = \frac{G}{p} \qquad\qquad \frac{K}{p} = \frac{1+e}{\kappa} = I_r \frac{2(1+\nu)}{3(1-2\nu)} \tag{3.57}$$

where I_r is the shear rigidity, and the shear modulus G is called G_{max} in engineering practices, which is often measured during site investigation. Poisson's ratio ν is rarely measured but is generally taken in the range $0.15 < \nu < 0.25$ without testing.

3.3.8 Initial soil state measures

In order to create a starting point, NorSand requires three state measures:

- Geo-static stress state p_i^{NC}: It is assigned using a single value of K0, which is equivalent to assuming a "green field" level-ground site as the starting point for any boundary value problem. The geo-static stress-state gives initial values for p_0 and q_0, and thus η_0. These are then used to compute the normally consolidated yield surface image stress as (i.e., equation 3.53 rewritten at geo-static stress-state conditions):

$$p_i^{NC} = p_0 exp\left(\frac{\eta_0}{M_i} - 1\right) \tag{3.58}$$

- Initial over-consolidation $p_{i,o}$: Over-consolidation pushes the yield surface away from the current stress-state thus:

$$p_{i,o} = R p_i^{NC} \tag{3.59}$$

  where $R \geq 1$ is the input over-consolidation ratio. It is worth noting that what is reported as heavily over-consolidated (i.e., soils characterized by $R \geq\geq 1$) is actually more accurately viewed as a dense soil. Thus, if modelling heavily over-consolidated deposits, it is suggested to use a dense choice for ψ_0 combined with more modest estimate of R to determine the initial position of the yield surface.

- Initial state parameter ψ_0: The initial value of the state parameter is assigned using a single value for each stratum. However, it is found that common depositional conditions for the soil produces the same soil state parameter despite the natural changes in gradation - in essence, both void ratio and the CSL change together. This shows up in CPT soundings which profiles commonly show near constant values of ψ within identifiable strata. For this reason, ψ becomes the basic input for boundary value problems using CSSM. The assigned psi_0 should be "characteristic" in the sense of the structural eurocode EN1997 (Marinelli, 2020).

3.3.9 Formulation summary

This section quickly recaps basic theory and NorSand. This report focuses on static liquefaction, which occurs when the effective stress becomes 0. To predict when liquefaction occurs, constitutive models are needed. Constitutive models are models which simulate and predict soil behaviour. In order to generalize models as much as possible, stress (σ'_q and σ'_m) and strain ($\dot{\varepsilon}_q$ and $\dot{\varepsilon}_v$) invariants are used, with a compression positive notation. These can be converted into triaxial invariants (q and p') as soil properties can be found using solely triaxial tests. Even though they are found using triaxial tests, they act as a reference point for all other stress combinations.

Soils exist within a whole spectrum of densities (or void ratio e), but have a unique CSL (First Axiom), which is the ultimate state the soil will reach when sheared indefinitely (Second Axiom).

$$e_c = \Gamma - \lambda ln(\sigma'_{m,c}) \tag{3.60}$$

Upon shearing, soils with a negative state parameter dilate whereas soils with a positive state parameter contract (i.e., do not dilate). In short, soil behaviour can be expressed in terms of dilatancy (dense) or lack of dilatancy (loose).

$$\psi = e - e_c \tag{3.61}$$

Dilatancy (equation 3.62) depends on state (state-dilatancy) and stress (stress-dilatancy).

$$D^p = \frac{\dot{\varepsilon}_v}{\dot{\varepsilon}_q} \tag{3.62}$$

State-dilatancy in NorSand is found to have the relationship:

$$D^p_{min} = \chi_i \psi_i \tag{3.63}$$

where D^p_{min} is the maximum dilatancy (which occurs at η_{max}) found in dense soils, χ_i is a material property and ψ_i is the image state parameter. Material property χ_i relates maximum dilatancy to the image state parameter for each sand. It is defined by χ_{tc}, which is found under drained triaxial conditions:

$$\chi_i = \frac{\chi_{tc}}{(1 - \chi_{tc}\lambda/M_{tc})} \tag{3.64}$$

The image state parameter ψ_i, which defined at the image critical state (figure **??**) and is unique for each yield surface, can be determined with:

$$\psi_i = e - e_i = \psi + \lambda ln\left(\frac{\sigma'_{m,i}}{\sigma'_m}\right) \tag{3.65}$$

Stress-dilatancy in NorSand has the relationship in the form:

$$D^p = M_i - \eta \tag{3.66}$$

where D^p is the plastic dilatancy, M_i is the image critical friction ratio and $\eta = \frac{\bar{\sigma}_q}{\bar{\sigma}_m}$ is the stress ratio. It is found that the critical friction ratio mobilizes, and evolves until reaching the final

critical friction ratio M. This mobilized critical friction ratio M_i is anchored to the image state and is defined as:

$$M_i = M(\theta)\left(1 - \frac{ND^p_{min}}{M_{tc}}\right) = M(\theta)\left(1 - \frac{N\chi_i|\psi_i|}{M_{tc}}\right) \tag{3.67}$$

The general critical friction ratio $M(\theta)$ can be defined, using the critical friction ratio found in triaxial tests M_{tc}, as:

$$M(\theta) = M_{tc} - \frac{M^2_{tc}}{3 + M_{tc}} cos\left(\frac{3\theta}{2} + \frac{\pi}{4}\right) \tag{3.68}$$

The yield surface in NorSand (Figure 3.18) is defined by:

$$f(\sigma'_q, \sigma'_m, \sigma'_{m,i,max}) = \sigma'_q - M_i\left[1 - ln\left(\frac{\sigma'_m}{\sigma'_{m,i}}\right)\right]\sigma'_m \tag{3.69}$$

Its internal cap is defined as:

$$\sigma'_{m,i,max} = \sigma'_m exp\left(-\frac{D^p_{min}}{M_{tc}}\right) = \sigma'_m exp\left(-\frac{\chi_i\psi_i}{M_{tc}}\right) \tag{3.70}$$

where $\sigma'_{m,i,max}$ is the maximum allowed $\sigma'_{m,i}$ for that current state. Hardening of the yield surface depends on he difference between the hardening parameter $\sigma'_{m,i}$, which is also anchored to the image state, and $\sigma'_{m,i,max}$, and is defined as:

$$\dot{\sigma}'_{m,i} = H\left[\sigma'_{m,i,max} - \sigma'_{m,i} - S_{soft}\right]\dot{\varepsilon}_q \tag{3.71}$$

Elasticty in NorSand is captured with the shear rigidity I_r and ν as these can be used to determine the bulk modulus as well:

$$I_r = \frac{G}{\sigma'_m} \tag{3.72}$$

4 Parametric and Stress-path Analysis

NorSand has been implemented into PLAXIS, which is a geotechnical analysis software capable of performing advanced finite element or limit equilibrium analysis of soil and rock deformation and stability, as well as soil structure interaction and groundwater and heat flow.

Before applying NorSand to research real-life case studies, its numerical behaviour must be determined, which in this report is done in the Soil Test facility of PLAXIS by means of single stress point analysis. First, a parametric analysis is done to determine the influence of each parameter. Lastly, the stress-path responses are determined for different sand states and boundary conditions.

4.1 Model parameters

This section quickly recaps the parameters that exist within NorSand:

- G_{ref}: Reference value of the shear modulus at the reference pressure.
- p_{ref}: Reference mean pressure (generally the common value of 100 kPa is used).
- n_G: Exponent of the power-law elasticity.
- ν: Poisson's ratio.
- M_{tc}: Friction ratio at critical state in triaxial conditions.
- N: Material parameter controlling the maximum stress ratio as a function of the minimum dilatancy.
- χ_{tc}: Material parameter which governs the inclination of the minimum dilatancy as a function of the state parameter.
- H_0 & H_ψ: Hardening parameters.
- R: Over-consolidation ratio.
- S: Softening flag.
- ψ_0: Initial value of the state parameter.

Elastic properties used in NS are G_{ref}, n_G and ν (equation 4.1). NS anchors elasticity to $G_{ref} \equiv G_{100}$, which is the value of the mean effective stress at the reference pressure p_{ref} equal to 100 kPa (a widespread convention), combined with an exponent n_G for a power-law trend, thus introducing the stress-dependency on this modulus. Commonly, Poisson's ratio ν is not measured and 0.2 is adopted as "not unreasonable" based on the extensive testing of Ticino sand.

$$G = G_{ref} \left(\frac{p}{p_{ref}} \right)^{n_G} \tag{4.1}$$

During undrained loading the rate of change of p can easily become faster than the basic hardening law, thus leading to $p_i > p_{i,max}$ (contrary to the basic principle of the hardening limit). For this reason, a softening term S_{soft} is added to the hardening law resulting to a further decrease of the image stress p_i during undrained conditions (i.e., for drained loading $S_{soft} \equiv 0$). In other words, it decreases (softens) the peak stress.

Plastic hardening parameter H. Plastic hardening modulus is the only NS-specific property as it relates only to the NS hardening law. There is an element of softening associated with increasing η, and better fits are obtained to test data if that is recognized. Thus, $H = H_0 - H_\psi \psi$ is used for the hardening modulus. Both H_0 and H_ψ are determined by optimization a set of drained triaxial tests which include loose and dense states. Where using only H_0 makes H a static parameter, using H_ψ adds a dependence on the evolving ψ and makes H dynamic.

4.2 Parametric analysis

The first step of the numerical behaviour is to systematically determine the effects of the model parameters on the computed behaviour.

4.2.1 Analysis results

Each model parameter is changed over a large enough range to clearly see an effect, but within the domain of realistic values for sands in general. Tables from different sources (Been and M. Jefferies, 2015, Ghafghazi, 2011, Marinelli, 2020, and Shuttle and M. Jefferies, 2010) are used as a reference to establish this domain. The baseline parameters are given in Table 4.1 and do not represent any sand in particular.

Table 4.1: Baseline parameters for parametric analysis

G_{ref}/p_{ref}	p_{ref} [kPa]	n_G	ν	Γ	λ_e	M_{tc}	N	χ_{tc}	H_0	H_ψ	R	S	ψ_0	p_0
350	100	0.5	0.2	1	0.03	1.2	0.35	4	300	0	1	0	-0.15/0.15	200

The analysis is done in triaxial compression for each parameter in undrained (TXU) and drained conditions (TXD), for dense and loose sand, from an initial consolidation pressure of $p_0 = 200$ kPa. The range for each parameter is tabulated as well (table 4.2).

Table 4.2: Parametric analysis

I_r ($p_{ref} = 100$)	M_{tc}	N	χ_{tc}	H_0	H_ψ
35, 350, 3500	1.1, 1.2, 1.3	0.25, 0.35, 0.45	3, 4, 5	100, 300, 500	0, 1000, 3000

Shear rigidity I_r

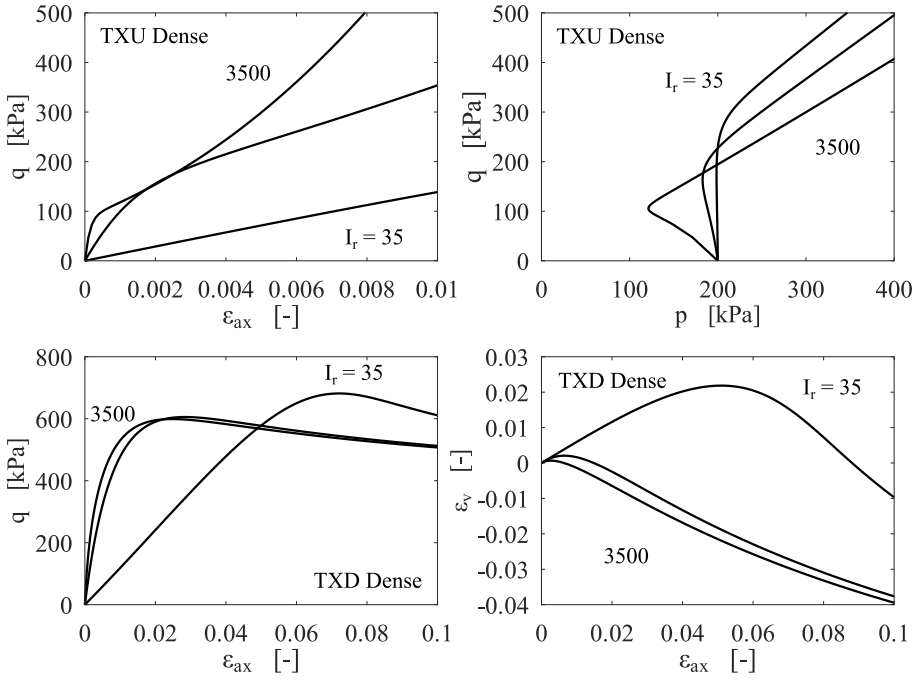

Figure 4.1: Parametric analysis of shear rigidity I_r on dense soil for the values I_r = [35, 350, 3500].

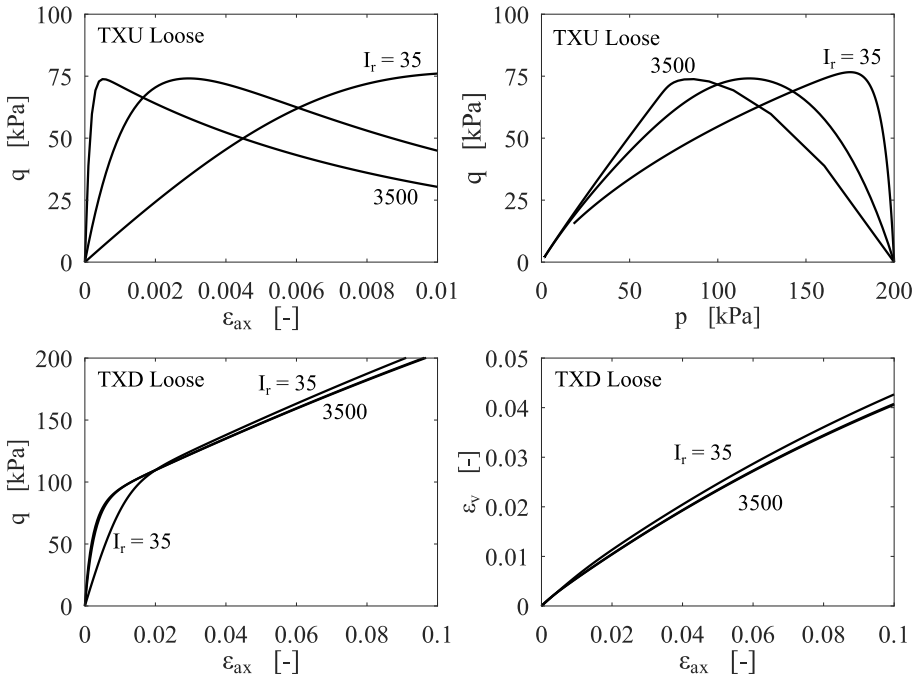

Figure 4.2: Parametric analysis of shear rigidity I_r on loose soil for the values I_r = [35, 350, 3500].

Critical friction ratio M_{tc}

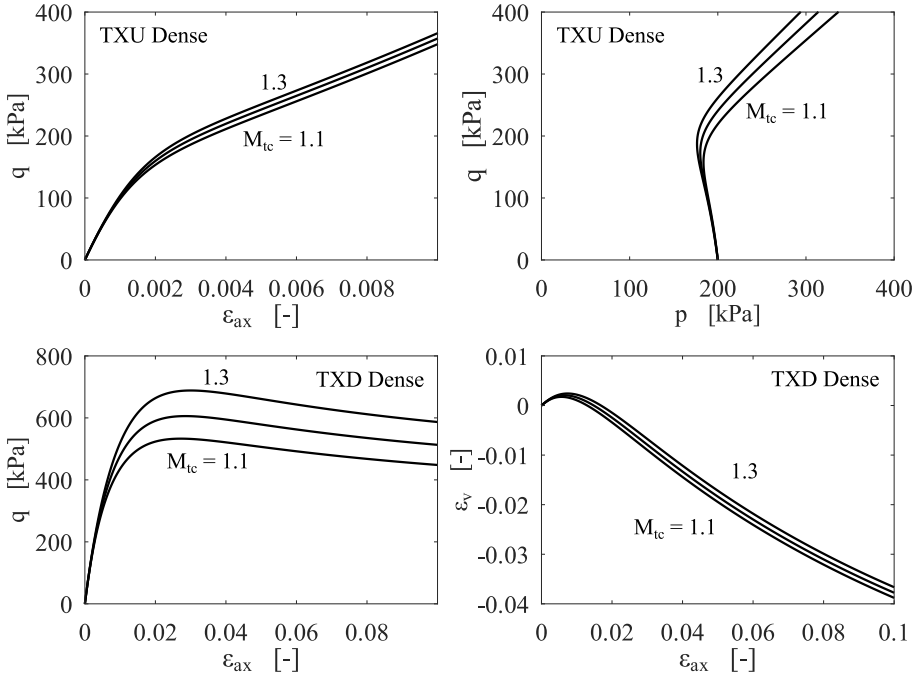

Figure 4.3: Parametric analysis of critical friction ratio M_{tc} on dense soil for the values M_{tc} = [1.1, 1.2, 1.3].

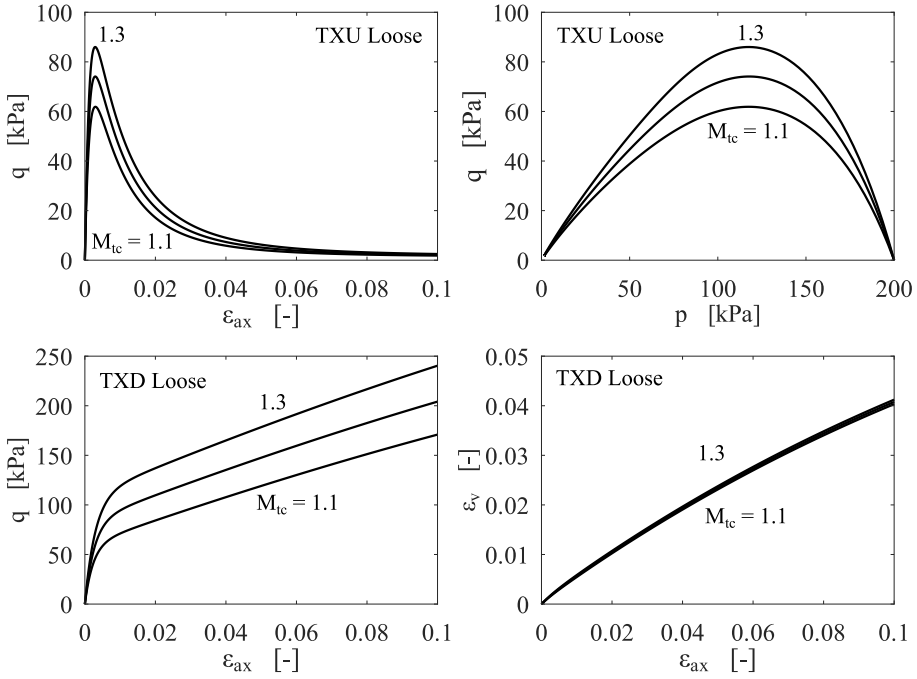

Figure 4.4: Parametric analysis of critical friction ratio M_{tc} on loose soil for the values M_{tc} = [1.1, 1.2, 1.3].

Volumetric coupling coefficient N

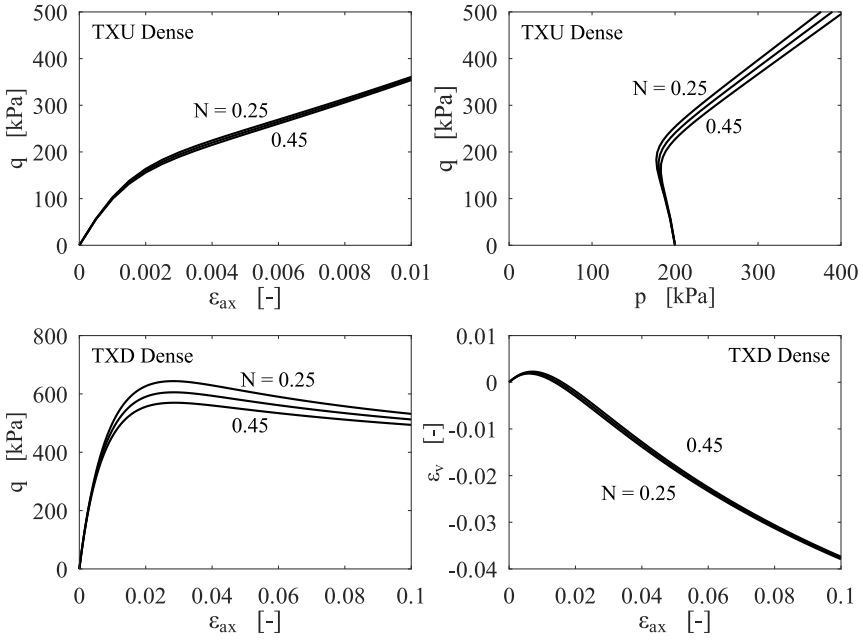

Figure 4.5: Parametric analysis of the volumetric coupling parameter N on dense soil for the values N = [0.25, 0.35, 0.45].

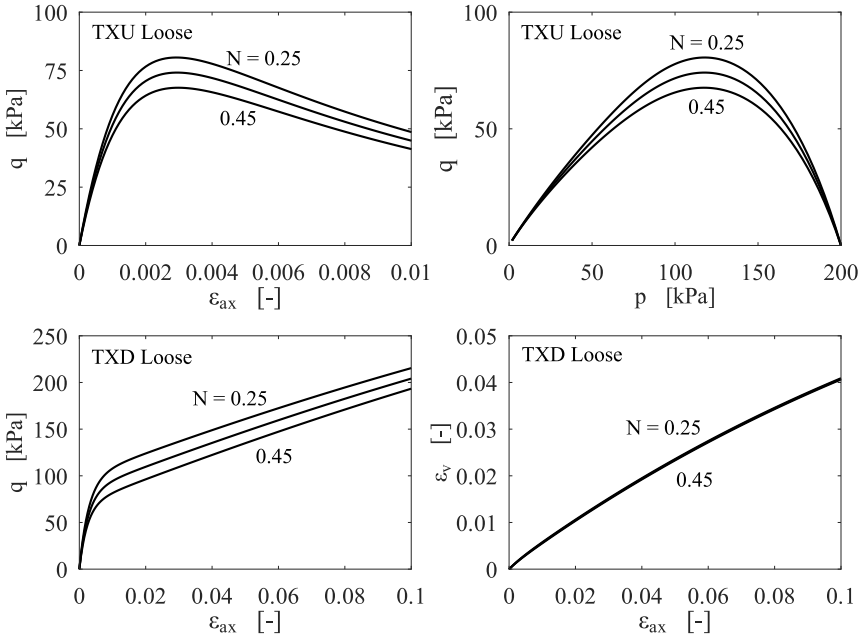

Figure 4.6: Parametric analysis of the volumetric coupling parameter N on loose soil for the values N = [0.25, 0.35, 0.45].

Soil property χ_{tc}

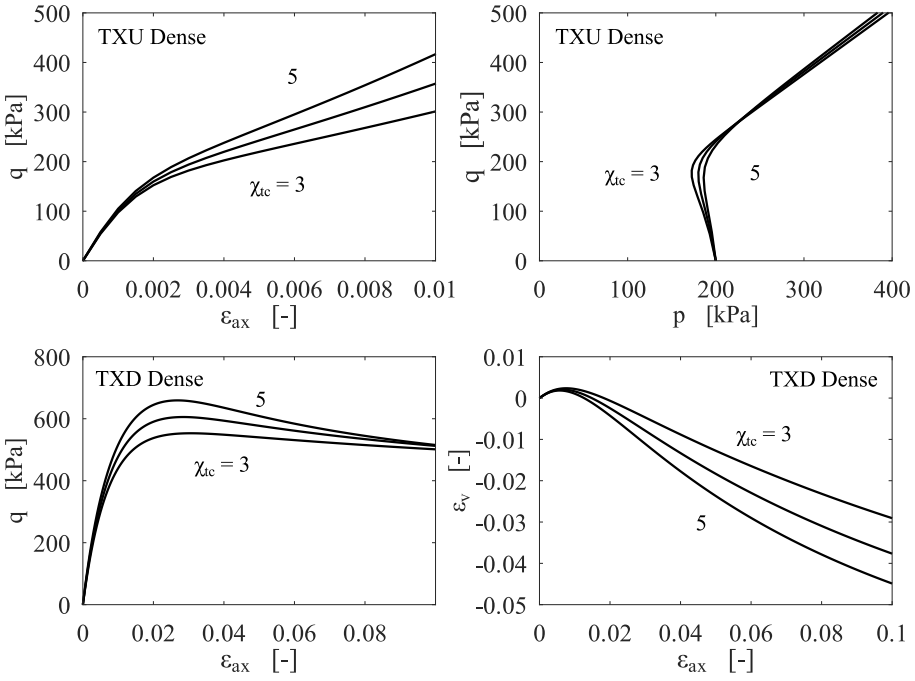

Figure 4.7: Parametric analysis of χ_{tc} on dense soil for the values $\chi_{tc} = [3, 4, 5]$.

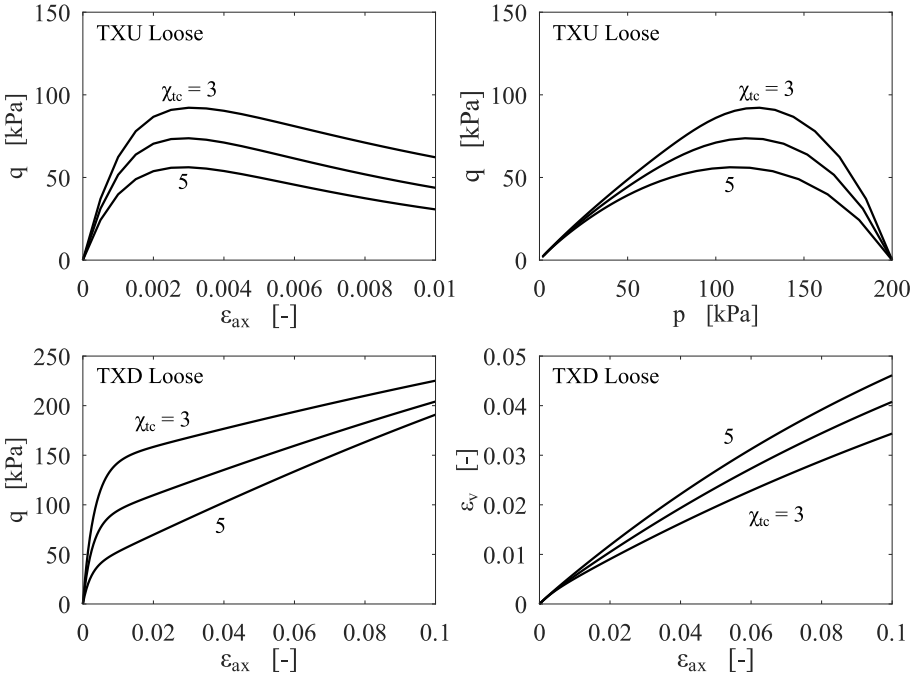

Figure 4.8: Parametric analysis of χ_{tc} on loose soil for the values $\chi_{tc} = [3, 4, 5]$.

Hardening parameter H_0

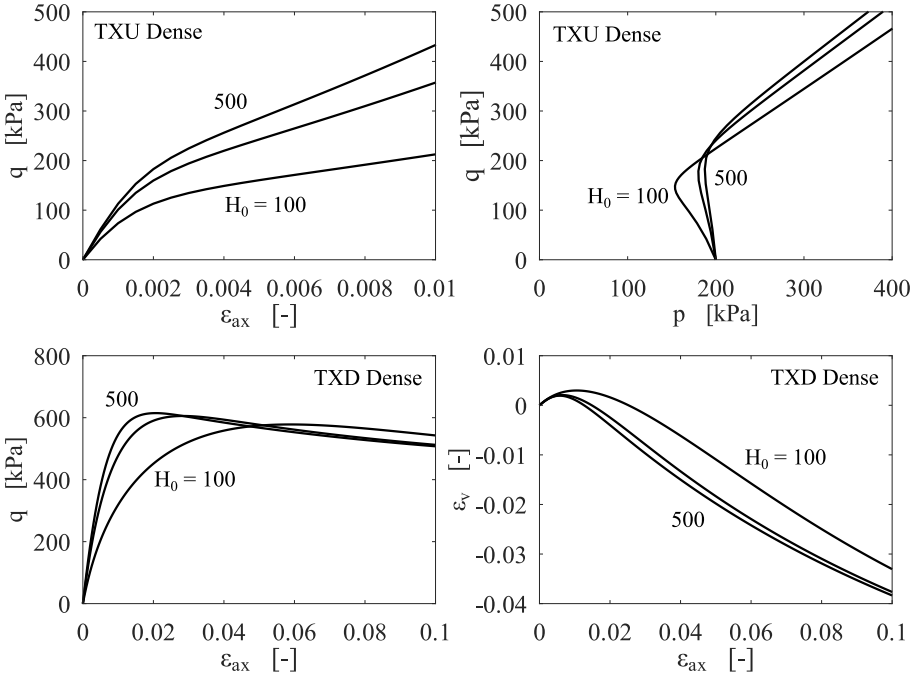

Figure 4.9: Parametric analysis of the hardening parameter H_0 on dense soil for the values H_0 = [100, 300, 500].

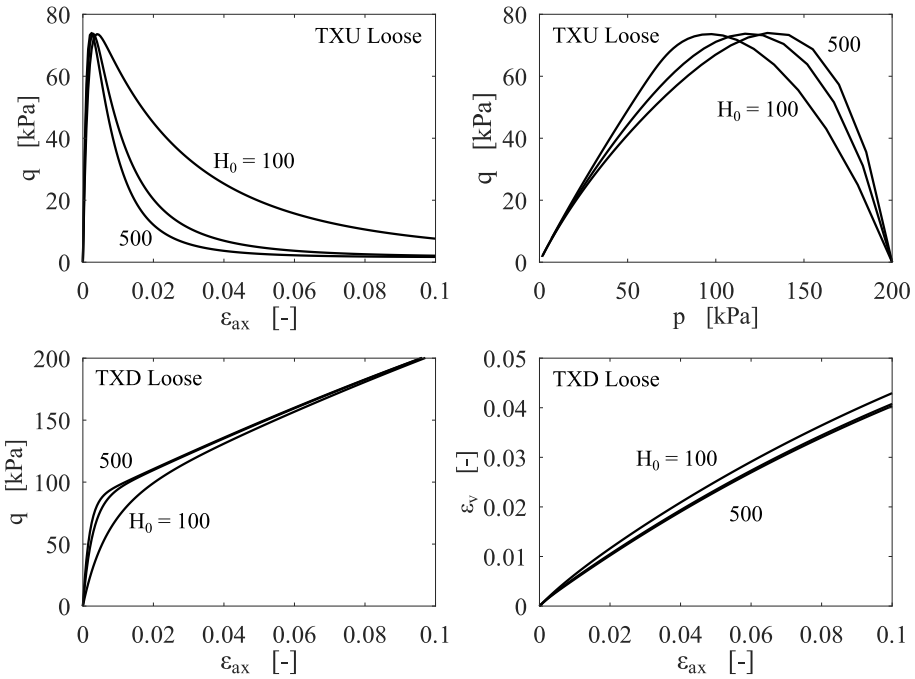

Figure 4.10: Parametric analysis of the hardening parameter H_0 on loose soil for the values H_0 = [100, 300, 500].

Hardening parameter H_ψ

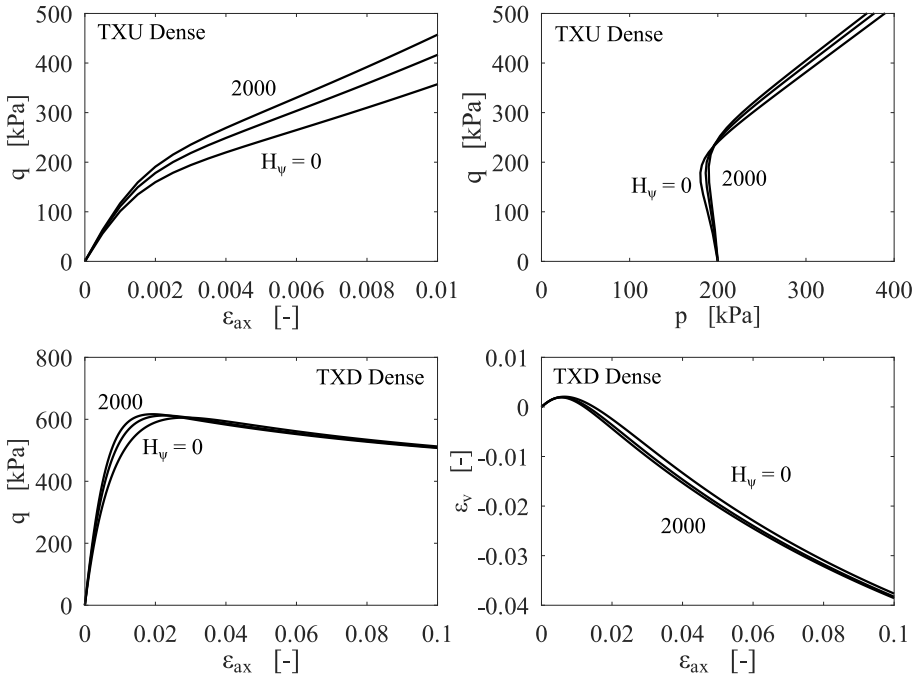

Figure 4.11: Parametric analysis of the hardening parameter H_ψ on dense soil for the values H_ψ = [0, 1000, 2000].

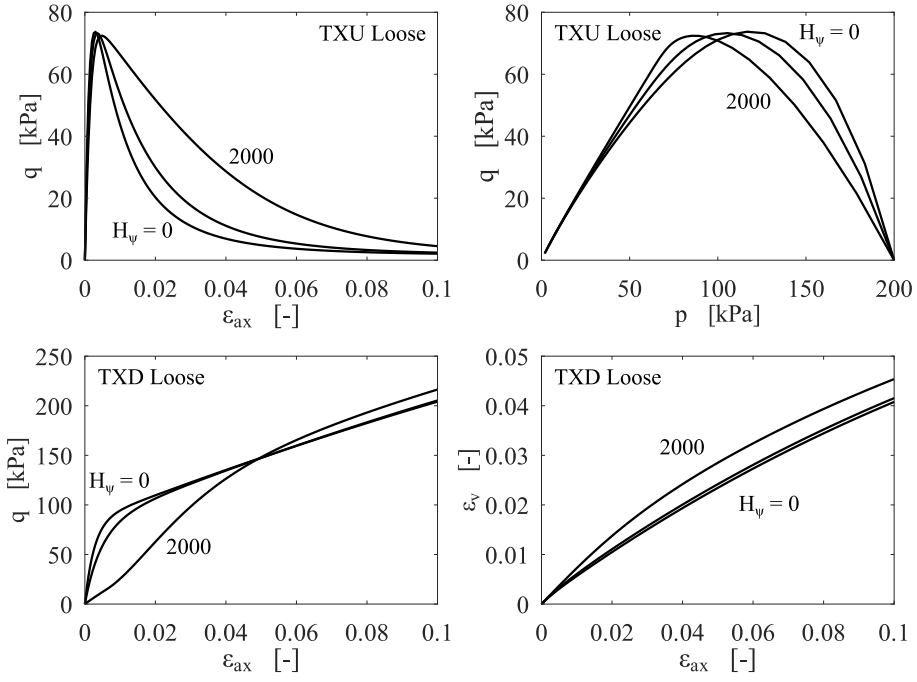

Figure 4.12: Parametric analysis of the hardening parameter H_ψ on loose soil for the values H_ψ = [0, 1000, 2000].

4.2.2 Discussion: Parametric analysis

The influence of the shear rigidity on dense undrained sand (Figure 4.1) shows that the stiffer the sand (i.e., the higher I_r) the quicker it tends to maximum dilation resulting in very strong negative pore pressures, i.e., high increase of mean effective stress and a higher peak strength. The upper left sub-figure shows a distorted picture: in reality the graph for $I_r = 3500$ goes way up for the same axial strain as the others. The current range for the figure is chosen such that clearly illustrates the initial behaviour. To sum up, increasing I_r in dense sands in undrained conditions increases the peak strength. For drained conditions there seems to be a threshold where increasing I_r does not really affect the behaviour anymore. A more comprehensive analysis is needed to find that threshold.

In loose sands, the effect of increasing I_r is clear: it accelerates the process of reaching the CSL and liquefaction, seen in the top left sub-figure of Figure 4.2. Alternatively, it offsets reaching the peak strength, shown in the top right sub-figure in Figure 4.2. Changing I_r in drained conditions has no effect on loose sands.

Changing the critical friction ratio has very little effect on the volumetric strain. However, increasing M_{tc} has the expected effect of increasing the peak strength in both drained dense and undrained loose tests (equation 4.2). Since soil has a tendency to follow roughly the same trajectory during loading (e.g., seen in Figure 3.15), increasing M_{tc} results in increasing the peak strength at essentially same maximum dilatancy (since D_{min} is mostly unaffected as χ_{tc} remains unchanged).

$$\eta_{max} = M_{tc} - (1 - N)D_{min} \tag{4.2}$$

The biggest effect of increasing the volumetric coupling coefficient N is seen when looking at the change in peak strength: increasing the volumetric coupling coefficient N decreases the peak strength in both undrained and drained conditions, in both dense and loose sands.

Increasing χ_{tc}, which means a larger minimum dilatancy for the same state parameter value (equation 4.3), shows that it increases the peak strength in drained dense sands but has the opposite effect in loose sands in undrained conditions, i.e., it decreases the peak strength.

$$D_{min} = \chi_{tc}\psi \tag{4.3}$$

Increasing H_0, which increases H as well (equation 4.5), results in quicker hardening (equation 4.4) and therefore its peak strength is reached faster. In undrained condition for dense sands, this results in a stronger increase in mean effective stress p. Dense sands in drained conditions only see a sharper rise to peak strength. Loose sands do not see a decrease in peak strength, but a quicker path to liquefaction when H_0 is increased. This is illustrated by a softer curve in the top right sub-figure in Figure 4.10.

$$\dot{p_i} = \left[H \frac{p}{p_i} \left(\frac{M_i}{M_{tc}} \right) (p_{i,max} - p_i) - S_{soft} \right] \dot{\varepsilon}_q \tag{4.4}$$

$$H = H_0 - H_\psi * \psi \tag{4.5}$$

The hardening parameters H_0 and H_ψ shows similar effects when changed. This makes sense when looking at the equation for the hardening modulus H. Caution is needed, however, as increasing H_ψ for dense sands has the same effect as increasing H_0. Because as the state parameter is negative, it cancels out the negative signs in equation 4.5. But in loose sands, increasing H_{psi} has the opposite effect as H_0.

4.3 Stress-path response

Different stress evolutions are described in this section. The first sub-section illustrates the behaviour of dense and loose sand in drained and undrained conditions. The second describes the effects of the softening flag on the stress-path on loose undrained soil.

4.3.1 Stress-path response: general soil conditions

The stress-path response shown in Figures 4.13 to 4.16 illustrate the constitutive behaviour of the NorSand model more clearly for dense and loose sand in drained and undrained conditions. The input parameters are the same as the baseline values used in the previous section, but are re-tabulated in Table 4.3. An initial isotropic consolidation pressure $p_0 = 200$ kPa is used for all stress-path responses. These figures show: the stress path and the corresponding yield surface in combination with the hardening variables (i.e., the image stress p_i and its maximum value $p_{i,max}$ at that state), thus showing their evolution during the loading path in sub-figures a; the evolution of the shear stress and the dilatancy in sub-figures b; the difference between $p_{i,max}$ and p_i, which characterizes the incremental hardening (equations 3.70 and 3.71), in sub-figures c; and the road to critical state, depicted by ψ and ψ_i tending to zero, in sub-figures d.

Table 4.3: Baseline parameters for stress path response

G_{ref}/p_{ref}	p_{ref} [kPa]	n_G	ν	Γ	λ_e	M_{tc}	N	χ_{tc}	H_0	H_ψ	R	S	ψ_0
350	100	0.5	0.2	1	0.03	1.2	0.35	4	300	0	1	0	-0.15 or 0.15

Recalling the hardening rule helps to explain the evolution of stress paths:

$$\dot{p}_i = \left[H \frac{p}{p_i} \left(\frac{M_i}{M_{tc}} \right) (p_{i,max} - p_i) - S_{soft} \right] \dot{\varepsilon}_q \tag{4.6}$$

where

$$p_{i,max} = exp\left(-\frac{D^p_{min}}{M_{tc}} \right) = exp\left(-\frac{\chi_i \psi_i}{M_{tc}} \right) \tag{4.7}$$

The evolution of the drained dense test (Figure 4.13) stops before the soil reaches critical state, which is indicated by the circle labeled q_{cs}. This figure clearly shows how hardening stops, and peak strength is reached, when $p_i = p_{i,max}$. However, since $\psi_i \neq 0$, a difference occurs again between p_i and $p_{i,max}$ after further shearing (subplot d). Consequently, the soil then undergoes softening as the difference $p_{i,max} - p_i$ turns negative (note that this difference is indeed small). Subplot b also illustrates how the soil contracts ($D^p > 0$) during the first part of shearing, and then quickly turns into dilation ($D^p < 0$), with the peak of that graph indicating maximum dilation. Additionally, it can be seen how dilation occurs while the soil hardens.

Figure 4.14 illustrates how the undrained dense soil has a tendency to harden indefinitely as the difference between p_i and $p_{i,max}$ is kept from reaching 0 (see subplot c). In other words, the soil keeps increasing in strength as long as it is sheared in undrained conditions and will not reach critical state.

Drained loading of a loose soil (Figure 4.13) is fairly straight-forward. What is interesting, however, is the quick increase in size of the yield surface during first few steps of axial deformation - this is where the difference between $p_{i,max}$ and p_i is relatively large. At the same time, one can observe from subplot b that contraction starts off at a high rate, but quickly slows down. After the difference turns really small, but not 0 (subplot c), hardening occurs at a slower pace and continues until critical state is reached.

Undrained loading of loose soil might have the most complicated evolution. The biggest difference compared to the other stress-paths is how quickly difference between p_i and $p_{i,max}$ turns negative, meaning $p_i > p_{i,max}$. This indicates that, after the mean stress decreases due to pore pressure increase, softening occurs very quickly. Note that softening, which in this case is not true softening behaviour, which is where soil degradation occurs, but a softening 'trick' enforced by NorSand to simulate the undrained behaviour where the pore pressure increases.

Model response of dense soils

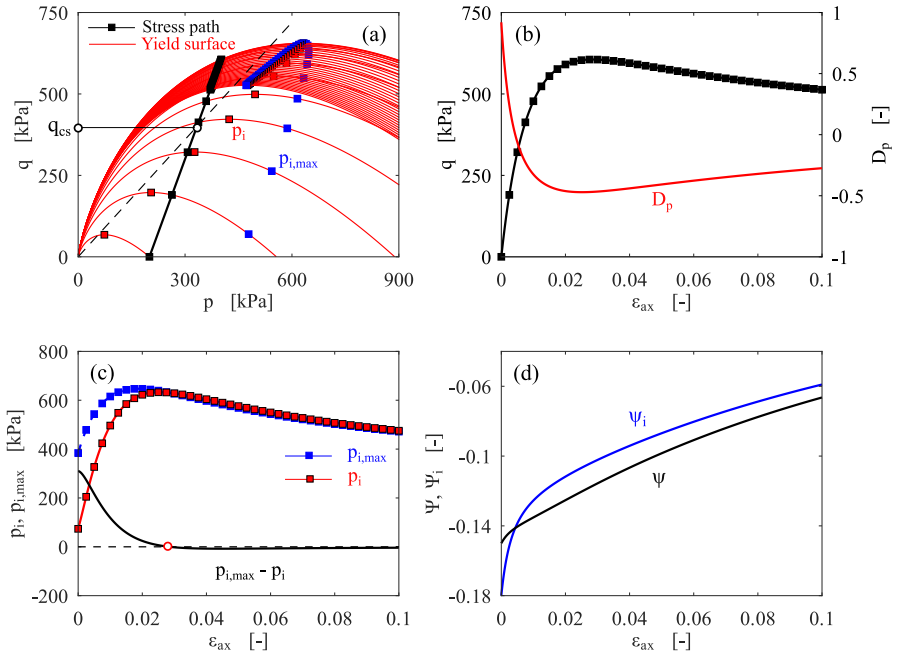

Figure 4.13: Model response during a drained triaxial test on a dense sand ($\psi_0 = -0.15$) with the input parameters given in Table 4.3.

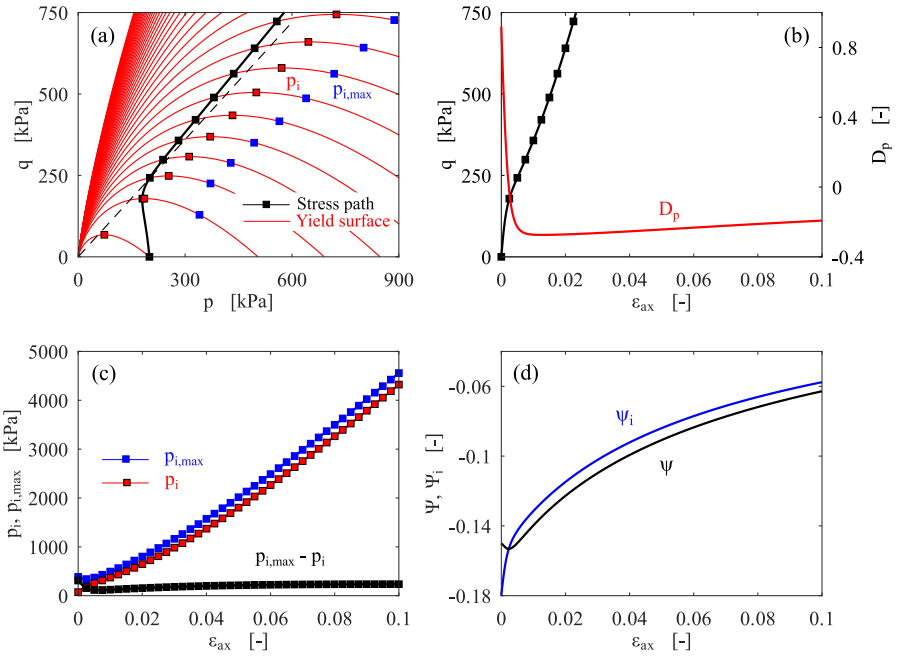

Figure 4.14: Model response during an undrained triaxial test on a dense sand ($\psi_0 = -0.15$) with the input parameters given in Table 4.3.

Model response of loose soils

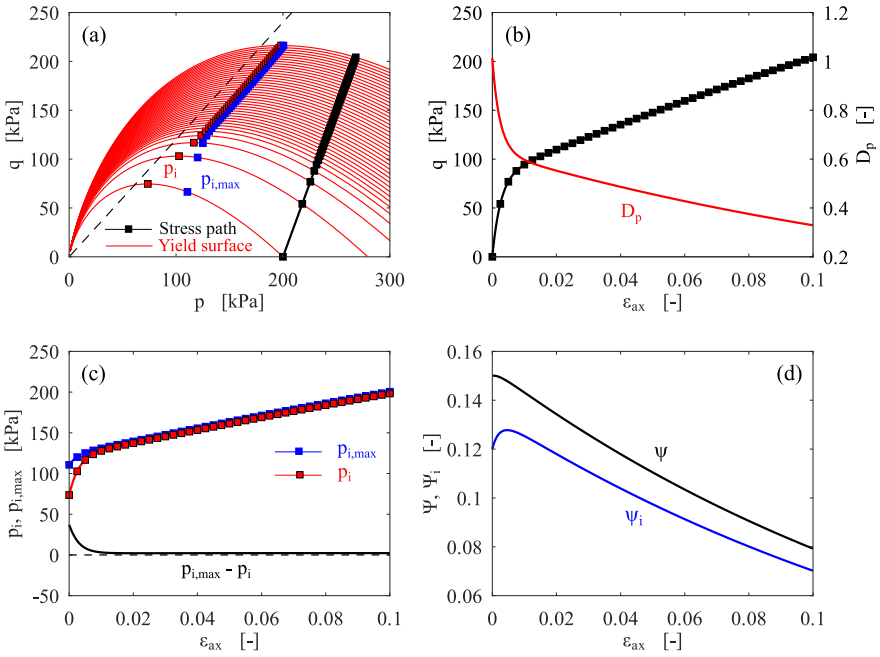

Figure 4.15: Model response during a drained triaxial test on a loose sand ($\psi_0 = 0.15$) with the input parameters given in Table 4.3.

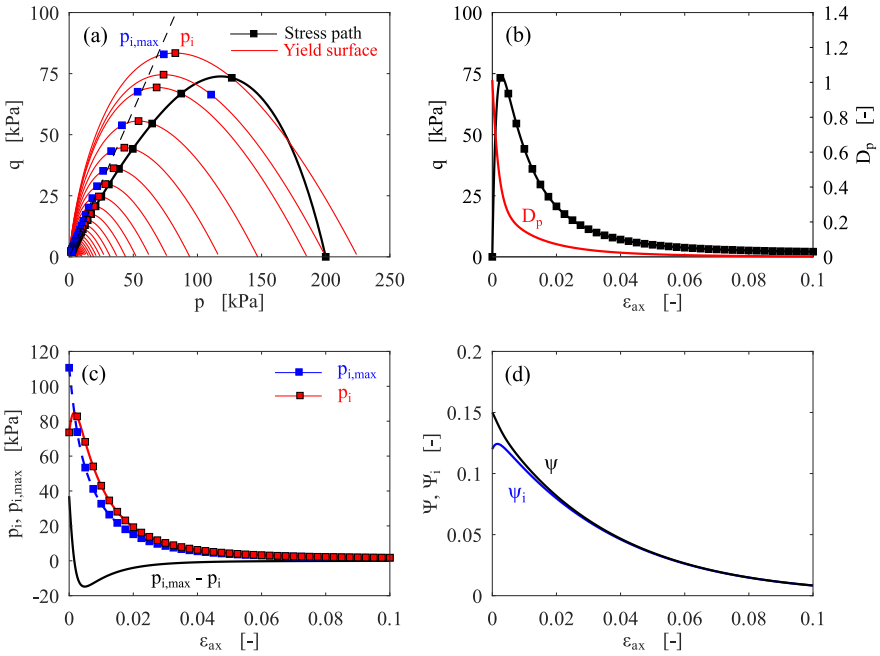

Figure 4.16: Model response during an undrained triaxial test on a loose sand ($\psi_0 = 0.15$) with the input parameters given in Table 4.3.

4.3.2 Stress-path response: softening flag

This section covers three elements: the difference in the behaviour of loose soil in undrained conditions when the softening flag is deactivated or activated; the re-hardening behaviour loose soil in undrained behaviour can exhibit; and the effect of increasing the consolidation pressure. In order to clearly show the to-be-described behaviour in this section, different parameters must be used:

Table 4.4: Parameters for stress path response

G_{ref}/p_{ref}	p_{ref}	n_G	ν	Γ	λ_e	M_{tc}	N	χ_{tc}	H_0	H_ψ	R	S	ψ_0	p_0
300	100	1.0	0.15	0.875	0.03	1.27	0.35	4	100	0	1	0/1	0.03	100/500

The figures in this section show: the yield-surfaces at select points, such as the beginning and the end of the test, and their related hardening variables in sub-figures a; the evolution of the shear stress and the dilatancy in sub-figures b; the stress path in the non-logarithmic compression plane with the aforementioned hardening variables in sub-figures c; and the difference between $p_{i,max}$ and p_i, which characterizes the incremental hardening, in sub-figures d.

The evolution of the undrained loose test where the softening flag is turned off, illustrated in Figure 4.17 ($\psi_0 = 0.03$), shows similar behaviour as seen in Figure 4.16 ($\psi_0 = 0.15$). The difference, however, is that the effect of softening is much stronger in Figure 4.16 than seen in Figure 4.17 due to looser state of the former resulting in a stronger reaction to undrained shearing.

Activating the softening flag gives interesting results (Figure 4.18). One must not forget that the point at which the soil arrives at critical state does not change when the softening flag is activated. The first effect of $S = 1$ is that the peak strength is reduced. This is attributed to larger decrease of p_i due to S_{soft} - in other words $\dot{p_i}$ becomes more negative resulting in earlier softening.

The next part of the evolution shows how the stress-path crosses the critical state line (i.e., $\psi = 0$ for a moment), shown in sub-figure c. The stress-path keeps going, even though $\psi = 0$, since there is still a difference between $p_{i,max}$ and p_i, resulting in further softening. Note that sub-figure d only shows a positive difference between $p_{i,max}$ and p_i, indicating that only hardening should occur throughout the evolution, but one must not forget that S_{soft} contributes to the further decrease, resulting in $\dot{p_i} < 0$ and thus softening.

Then, there comes a point where re-hardening occurs after softening, which is indicated by yield surface 3 in sub-figure a. This is explained as the stress-path crosses the CSL and continued on softening, the soil turned slightly dense (i.e., $\psi < 0$). This continues until $\dot{p_i} > 0$, to which there is hardening until the soil reaches true critical state where $\psi = 0$ and there is no more difference between $p_{i,max}$ and p_i.

Figures 4.19 and 4.20 show that an increase in consolidation pressure results in an increase in size but no change in shape if all other parameters are kept the same. Also, even though the values differ, the movement of the stress-paths remain the same.

Model response difference between $S = 0$ and $S = 1$

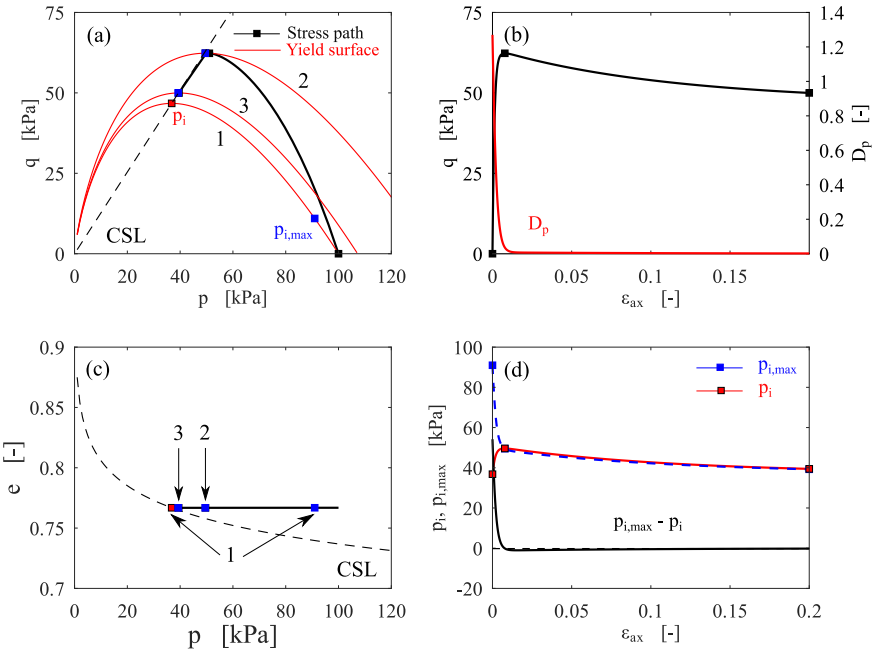

Figure 4.17: Model response during an undrained triaxial test on a loose sand with the softening flag turned off ($S = 0$ and $p_0 = 100$ kPa). The input parameters are given in Table 4.4.

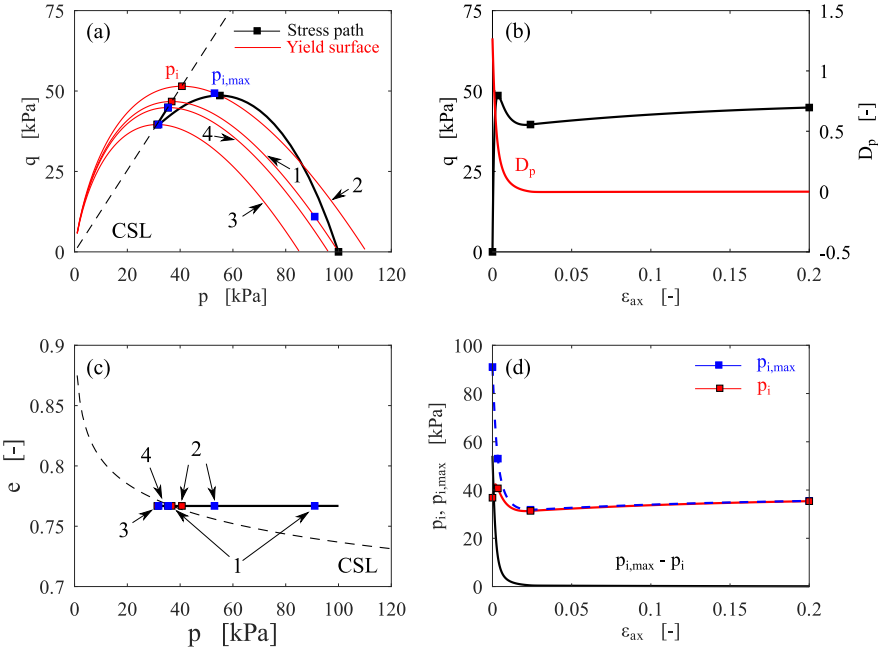

Figure 4.18: Model response during an undrained triaxial test on a loose sand with the softening flag turned on ($S = 1$ and $p_0 = 100$ kPa). The input parameters are given in Table 4.4.

Model response difference between $S = 0$ and $S = 1$ at a higher consolidation pressure

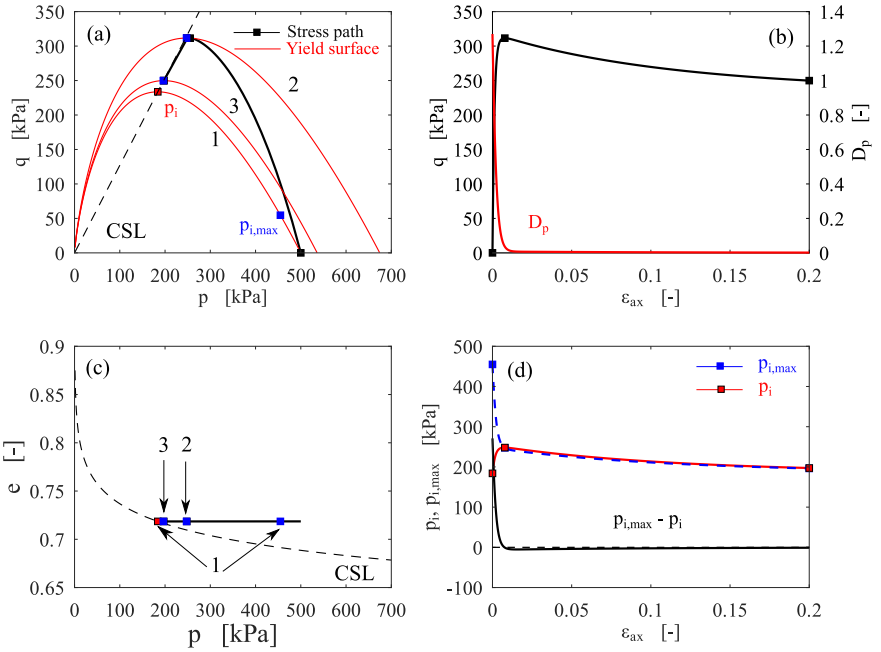

Figure 4.19: Model response during an undrained triaxial test on a loose sand with the softening flag turned off ($S = 0$ and $p_0 = 500$ kPa). The input parameters are given in Table 4.4.

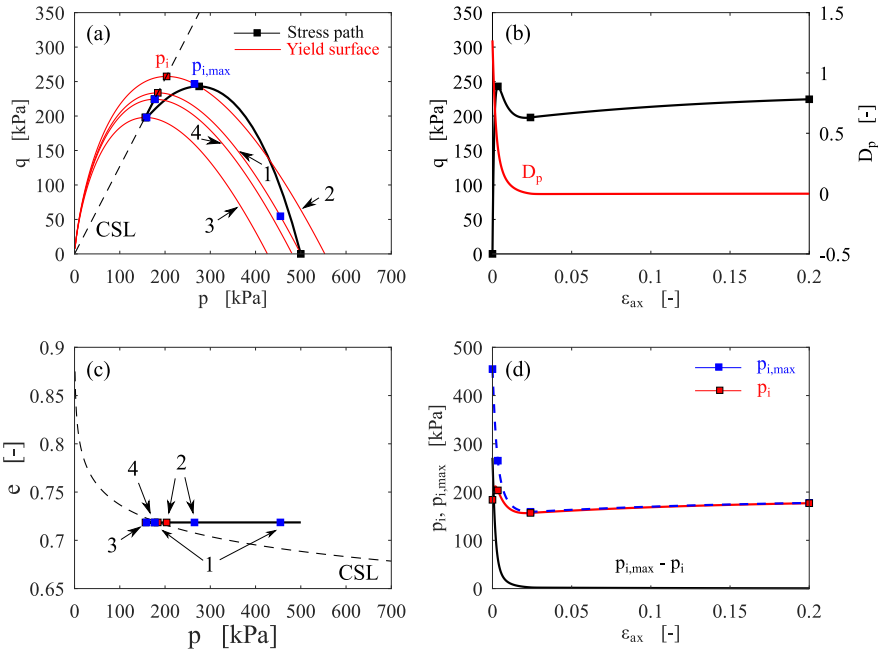

Figure 4.20: Model response during an undrained triaxial test on a loose sand with the softening flag turned on ($S = 1$ and $p_0 = 500$ kPa). The input parameters are given in Table 4.4.

5 Verification and Validation

After new models are implemented, they must be verified to ensure they are in fact the same model that was originally developed and validated to determine if it approximates sand behaviour as intended. Verification is done with two methods: verification by checking the output of PLAXIS NorSand with the values calculated with formulation on which the model is based (section 5.1); and verification by comparison between the newly integrated NorSand in PLAXIS and an original implementation of NorSand, produced by the authors of the model (section 5.2). Validation is done by comparing PLAXIS NorSand to experimental lab test data (section 5.3), which can be found on the website of the publisher of the book written by Been and M. Jefferies, 2015: http://www.crcpress.com/product/isbn/9781482213683.

5.1 Original formulation versus PLAXIS NorSand

Solving problems can be done analytically or numerically. An analytical solution involves framing the problem in a well-understood form and calculating the exact solution. A numerical solution means making guesses at the solution through iterations until the solution is accurate enough. As NorSand is a plasticity model, which is strongly non-linear, calculating the stress-path manually would be extremely difficult and is not a closed-form solution. As such, there exists no analytical solution for the stress path. Instead, to further verify PLAXIS NorSand a comparison is made between the output of PLAXIS NorSand and the solution of the formulation on which the implementation is based on. The peak strength and their related mobilized friction ratio in both dense drained and loose undrained condition are chosen as reference points for the verification.

5.1.1 Formulation

Before diving into the formulation and different processes for the comparison, it is important to highlight that the original formulation will have an initial input that was an output of PLAXIS NorSand. This will be further expanded on when the processes are explained.

Soil behaviour has been observed to follow the formulation given in equation 5.1, which is a re-written form of the Dafalias dilatancy equation:

$$M_i = \eta + D \tag{5.1}$$

As mentioned in section 3.3.5, a more direct relationship between the mobilized friction ratio M_i and the state parameter ψ is determined as:

$$M_i = M_{tc} + ND_{min} = M_{tc} - N\chi_{tc}|\psi| \tag{5.2}$$

This equation is, in essence, directly used in the PLAXIS implementation of NorSand. These two equations are used to determine the peak strength η_{max} for the original formulation.

Since the loose test is done in undrained conditions, there is no volumetric strain. As such, the process to arrive at the peak for the formulation is different than that for the dense drained test. Both processes will be explained separately.

Process dense drained test

After running the implementation, using the parameters given in Table 5.2 and $\psi_0 = -0.15$, the program outputs, after a little bit of post processing, η_{max} and D_{min}. This D_{min}, along with M_{tc} and N that were known beforehand (Table 5.2), will then be used as an input for the original formulation (equation 5.2) to determine M_i ($M_{i,form}$). Then, both $M_{i,form}$ and D_{min}, recall that peak strength occurs at maximum dilation, are used in equation 5.1 to determine η_{max} ($\eta_{max,form}$). Equation 5.1 is also used to determine the mobilized friction ratio at peak strength for the implementation ($M_{i,PLAXIS}$).

Process loose undrained test

Since undrained conditions does not allow for volumetric strain, there is no related maximum dilation at peak strength for the undrained loose test. Instead, the state parameter at peak strength from PLAXIS is used as an input in equation 5.2 to determine $M_{i,form}$. Similarly, the peak strength for the original formulation can be determined using a modified version of equation 5.1:

$$\eta_{max} = M_{i,form} - \chi_{tc}\psi \tag{5.3}$$

The peak strength and the related state parameter, which are extracted from the output of the implementation, are used to determine $M_{i,PLAXIS}$ using equation 5.3.

5.1.2 Test results

Following the steps presented in the previous section it is possible to determine and compare the mobilized friction ratio and the peak strength for both the original formulation and the implementation for dense drained and loose undrained tests. The results are given in the table below. Figure 5.1 illustrates the peak strength and the related minimum dilation at that point.

Table 5.1: Original formulation and PLAXIS NorSand mobilized friction ratio M_i and peak strength η_{max} results.

	Dense drained		Loose undrained	
	M_i	η_{max}	M_i	η_{max}
Original formulation	1.0767	1.429	1.0160	0.4904
PLAXIS NorSand	1.0801	1.4324	1.0465	0.5208

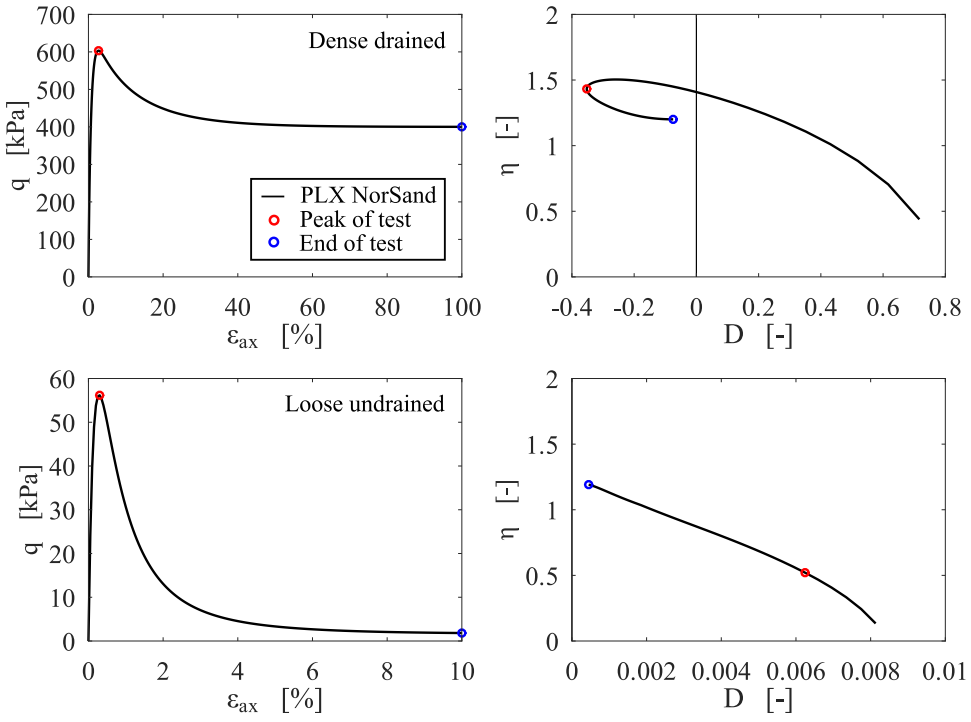

Figure 5.1: Illustration of the peak stress points from which the model data is extracted.

Table 5.2: Parameters for comparison between PLAXIS (PLX) NorSand and original formulation at peak strength.

Γ	λ_e	M_{tc}	N	χ_{tc}	H_0	H_ψ	G_{max} *at* p_0	n_G	ν	ψ_0	p_0	R	S
1	0.030	1.20	0.35	4	300	0	70	0.5	0.2	-0.15 or 0.15	200	1.0	0

5.1.3 Discussion: Original formulation versus PLAXIS NorSand

Even though the verification is not done in the classical sense, i.e., comparing a numerical solution with an analytical solution, the applied process still allowed for some comparison to check whether the implementation arrives at realistic values for a reference point (in this case peak strength).

It can be seen from Table 5.1 that PLAXIS NorSand consistently produces higher values than the original formulation. Comparison for the dense drained test indicates a very small difference between values for both the mobilized friction ratio M_i and peak strength η_{max}. Comparison for the loose undrained test shows a slightly bigger difference.

Lastly, it is worth noting that the $D-\eta$ plot in Figure 5.1 for the loose undrained test is quite unrepresentative. Strictly speaking, undrained tests result no volumetric strains and therefore $D = 0$ throughout the test as well. However, as the PLAXIS implementation uses Young's modulus of water, which is very large, in its stiffness matrix to calculate the elastic response during undrained loading there is still some, albeit negligibly small, volumetric strain. As such, one can still plot the evolution of the dilatancy versus the stress ratio for loose undrained tests, which interestingly somewhat follows the same path for loose drained tests (see subplot b of Figure C.5 in Appendix C.3).

5.2 VBA NorSand versus PLAXIS NorSand

One of the first implementations of NorSand by the authors of NorSand is done in Visual Basic for Applications (VBA) on Excel and is modeled with a purely explicit strategy using forward Euler method. This VBA version of NorSand (VBA NorSand) is what the PLAXIS version of NorSand (PLAXIS NorSand) will be compared to. The process is done in two steps: first, different tests are used to properly calibrate the VBA NorSand. Then, after a proper fit is established, the same input values are fed into the PLAXIS NorSand. In essence, the more true to the original, the more the VBA and PLAXIS NorSand should overlap. Even though PLAXIS NorSand employs a slightly different strategy than VBA NorSand, e.g., automatic sub-stepping with error control to further enhance the model, the outputs of both versions should mostly overlap nonetheless. The verification process is done in the context of triaxial and direct simple shear tests. As undrained direct simple shear (DSSU) data is very scarce and the VBA NorSand does not model drained direct simple shear (DSSD) well, it was opted to simply use variables that do not describe a particular soil in order to establish the overlap between VBA and PLAXIS NorSand.

5.2.1 Determined soil properties from lab tests

The experimental data is derived from tests done on Erksak 330/0.7, where the first number denotes the D_{50} of sand in micrometers (e.g., 330 μm = 0.360 mm for Erksak) and the second number the fines content in percentage (e.g., 0.7% for Erksak). The soil properties derived from this data are shown in figure 5.2. Each soil property is derived by processing triaxial test data. Parameter N and critical friction ratio in triaxial conditions M_{tc}, illustrated in subplot a, can be found by plotting the maximum stress ratio η_{max} at maximum dilatancy D_{min} of multiple drained dense tests (figure 3.15 shows one such point of a test). M_{tc}, the point where soil has arrived at critical state, is found at the intersection where $D_{min} = 0$. Subplot b shows how plotting the state parameter at the point of maximum dilatancy - again, from dense drained triaxial tests - gives a linear relationship, which has the slope χ_{tc}. The CSL in subplot c is derived by fitting a line, in log-scale, through the endpoints of tests where critical state is reached - these points are generally from undrained loose tests as they tend to quickly reach critical state.

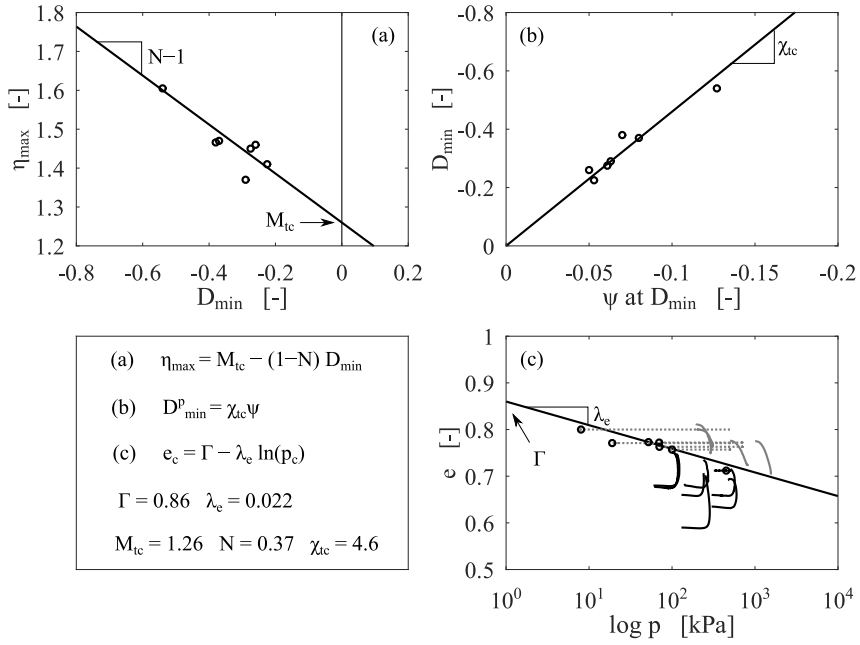

Figure 5.2: Illustration of derivation of soil properties for Erksak 330/0.7. The black graphs in subplot c are that of dense tests, whereas the grey lines represent loose tests.

5.2.2 Calibration and comparison

This section shows the extent to which VBA NorSand and PLAXIS NorSand overlap while using the same parameter set. These parameters will also show how far they deviate from the lab test-determined soil parameter. One can appreciate that these results are both a form of verification, in that they show the similarities between the original implementation and the new one, but also a form of validation, in that they show how well the constitutive model is able to simulate lab tests. Further validation is done in section 5.3.

The similarity between the VBA and PLAXIS NorSand are illustrated in figures 5.3 to 5.6. Four different tests (table 5.3) are used to calibrate VBA NorSand. These tests range from drained to undrained on dense and loose sands. The resulting parameters, which were then used as the input for PLAXIS NorSand, are given in table 5.4. Figure 5.7 compares the VBA and PLAXIS NorSand in DSSU conditions without calibration, where the variables, that do not describe any soil in particular, are given in table 5.5.

Table 5.3: Test values of Erksak 330/0.7 monotonic triaxial tests. MT = moist tamped and WP = wet pluviated.

Test	ψ_0	p_0 (kPa)	G_0 (MPa)	Preparation method
1. CID_D664 (dense drained)	-0.101	300.3	158	WP
2. CIU_L602 (dense undrained)	-0.012	500.1	161	MT
3. CID_D681 (loose drained)	0.068	1005.4	194	MT
4. CIU_C609 (loose undrained)	0.076	499.7	129	MT

Table 5.4: Calibrated parameters to the triaxial tests. T = Test.

CSL			Plasticity					Elasticity						
T	Γ	λ_e	M_{tc}	N	χ_{tc}	H_0	H_ψ	G_{max} at p_0	n_G	ν	ψ_0	p_0	R	S
1.	0.86	0.022	1.27	0.40	5.2	30	1000	160	0.5	0.2	-0.101	300	1.0	0
2.	0.86	0.022	1.26	0.37	4.6	50	0	160	0.5	0.2	-0.012	500	1.3	0
3.	0.86	0.022	1.21	0.37	4.6	60	0	190	0.5	0.2	0.068	1005	1.0	0
4.	0.86	0.022	1.17	0.45	5.5	140	100	55	0.5	0.2	0.076	500	1.15	1

VBA NorSand versus PLAXIS NorSand: dense triaxial tests

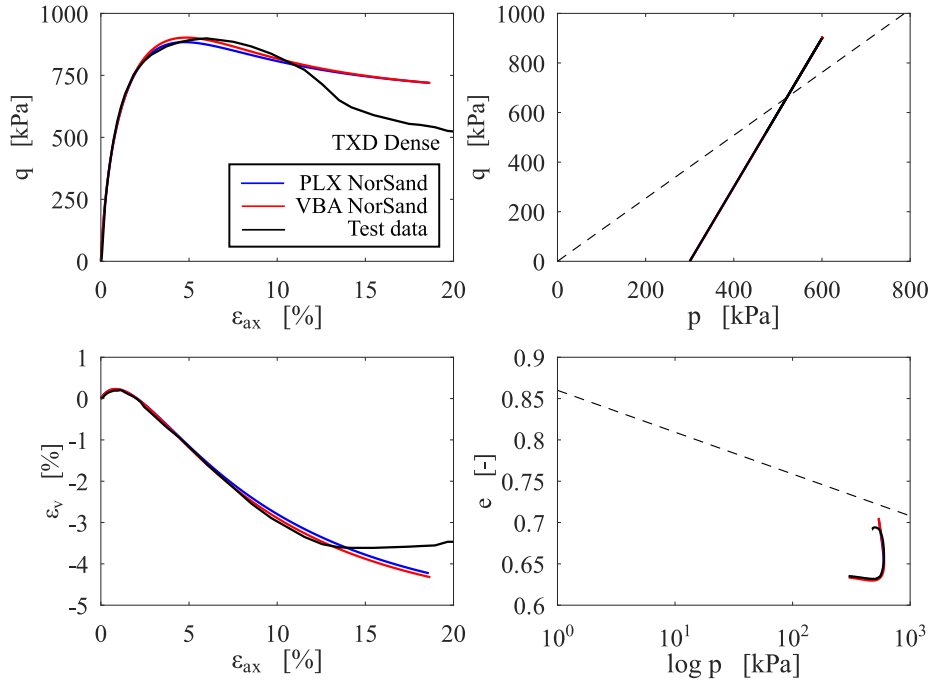

Figure 5.3: Calibrated comparison between PLAXIS (PLX) NorSand, VBA NorSand and dense drained triaxial (CID_D664) test data.

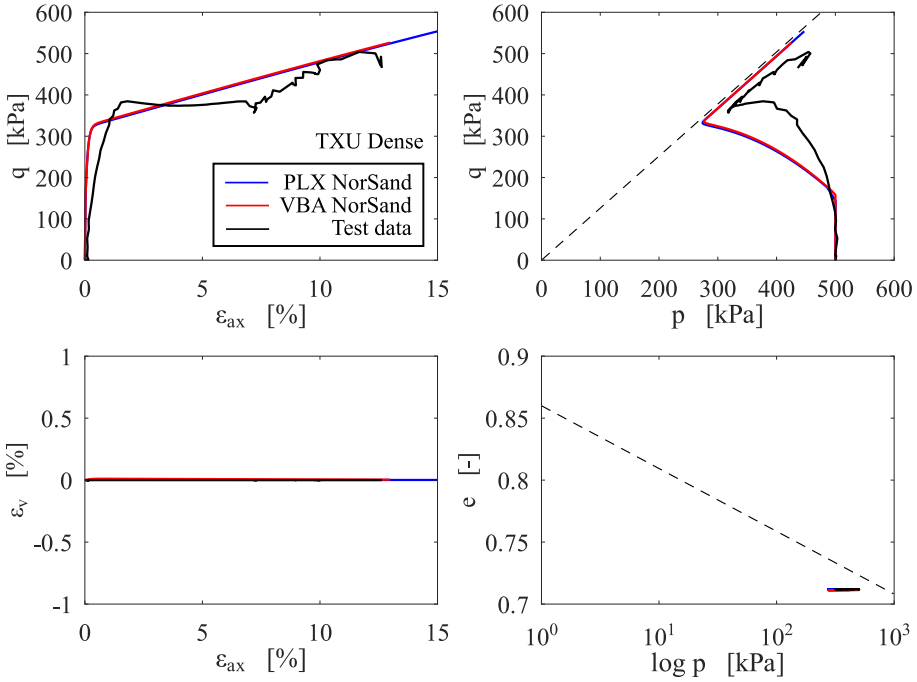

Figure 5.4: Calibrated comparison between PLAXIS (PLX) NorSand, VBA NorSand and dense undrained triaxial (CIU_L602) test data.

VBA NorSand versus PLAXIS NorSand: loose triaxial tests

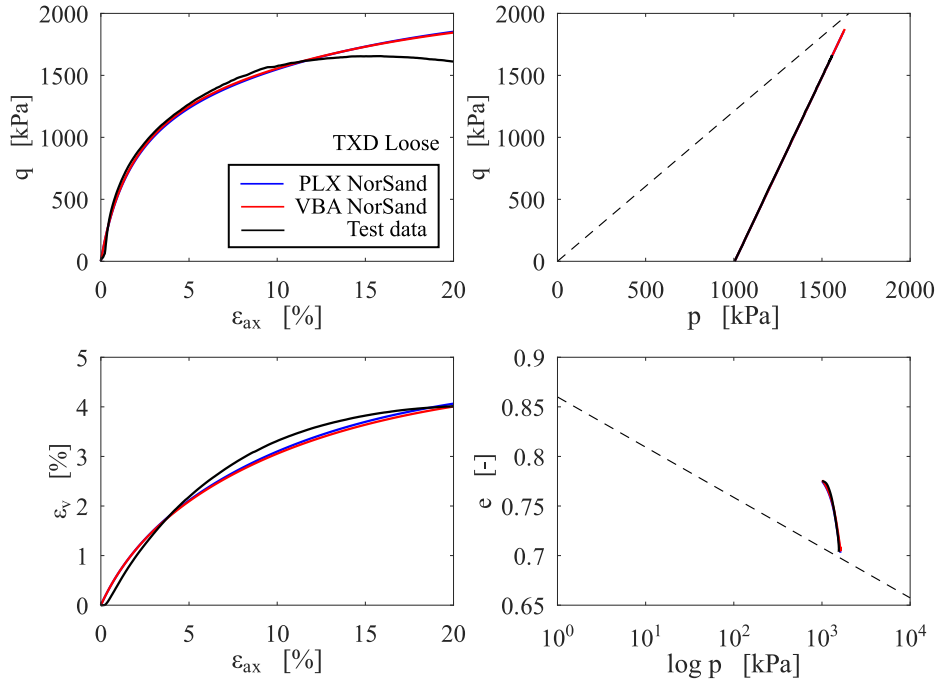

Figure 5.5: Calibrated comparison between PLAXIS (PLX) NorSand, VBA NorSand and loose drained triaxial (CID_D681) test data.

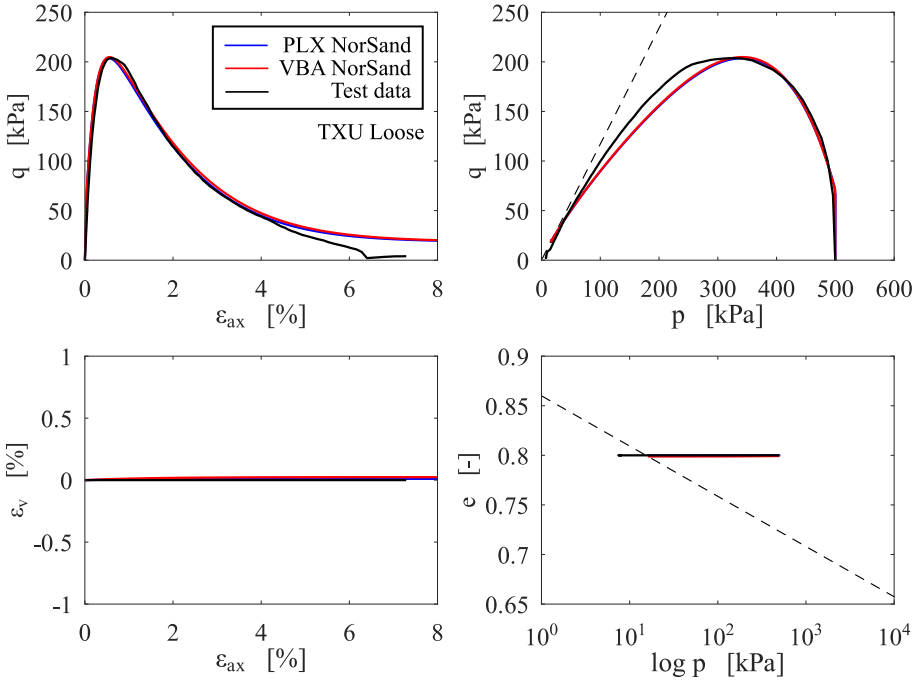

Figure 5.6: Calibrated comparison between PLAXIS (PLX) NorSand, VBA NorSand and loose undrained triaxial (CID_G154) test data.

VBA NorSand versus PLAXIS NorSand: dense and loose DSSU tests

Without going into too much detail, this section will quickly explain what the direct simple shear test entails and show the results of the comparison between the two implementation of NorSand in undrained conditions.

Figure 2.2 from section 2.2 illustrates how direct simple shear (DSS) tests can also give information about soils, such as the horizontal shear strength τ_{max}, cohesion c and friction angle ϕ (see Appendix B). The sample is consolidated in one direction as it is constrained horizontally (i.e., no lateral strain) - this keeps the sample in a K_0 condition, to simulate the deposition of natural soils. In a DSS test the sample can be constrained by different methods: a stack of metal rings, a wire reinforced membrane or a confining cell pressure, with plane strain conditions as a result. One should keep in mind that, contrary to triaxial tests where the stresses can be expressed in the p-q space (as $\sigma_2 = \sigma_3$), DSS tests are commonly expressed in shear stresses.

As mentioned before, the comparison between PLAXIS NorSand and VBA NorSand for undrained direct simple shear conditions is done without the calibration of lab tests as they were scarce and insufficiently accurate to be useful. As such, they are compared with the use of variables, given in table 5.5, that does not describe any particular soil.

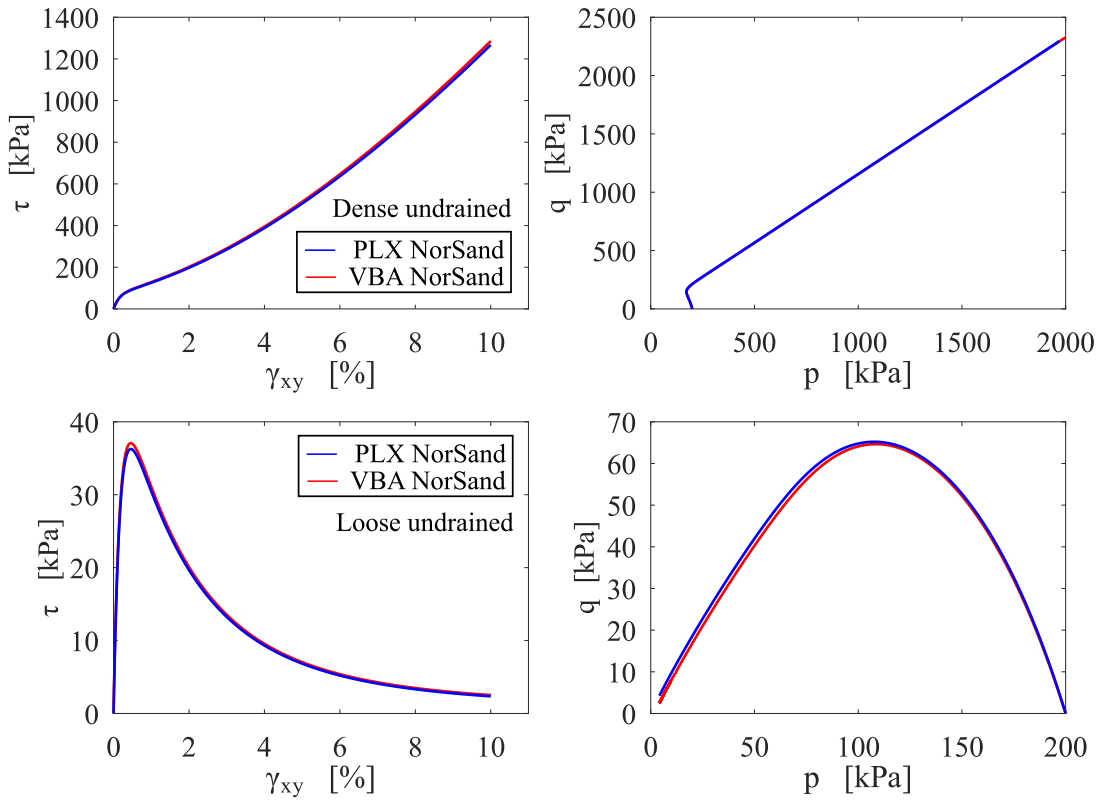

Figure 5.7: Comparison between PLAXIS (PLX) NorSand and VBA NorSand in DSSU conditions.

Table 5.5: Parameters of no particular soil for comparison between PLAXIS (PLX) NorSand and VBA NorSand in DSSU conditions.

Γ	λ_e	M_{tc}	N	χ_{tc}	H_0	H_ψ	G_{max} at p_0	n_G	ν	ψ_0	p_0	R	S
1	0.030	1.20	0.35	4	300	0	70	0.5	0.2	-0.15 or 0.15	200	1.0	0

5.2.3 Discussion: VBA NorSand versus PLAXIS NorSand

In an ideal world, one set of soil parameters (i.e., CSL, plasticity and elasticity parameters), most of which have been derived from the data mentioned in section 5.2.1, along with different initial parameters (e.g., state parameter and consolidation pressure), are used as input parameters while acquiring accurate results.

It became evident, however, in order to fit individual lab test data as best as possible, the soil properties had to be treated as if they had 'freedoms', meaning that the values can deviate from what has been determined from lab test data (Figure 5.2). One explanation for the difference in properties from test to test, even when applied to the same sand-type (e.g., Erksak 330/0.7), is due to the inherent and unrepresented aspect of soil called 'fabric'. This difference in fabric can, among other influences, arise due to different preparation methods (Been and M. Jefferies, 2015).

Overall, in triaxial conditions, calibration of the models resulted in decent approximation of the experimental data. The first parameter that stood out was that an R larger than 1.0 was needed for both undrained tests, even though the tests were prepared without over-consolidating the samples. This further emphasises that all parameters must be regarded as having "freedoms" and thus used in order to properly calibrate the models.

Another parameter that deviated from test data, albeit expected, was the need for a lower M_{tc} for the loose samples. It was observed in Been, Hachey, and M. Jefferies, 1991 (Figure C.7) that looser soils had a lower critical state friction angle ϕ'. This was also touched upon by Been and Jefferies (2015) when it was observed that loose sands consistently required lower M_{tc} values for NorSand to properly match experimental data. An explanation could be that values of M_{tc}, determined by use of regression lines (figure 3.17), are larger than the critical friction ratio at critical state M_{tc} found in loose sands. This is illustrated in figure C.5 in Appendix C.3, where sub-figure b indicates a trend-line with a lower M than those found in a and c. As such, because the M_{tc} for dense sands are larger, it results in "pulling up" of the regression line in sub-figure c. Therefore, a lower M_{tc} is required when calibrating for loose sands.

Aside from the need to utilize all parameters to calibrate each test individually, inputting the resulting values in both VBA NorSand and PLAXIS NorSand gave very similar outputs.

As there were no proper experimental DSSU lab tests available, only a verification was done. The DSSU tests show a very good agreement in their results. The main observable difference, although negligible, is the minimal difference in strength: the strength determined in VBA NorSand is slightly larger than that of PLAXIS NorSand. One reason for this difference could be that the time stepping in the VBA implementation is larger (i.e., smaller number of steps and therefore a courser solution) than that of PLAXIS NorSand, resulting in an over-estimation of the strength. But, again, the difference is essentially negligible.

5.3 First-order lab test data approximation

Recall that a part of the single stress point analysis was done in the previous chapter in section 5.2, where the model was calibrated to each individual lab test. Section 5.3.1 goes further into comparing the model output to experimental data, but now only with one soil parameter set per sand type. This comparison can be seen a first-order approximation and can illustrate the limitations of the model.

Monotonic loading in triaxial tests of three different sands are used as reference data. These tests differ from drained to undrained on loose and dense sands. If a dense or loose test in drained or undrained conditions is unavailable, the test that comes closest to it will be used as a substitute (e.g., a dense undrained test for Nerlerk is substituted with a loose undrained test where $\psi_0 = 0.015$). The sands used for validation are Erksak 330/0.7, Nerlerk 270/1, and Ticino-4 530/0. Afterwards, the results are discussed in section 5.3.2

5.3.1 Soil description and results

Erksak

Test data of Erksak 330/0.7 is the first sand to which NorSand was calibrated. Erksak was used as a core-fill for a caisson-type drilling unit called the Molikpaq, deployed in the Beaufort Sea by Gulf Canada Resources Ltd. The sand was extensively tested both in-situ and in the laboratory. The parameters and test values are summarized in tables 5.6 and 5.7, respectively. These values are based on those found in table 3-2 in Shuttle and M. Jefferies, 2010, which contain examples of calibrated soil property sets for NorSand. The results are shown in figures 5.8 and 5.9, which are for dense and loose sand, respectively.

Table 5.6: General parameters for Erksak 330/0.7 monotonic triaxial calibration. MT = moist tamped and WP = wet pluviated.

G_{ref}/p_{ref}	p_{ref} $[kPa]$	n_G	ν	Γ	λ_e	M_{tc}	N	χ_{tc}	H_0	H_ψ	R
150 - 1000	100	0.5	0.2	0.817	0.014	1.26	0.3	4.1	WP: 70	WP: 1400	1
									MT: 130	WP: 1400	

Table 5.7: Test values of Ersak 330/0.7 monotonic triaxial tests. MT = moist tamped and WP = wet pluviated.

Test	ψ_0	p_0 (kPa)	G_{ref}	H_0	H_ψ	S	Preparation method
CIU_G635 (dense undrained)	-0.158	200	35E3	130	1400	0	MT
CID_G762 (dense drained)	-0.139	250	100E3	70	1400	0	WP
LIQ_G604 (loose undrained)	0.056	700	15E3	130	1400	1	MT
CID_G685 (loose drained)	0.069	194	100E3	130	1400	0	MT

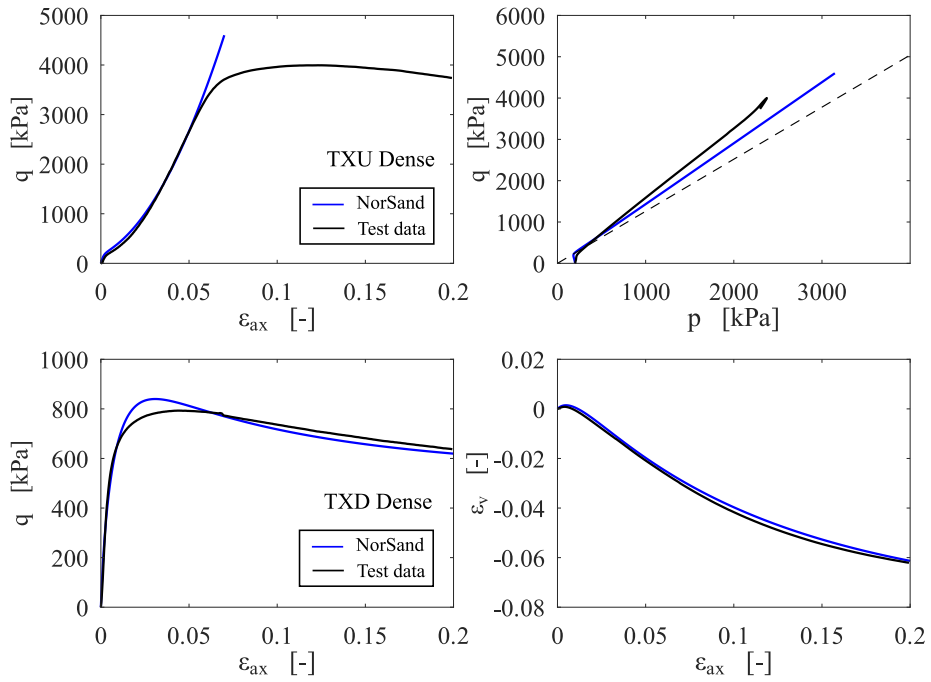

Figure 5.8: Calibration attempt of NorSand to dense Erksak 330/0.7 sand in triaxial compression. Top row sub-figures correspond to the undrained test (CIU_G635) while the bottom sub-figures correspond to the drained test (CID_G762).

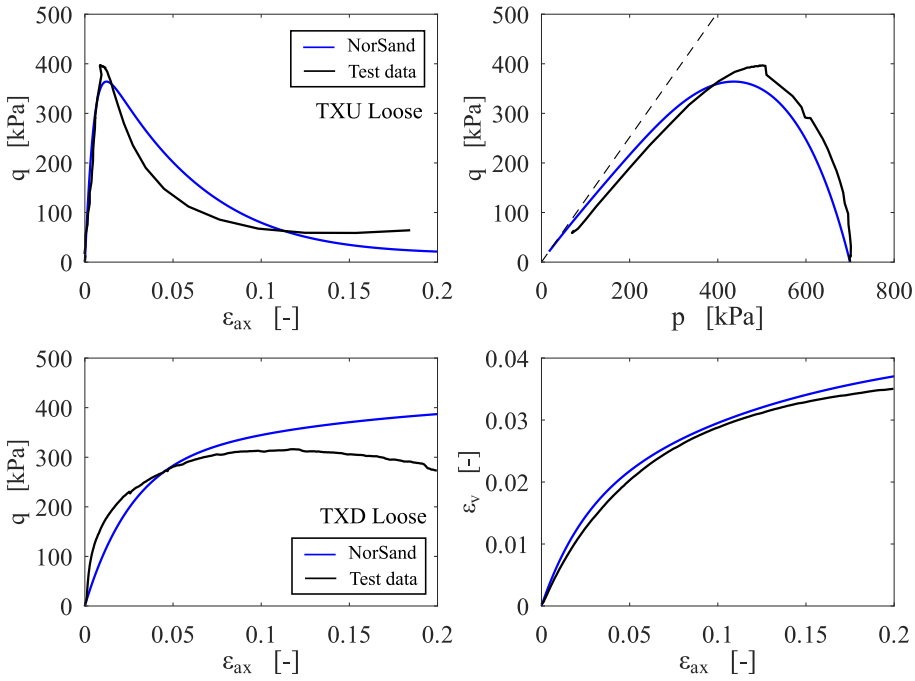

Figure 5.9: Calibration attempt of NorSand to loose Erksak 330/0.7 sand in triaxial compression. Top row sub-figures correspond to the undrained test (LIQ_G604) while the bottom sub-figures correspond to the drained test (CID_G685).

Nerlerk

Nerlerk B-67 was to be an exploration well drilled in 45m of water, with the Dome Petroleam's platform founded on a 36m high sand berm constructed on the seabed, in the Canadian Beaufort Sea during the winter in 1983/1984. As such a large volume was needed for the fill, the local Nerlerk barrow was used. During construction, the Nerlerk berm succumbed to liquefaction due to static loading, prompting additional interest into extensive research of the structure and soil. The data that came out of that research is used in this paper.

The parameters and test values are summarized in tables 5.8 and 5.9, respectively. These values are based on those determined directly from sand lab test data, provided by the download link from Been and M. Jefferies, 2015. The elasticity parameter G_{ref} was determined from Figure 9.13 (middle line) in Been and M. Jefferies, 2015 and the hardening parameters H_0 and H_{psi} were taken from Table 1 of Marinelli, 2020. The results are shown in Figures 5.10 and 5.11, which are for dense and loose sand, respectively.

The available experimental data set of Nerlerk did not include any dense undrained triaxial tests. As such, a loose undrained test with the least positive state parameter is chosen as a substitute (test GIU_G107).

Table 5.8: General parameters for Nerlerk 270/1 monotonic triaxial calibration. MT = moist tamped and WP = wet pluviated.

G_{ref}/p_{ref}	p_{ref} $[kPa]$	n_G	ν	Γ	λ_e	M_{tc}	N	χ_{tc}	H_0	H_ψ	R
450	100	0.5	0.2	0.853	0.0208	1.26	0.38	4	MT: 85	MT: 75	1

Table 5.9: Test values of Nerlerk 270/1 monotonic triaxial tests. MT = moist tamped and WP = wet pluviated.

Test	ψ_0	p_0 (kPa)	S	Preparation method
CIU_G107 (loose undrained)	0.010	700	1	MT
CID_G157 (dense drained)	-0.170	204	0	MT
CIU_G103 (loose undrained)	0.069	501	1	MT
CID_G154 (dense drained)	-0.033	50	0	MT

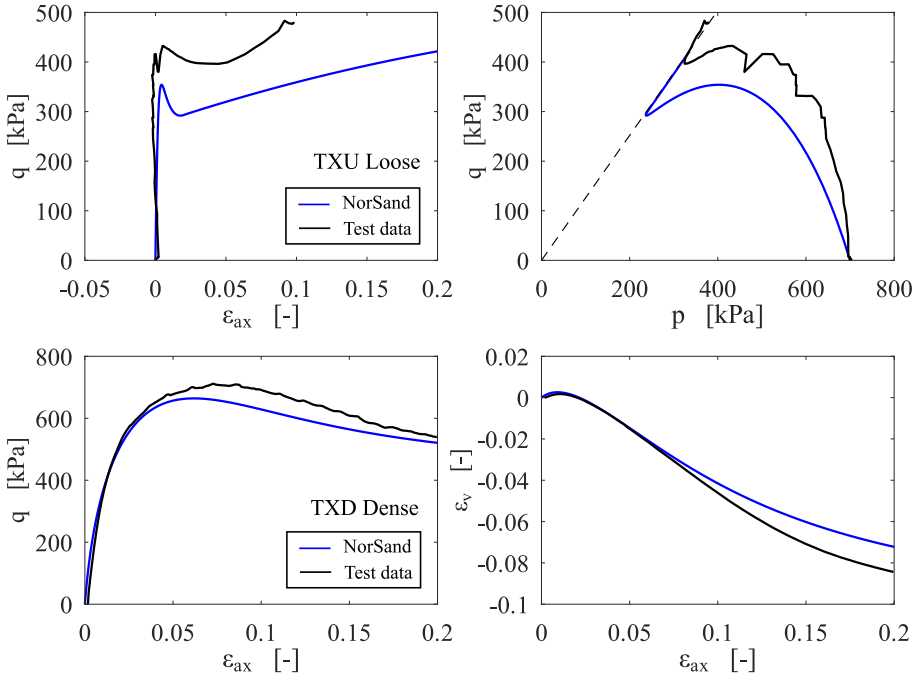

Figure 5.10: Calibration attempt of NorSand to dense Nerlerk 270/1 sand in triaxial compression. Top row sub-figures correspond to the undrained test (CIU_G107) while the bottom sub-figures correspond to the drained test (CID_G157).

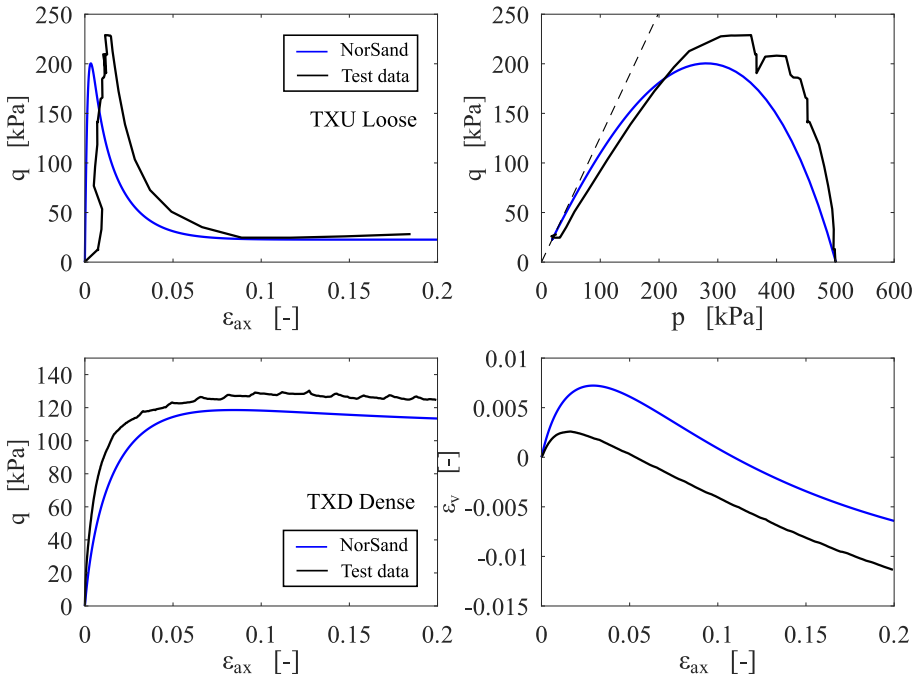

Figure 5.11: Calibration attempt of NorSand to loose Nerlerk 270/1 sand in triaxial compression. Top row sub-figures correspond to the undrained test (CIU_G103) while the bottom sub-figures correspond to the drained test (CID_G154).

Ticino-4

Ticino-4 differs from the previous two in the sense that it is a laboratory sand without any fines, whereas Erksak and Nerlerk are considered natural sands. Laboratory standard sands are used in academic studies to find, for example, how elasticity depends on stress and void ratio.

The parameters and test values are summarized in tables 5.10 and 5.11, respectively. These values are taken from table 3-2 in Shuttle and M. Jefferies, 2010. The elasticity parameter G_{ref} was determined from the $Gvs.p$ plot from sand lab test data, provided by the download link from Been and M. Jefferies, 2015. The results are shown in figures 5.12 and 5.13, which are for dense and loose sand, respectively.

The available experimental data set of Ticino did not include any loose drained triaxial tests. As such, a dense drained test with the least negative state parameter is chosen as a substitute (test CID_C262.

Table 5.10: General parameters for Ticino 530/0 monotonic triaxial calibration. MT = moist tamped and WT = wet pluviated.

G_{ref}/p_{ref}	p_{ref} $[kPa]$	n_G	ν	Γ	λ_e	M_{tc}	N	χ_{tc}	H_0	H_ψ	R
10.255	100	0.5	0.2	0.962	0.0248	1.23	0.3	3.5	MT: 115	MT: 420	1

Table 5.11: Test values of Ticino 530/0 monotonic triaxial tests. MT = moist tamped and WT = wet pluviated.

Test	ψ_0	p_0 (kPa)	S	Preparation method
LIQ_1102 (loose undrained)	0.0016	470.3	0	MT
CID_C264 (dense drained)	-0.117	206	0	MT
LIQ_1105 (loose undrained)	0.075	279	1	MT
CID_C262 (loose drained)	0.020	200	0	MT

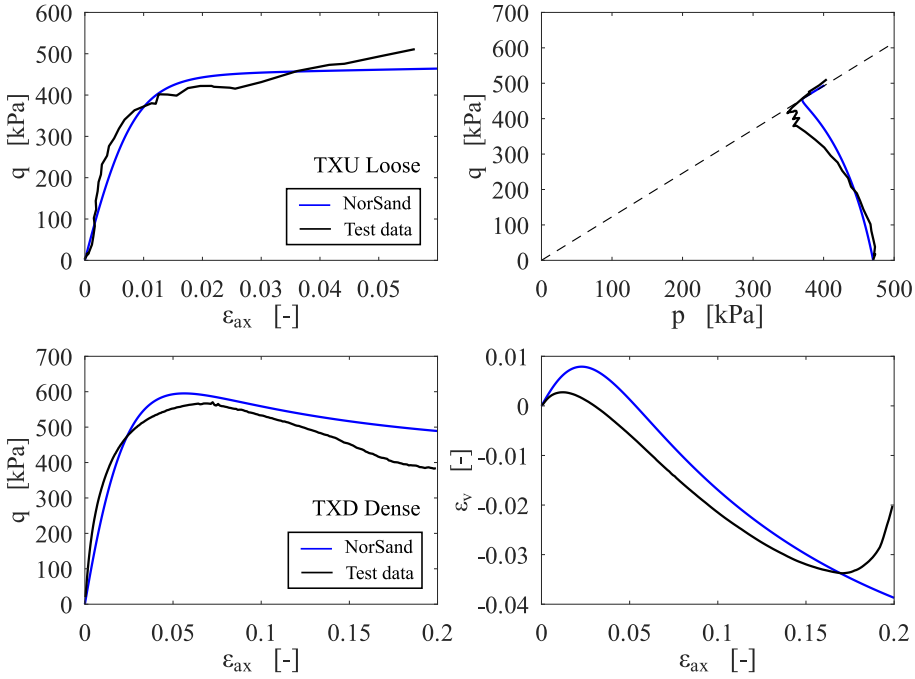

Figure 5.12: Calibration attempt of NorSand to dense Ticino 530/0 sand in triaxial compression. Top row sub-figures correspond to the undrained test (LIQ_1102) while the bottom sub-figures correspond to the drained test (CID_C264).

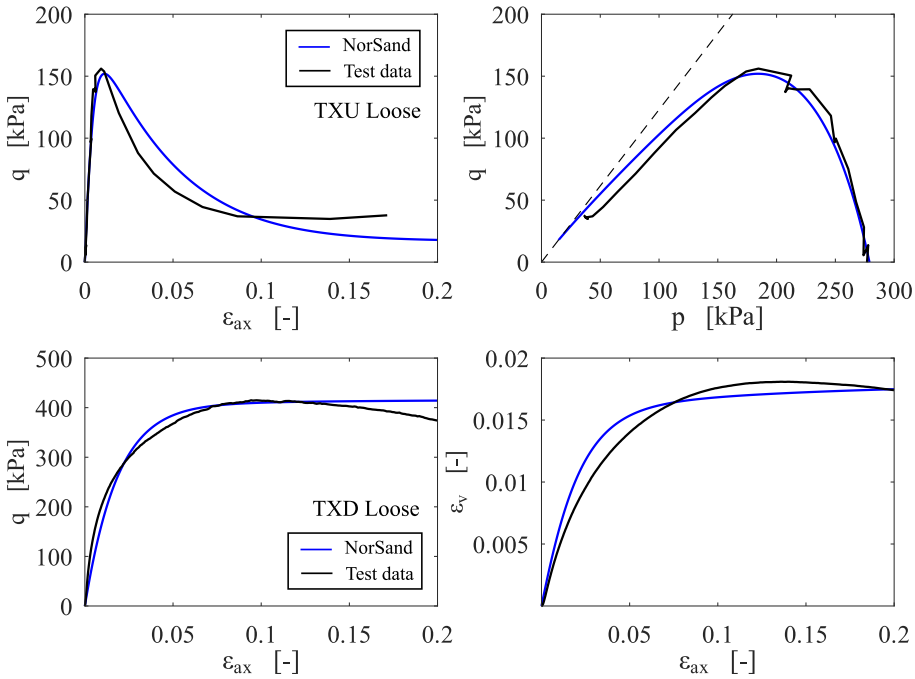

Figure 5.13: Calibration attempt of NorSand to loose Ticino 530/0 sand in triaxial compression. Top row sub-figures correspond to the undrained test (LIQ_1105) while the bottom sub-figures correspond to the drained test (CID_C262).

5.3.2 Discussion: First-order approximation

The main noticeable trend was the consistent need for activation of the softening flag ($S = 1$) during undrained loading of loose sands (left figure of the top row for all the loose sands). Immediate improvement was seen and the peak strength matched that of the experimental data more closely. Another consistent occurrence is the inherent behaviour of unending increase of peak strength during undrained loading of dense soils. Normally, as explained in section 2.3, during undrained loading of dense soil, the excess pore pressures will positively influence the effective stress up until the total pore pressure reaches $u = -100kPa$. After which, cavitation will occur and the water vaporizes, with soil collapse and a peak strength as a result. This natural phenomenon is not incorporated into the framework of NorSand. As such, one must keep this behaviour in mind when using the Soil Test facility of PLAXIS and make sure the 'cavitation cut-off' is activated during FEAs.

As seen in table 5.6, there is a range for G_{ref}. This is the only parameter - and only for this sand - that is treated as a 'freedom' (meaning it is not pre-set from parameter determination). As such, experimental data was immediately improved. Changing G_{ref} (or rigidity I_r) had no effect on loose sand in drained condition within NorSand, which is illustrated in section 4.2. For calibration of dense undrained Erksak data, NorSand only correctly approaches the experimental data up to 5% axial strain. Any further and the model continues to shoot straight up. At first glance, this would be attributed to the inherent tendency of the model to harden indefinitely. But, this is only part of the story: the soil sample has yet to reach the cavitation point as PLAXIS NorSand and the lab test part their ways at around 7% axial strain. Since the back-pressure (section A) of the test is at 1300 kPa and the excess pore pressure is at around -800 kPa at 7% axial strain, there is still around -600 kPa left before reaching the cavitation point - the soil sample should have increased in strength. One explanation for this could be a local collapse mechanism within soil, resulting in a decrease of negative excess pore pressure.

Other than the mismatch of peak strength in drained conditions, dense data is matched quite well. Aside from the over-estimation of residual strength for the loose drained test and under-estimation of the softening in the loose undrained test, loose Erksak sand is quite well approximated.

Calibration of Nerlerk sand in general seems to decently match experimental data. The biggest mismatch is seen in the strain plot for the dense test in drained conditions (bottom right of Figure 5.11). One explanation could be that the input value for the initial state parameter found in the experimental data is wrong, and must be less than $\psi_0 = -0.033$ (table 5.9). Another interesting mismatch is when the softening flag is activated for test CIU_G107 (top row of Figure 5.10). One explanation could be that since ψ_0 is so close to 0, the softening flag results in too much of a decrease in peak strength.

Overall, the behaviour of Ticino is very well approximated, considering one set of parameters is used.

All in all, using one set of input parameters can generally give a decent first-order indication of soil behaviour. It is good to note that post-peak behaviour is generally neglected when fitting the model to data. Because once peak strength is reached during experimental testing, strains localize and the average of strains over the whole sample no longer represents what is happening in the zone of shearing (which the model tries to replicate through single stress point analysis).

This analysis is not thorough enough as a small sample size is used. Also, for some sand-types various test conditions were not available, such as dense undrained lab test data for Ticino. To further validate the model, a wider range of test data could be used. Additionally, it would be wise to validate PLAXIS NorSand in plane strain conditions with use of experimental plane strain tests, such as the bi-axial or DSS test.

6 Application: FEA of a Submerged Landslide

This chapter goes through the application of the NorSand constitutive model in 2D PLAXIS through a slope stability analysis of a simplified 2D model of a submerged landslide such that the general behaviour of the constitutive model can be tested. First, a quick overview of failure modes of slopes are illustrated and their cause of instabilities are given. Then, without going into detail, the concept of the finite element method (FEM) is explained. Next, the set-up of the model is laid out. The influence of soil density on the slope behaviour is then explored. The differences between NorSand, Modified Cam-Clay and Mohr-Coulomb, are determined in subsection 6.5. Lastly, the FEA results are discussed.

6.1 Types of Slope Failures and Instability Mechanism

As the submarine structure will be brought to failure for the analysis, it is important to familiarize oneself with possible modes and mechanisms. A common mode of slope failure is a rotational slip along an almost circular failure surface (Duncan, Wright, and Brandon, 2014). 4 main types of slope failure can be described: Toe Failure, in which failure occurs along the surface that passes through the toe (Figure 6.1a); base failure, in which the failure surface passes below the toe (Figure 6.1b); slope failure, in which the failure occurs along a surface that intersects the slope above the toe (Figure 6.1c); compound failure, in which the failure is a combination of the rotational and translational slip and generally occurs when a hard stratum exists (Figure 6.1d).

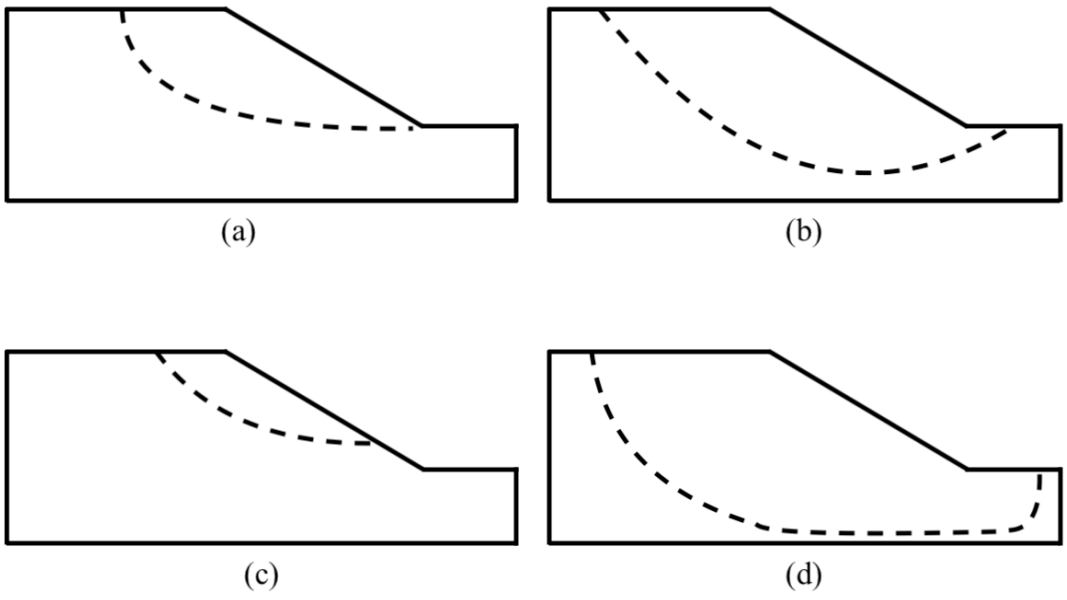

Figure 6.1: (a) Toe Failure, (b) Deep-Seated Failure, (c) Slope Failure, and (d) Compound Failure. Altered from Wanstreet, 2007.

As long as the shear strength of the soil is greater than the shear stresses it is subjected to, it will remain stable. Instability can occur due to two mechanism: either a decrease in shear strength, e.g., due to scouring, an increase in moisture content, excess pore water pressure, monotonic or cyclic loads, weathering, etc.; or an increase in shear stress due to weight of water causing saturation of soils, surcharge loads, seepage pressure, et cetera (Duncan, Wright, and Brandon, 2014).

6.2 Finite element analysis

Engineering problems, which are generally complex continuous physical problems, can be analyzed and solved with use of the finite element method (FEM). An FEM creates a mesh by discretization of a domain into smaller, simpler parts that are called finite elements, thus greatly simplifying the problem. It numerically solves differential equations that arise in engineering and mathematical modeling, such as structural analysis, heat transfer, fluid flow, mass transport etc. In practice, a finite element analysis (FEA) usually consists of three principal steps:

- Pre-processing: Constructing a to-be-analyzed model with the assigned material data, which is then divided into elements with the use of the FEM. If a finer mesh (i.e., more elements) is applied, then the accuracy of the analysis increases - but so does the computational power and time. However, an extremely fine mesh is rarely needed to sufficiently and effectively tackle engineering problems. By imposing boundary conditions, certain nodes will have fixed displacements, and others will have prescribed loads.
- Analysis: The behaviour of each element is analyzed, often by means of relationships between force and displacement. Then, the elements, which are linked together at discrete points called nodes, are solved in a large system of equations to determine how they relate to each other with the use of continuity equations (which make sure the elements do not overlap and/or rip):

$$[K_m]\{U\} = \{F\} \tag{6.1}$$

  where $\{U\}$ and $\{F\}$ are the displacements and externally applied forces, respectively, at the nodal points. The formation of the stiffness matrix $[K_m]$ is dependent on the type of problem being attacked.
- Post-processing: Plots of the output, such as stress, displacement, and strain can be produced to visualize the initial state and the effects of the problem statement. Using these results, one can, for example, iteratively apply changes to the model to reinforce a structure such that yielding does not occur anymore.

6.3 2-D underwater slope set-up

It is possible, with the use of properly chosen assumptions, to transform a three dimensional problem into a 2-D problem, immensely simplifying the problem statement. Plane-strain, in which there is zero strain in the direction normal to the axis of applied stress, is one such assumption. It is often applied in geotechnical engineering for very wide structures, such as tailings dams and underwater slopes. Since VBA NorSand has been validated in DSSU conditions, which occur in plane strain conditions, PLAXIS NorSand can indirectly be seen validated for those conditions as well. As such, NorSand can be applied in finite element analyses where plane strain is assumed. This section goes through the set-up of a finite element (FE) model of a submerged slope.

6.3.1 Initial and boundary conditions

The conditions are similar to the problem presented in Jefferies and Been (2015) where the loading process is aimed to simulate a flow liquefaction process which is triggered by applying a displacement of 20 cm on the top of the slope through a rigid slab (Figure 6.2) with the initial NorSand soil parameters representing a normally consolidated quartz sand with trace of silts (Table 6.1). With an attempt to simulate flow liquefaction, undrained conditions are prescribed to the entire finite element domain. In this deformation controlled approach, contrary to a load controlled approach where the post-failure modes are not available for analysis, one can track the evolution of stresses and displacements after 'failure' (which is the point of maximum applicable load). As failure progresses it is possible watch the evolution up to the state within the domain where the program fails to maintain equilibrium.

Table 6.1: NorSand parameters proposed in Jefferies and Been (2015) for the 2-D slope liquefaction model.

G_{ref}/p_{ref}	p_{ref} [kPa]	n_G	ν	Γ	λ_e	M_{tc}	N	χ_{tc}	H_0	H_ψ	R	S	ψ_0
300	100	1.0	0.15	0.875	0.03	1.27	0.35	4	100	0	1	0	0.03

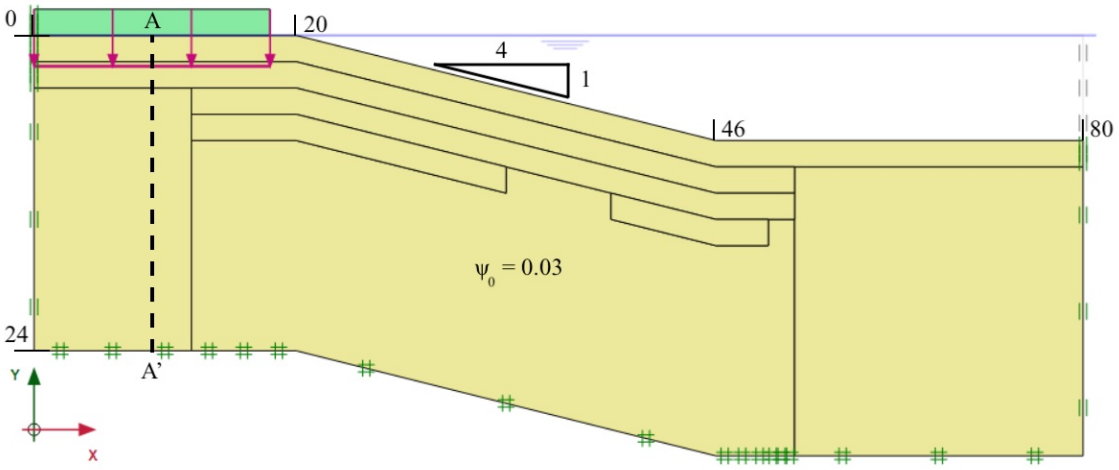

Figure 6.2: Initial and boundary conditions of the finite element problem solved with PLAXIS 2D.

The slope is 8 m high, with a 1V in 4H outer face. The foundation below the slope is at substantial depth so that the slope behaviour is not constrained by a strong base. It is assumed that the structure lies on top of a rigid bedrock with infinite stiffness with fixed bottom boundary conditions such that both lateral and vertical displacements are constrained. The boundary conditions of the mesh sides are fixed laterally to simulate the existence of soil beyond the described domain. Figures D.1 and D.2 in Appendix D.1 show how increasing the depth and width of the boundary conditions, while keeping everything else the same, have fairly little effect on the load capacity (i.e., they essentially share the same maximum applicable load) of the slope, even though their post failure evolutions differ. Figure 6.2 shows how, even though there are various soil sections, a single soil profile covers the entire domain. It was opted to disregard zones of different densities (or state parameters) to not over-complicate the FEAs due to time-constraints.

6.3.2 FEA phasing

The FEA of the slope is simulated in three phases:

- Phase 1: A K_0 $(= 1 - sin\phi)$ initialization where the initial stress, due to the soil weight, of the domain is updated without reaching equilibrium since no shear stresses are calculated with this initialization. A value of $K_0 = 0.5$ corresponds to a friction angle $\phi = 30°$, which is close to the friction angle determined with equation 6.2 and $M_{tc} = 1.27$:

$$sin\phi_{cv} = \frac{3M_{tc}}{M_{tc} + 6} \tag{6.2}$$

- Phase 2: A plastic loading phase with the assignment of soil properties to the model elements. A new initial stress state, which is in equilibrium, is calculated according to the constitutive model response to the stress field from phase 1.

- Phase 3: This phase can split into two sub-phases. First, the state variables are reset and recalculated according to the more appropriate stress field determined in phase 2. This guarantees the correct calculation of the state variables from the pre-determined densities of

the domain. The second part is a plastic loading phase where a 20 cm deformation is applied on top of the crest. This loading could also be viewed as additional lifts of fill placed on the top of the slope.

An important aspect to note is the fact that the arc-length control is activated during the FEAs to save computing time. When during the calculation it appears that the load to be applied is larger than the failure load, the calculation would then try to apply the load defined by the user over and over again without converging to a solution as the load can simply not be applied. Hence, the calculation will keep iterating. When using the arc-length control, the calculation will in fact accurately find how much of the load can really be applied. Additionally, arc-length control is combined with an automatic failure detection. This automatic failure detection says that if in 5 successive calculation steps the applied load has to be decreased in order for the calculation to converge, failure is assumed and the calculation stops (Van der Sloot, 2011). Figure D.3 in Appendix D.1 illustrates the difference between turning it off and on. An artifact of the arc-length control is thus the sudden decrease of vertical load and deformation on the structure, but these artifacts are manually removed in other figures for clarity. Figures, such as the total deviatoric strains throughout the domain in phase 3, are processed at steps before the automatic failure detection kicks in.

6.3.3 Mesh size

A 'medium' (one of the standard options for the meshing phase within PLAXIS) mesh size was chosen, which comes to 5754 elements, to save time but still retain sufficient accuracy. There is an observed mesh size dependency when applying different mesh densities to the domain while all other input remained the same (Figures D.4 to D.7 in Appendix D.1). The mesh influences the behaviour of slope rather than solely the constitutive model, where a finer mesh results in a lower bearing capacity and shallower failure surface compared to courses meshes. Since there is no one concrete correct solution for this analysis, one has more freedom to choose which element density fits best to perform said analyses.

6.4 Influence of different densities on slope behaviour

This section will explore the effects of different densities (i.e., state parameters) on the behaviour of the underwater slope. First, the effects of increasing the initial state parameter, where the soil goes from normally consolidated ($\psi_0 = 0.03$) to highly liquefiable ($\psi_0 = 0.07$), are illustrated in 6.4.1). Then, the effects of changing the domain from loose to dense are shown in subsection 6.4.2.

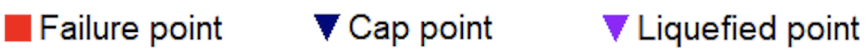

Figure 6.3: Relevant plastic point types found in the FEA plastic point figures.

To differentiate the plastic points according to the hardening process, the existing symbols used in PLAXIS output are employed with a different meaning: the failure points are plastic points at critical states; hardening points are points which are in plasticity; and liquefaction points, which are plastic points characterized by a stress ratio greater than the instability line (the line that goes through peak strength of a stress path). It is worth noting that liquefaction points are plotted also when the finite element analysis is performed in drained conditions, thus highlighting potential liquefaction phenomena occurring if soil conditions switch from drained to undrained.

6.4.1 FEA results: increase of initial void ratio in NorSand

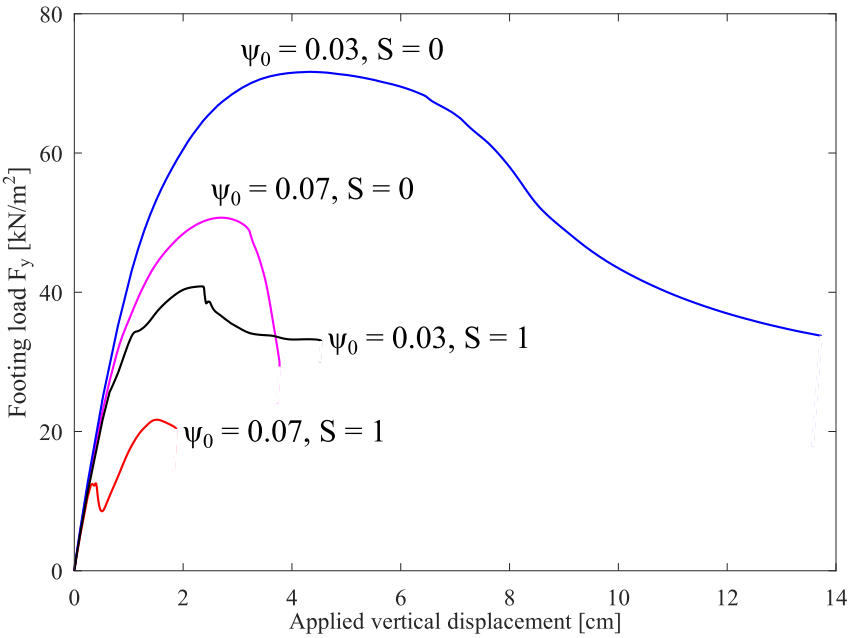

Figure 6.4: Load-displacement response under the rigid slab for different loose soils with the softening flag turned off and on.

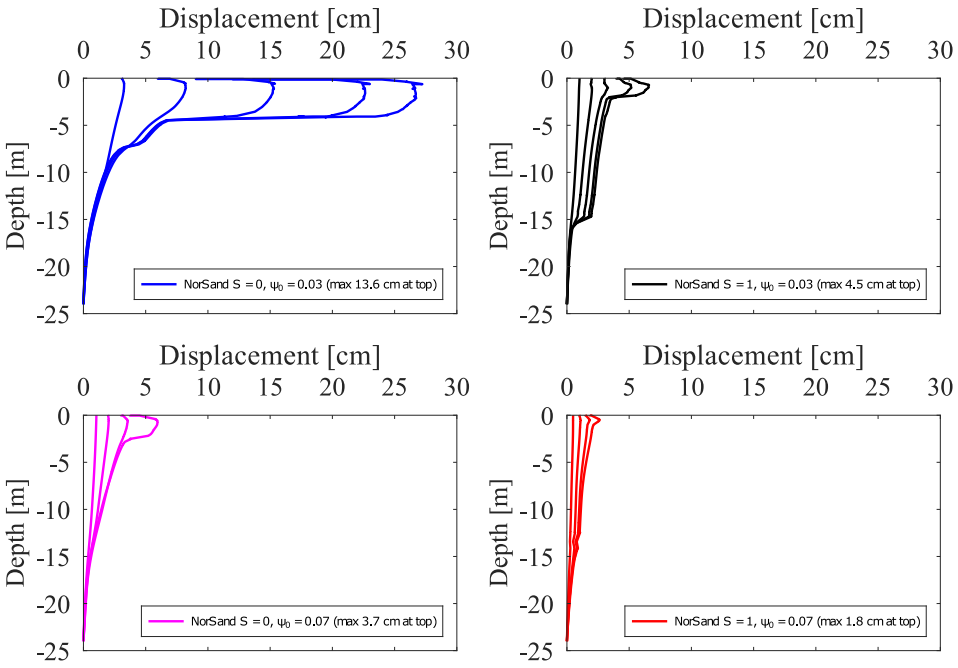

Figure 6.5: Evolution of the total displacement $|u|$ at section A-A'

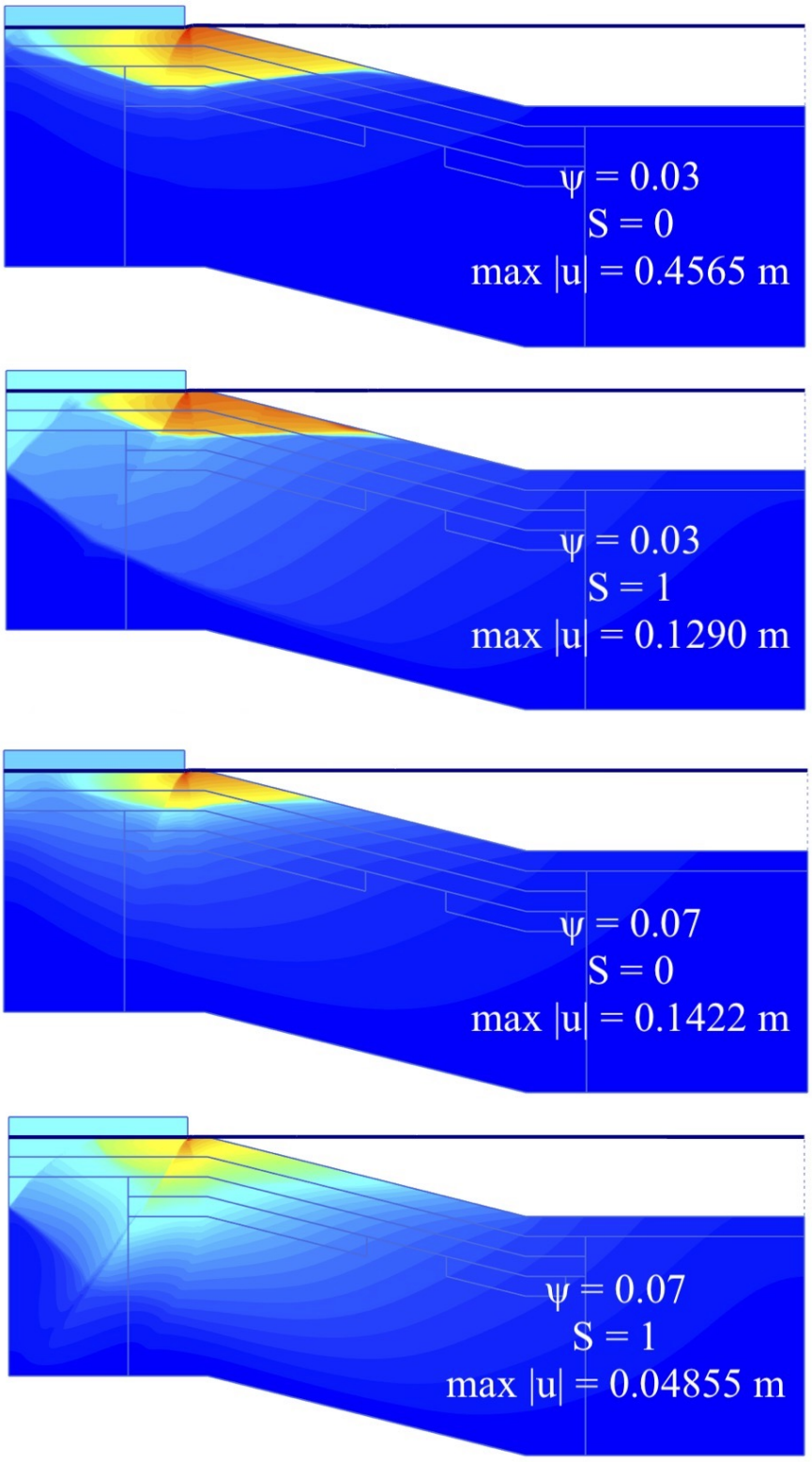

Figure 6.6: Total displacements $|u|$ at phase 3 for different loose soils. Parameters are given in Table 6.2.

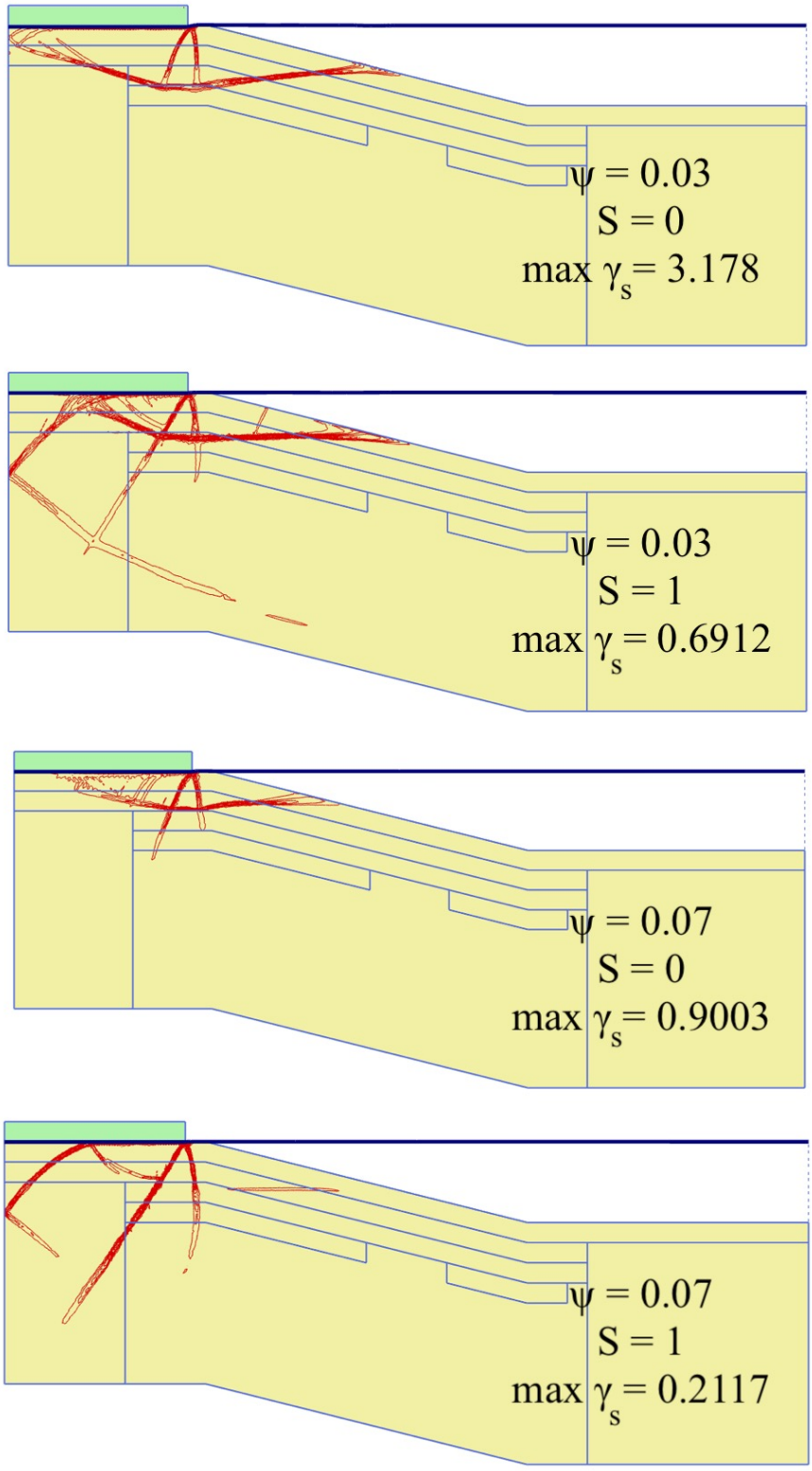

Figure 6.7: Total deviatoric strain at phase 3 for different loose soils. Parameters are given in Table 6.2.

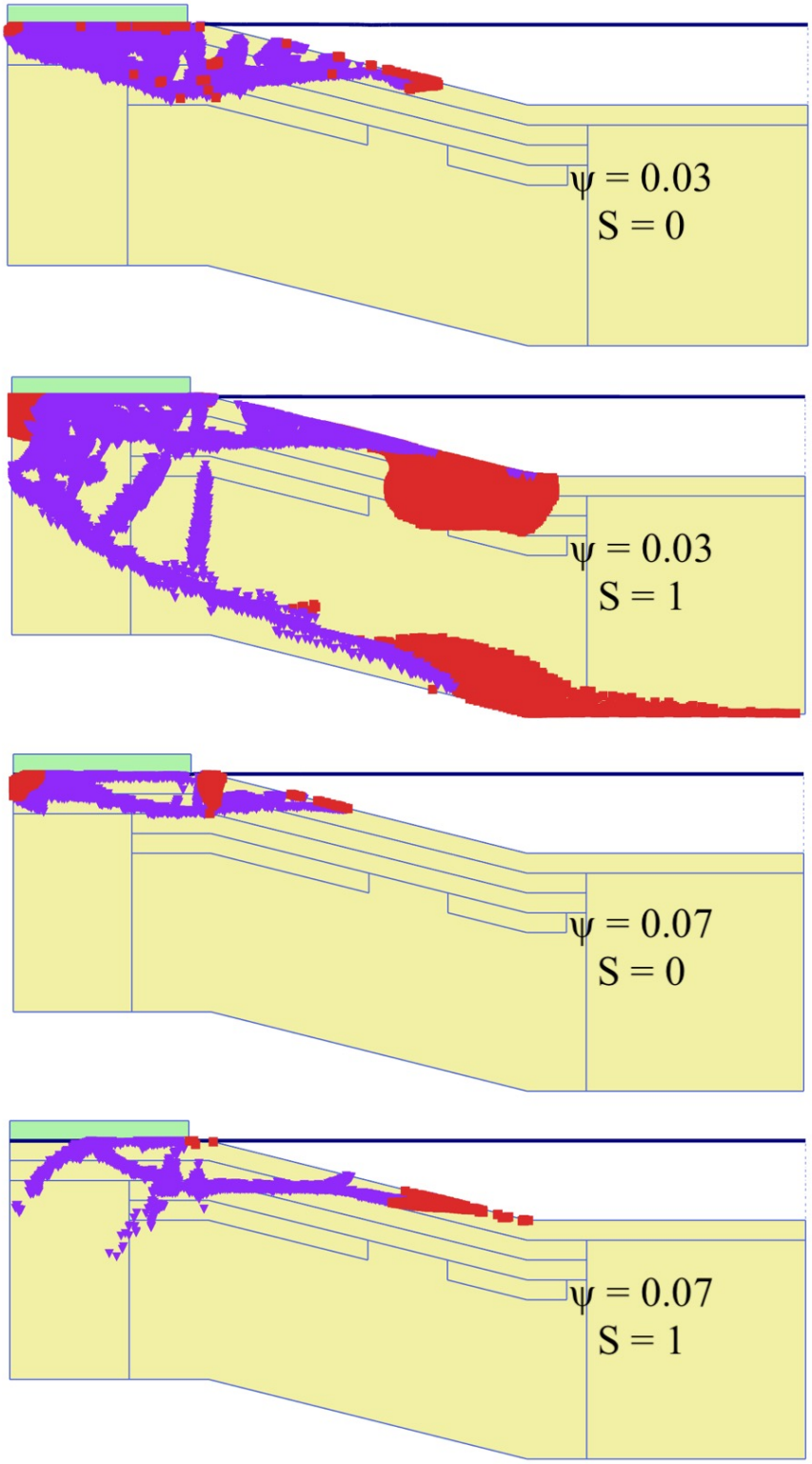

Figure 6.8: Plastic points at phase 3 for different loose soils. Parameters are given in Table 6.2.

6.4.2 FEA results: difference between dense and loose soil

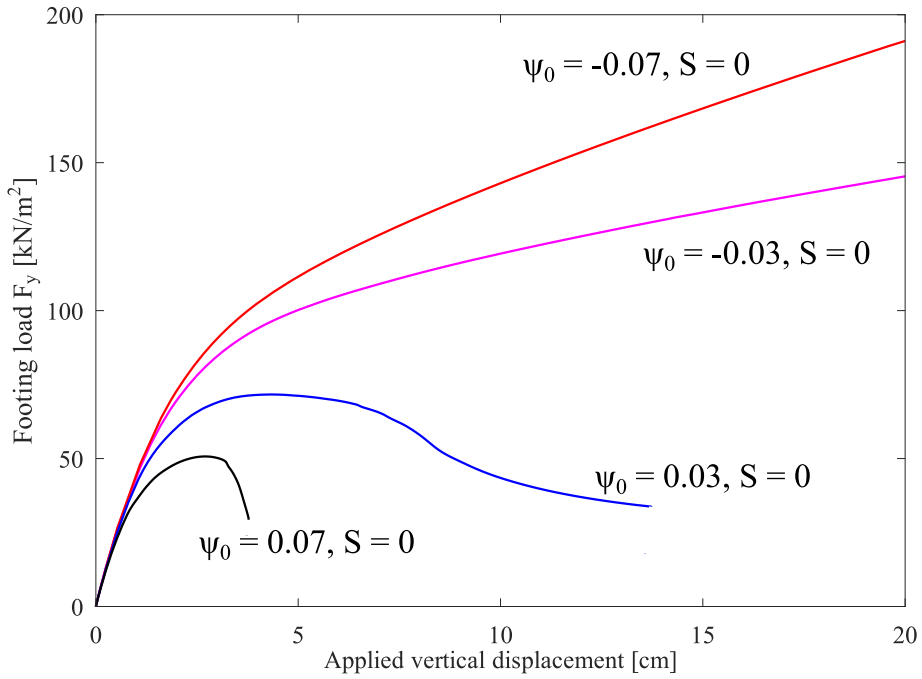

Figure 6.9: Load-displacement response under the rigid slab for each constitutive model.

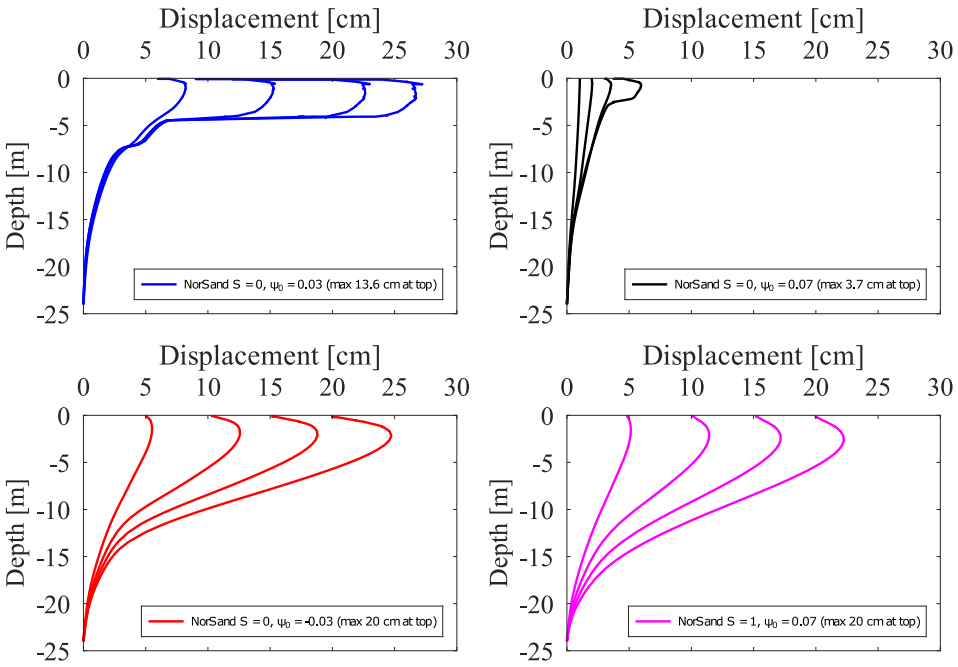

Figure 6.10: Evolution of the total displacement $|u|$ at section A-A'

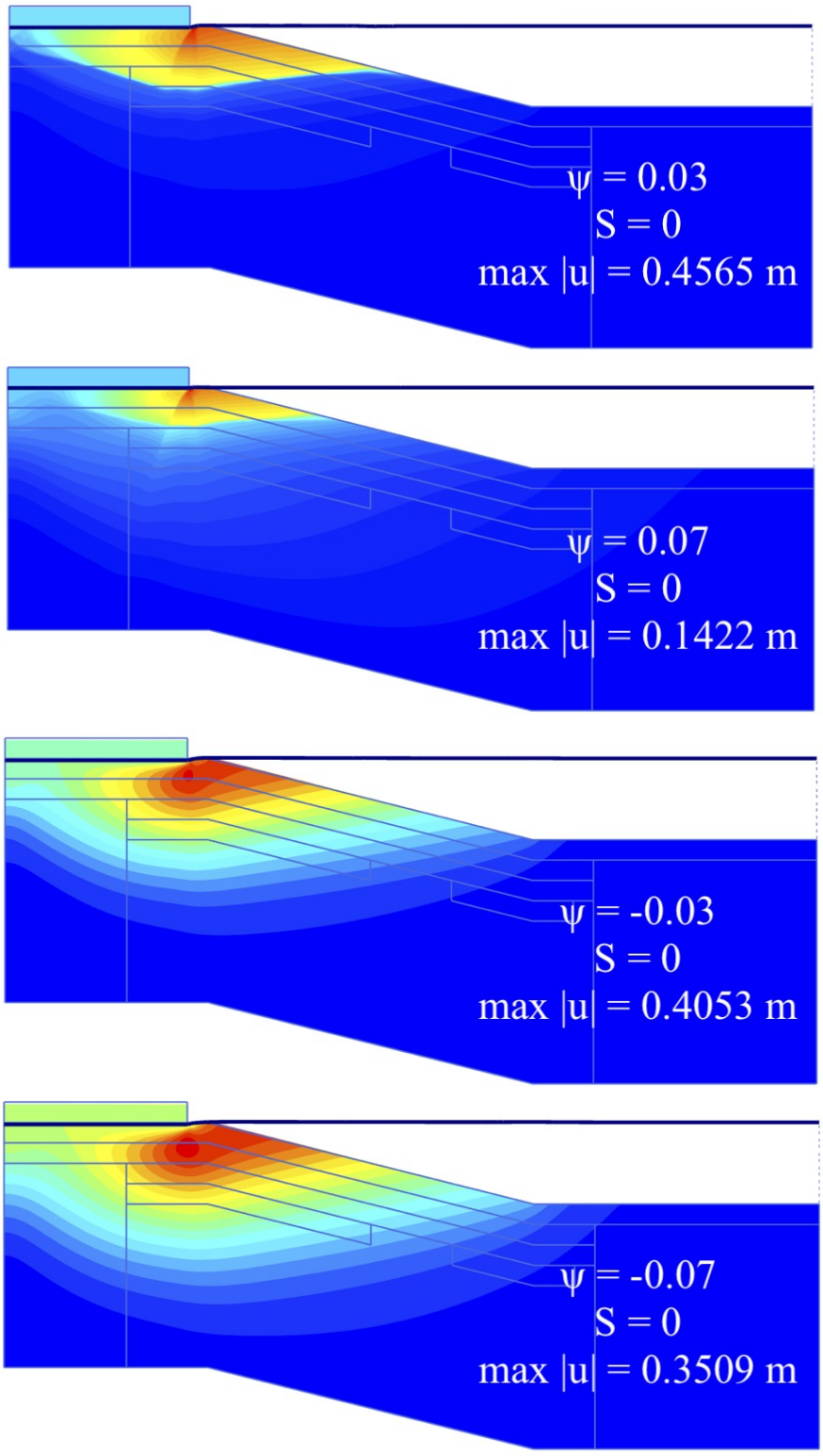

Figure 6.11: Total displacements $|u|$ at phase 3 for different densities. Parameters are given in Table 6.2.

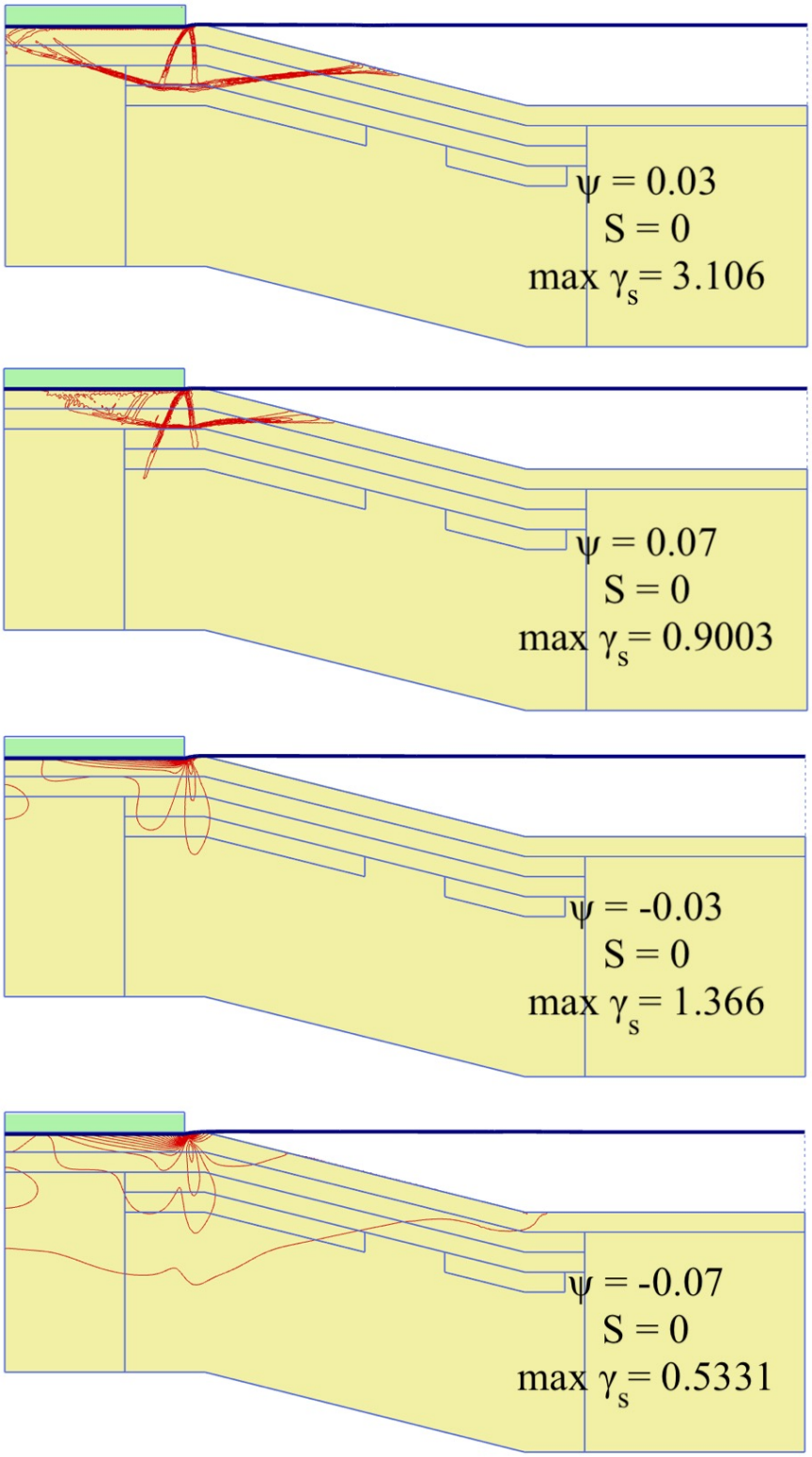

Figure 6.12: Total deviatoric strain at phase 3 for different densities. Parameters are given in Table 6.2.

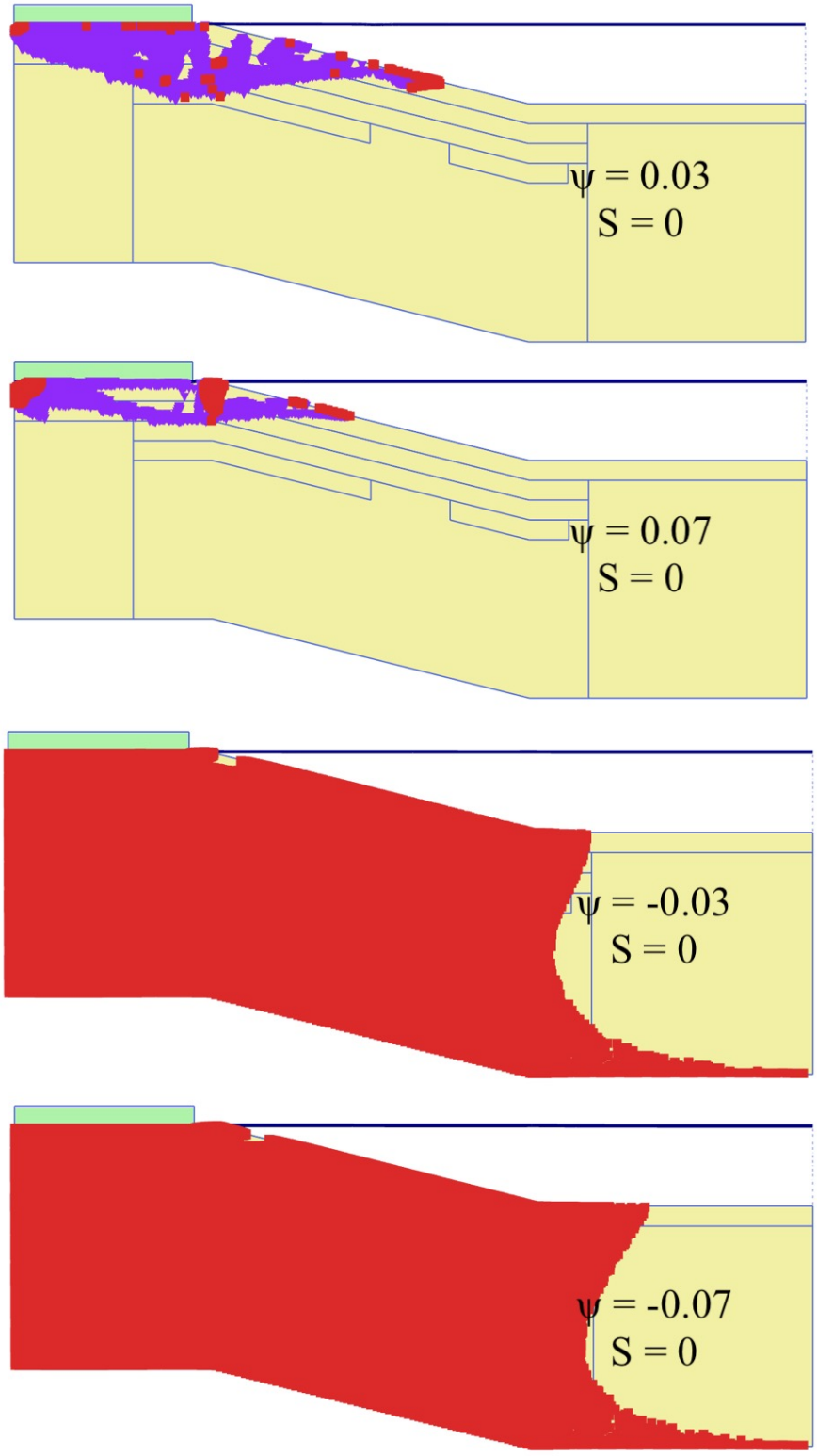

Figure 6.13: Plastic points at phase 3 for different densities. Parameters are given in Table 6.2.

6.5 NorSand versus Mohr-Coulomb and Modified Cam-Clay

This section will explore the liquefaction potential of a 2-D model (Figure 6.2) of a simple underwater slope when different constitutive models - NorSand, Mohr-Coulomb (MC), and Modified Cam-Clay (MCC) - are applied to the materials.

6.5.1 Parameter setup

Throughout the FEA, different constitutive models are assigned to the domain. To perform the comparison, the materials, albeit with different models, must more or less have the same properties. In other words, the material properties of a soil must be translated from one constitutive model to the other. To do so, the baseline parameters of NorSand, which correspond to normally consolidated behaviour ($\psi_0 = 0.03$), given in Table 6.1 are used to translate the input parameters from NorSand to the other two.

Importantly, one must adhere to certain contextual 'rules' during the calibration of the other models. For instance, in this FEA soils are assumed to be deposited without being over-consolidated (i.e., $R = 1$). And where NorSand shows a peak strength for normally consolidated loose sands in undrained conditions (which is also observed behaviour in experimental data), MCC does not. MCC does show peak strength, however, when the soil is modeled as over-consolidated. However, as the 'rules' dictate, the soil cannot be assigned an over-consolidation ratio larger than 1.

In the initial analysis performed by Jefferies and Been (2015), the softening flag was chosen as 0 ($S = 0$). S will be both deactivated and activated ($S = 1$) in this analysis, but the other constitutive models will be calibrated against the undrained behaviour of NorSand where $\psi_0 = 0.03$ and $S = 0$. Going from NorSand to MCC means dropping some of the NorSand specific-parameters. Luckily, parameter such as λ, ν and M_{tc} can be used directly within MCC. The initial void ratio can be chosen quite arbitrarily (generally taken as 0.5) as it has very little effect. Choosing the unload-reload stiffness κ comes with a bit of freedom as there is no clear indication of what value it should be. For now, it is chosen such that the peak strength in undrained conditions approximates that of NorSand with the softening flag turned off. Determining the values for Mohr-Coulomb is somewhat straightforward. The Young's modulus can be calculated from the shear modulus at the reference pressure with the following equation:

$$E = 2G(1 + \nu) \tag{6.3}$$

Since loose sands do not show cohesive behaviour, $c_{ref} = 0$. Additionally, no dilation angle is chosen to keep assumptions to a minimum (even though $\psi = 0$ in itself is one) and maintain a straightforward approach with MC. It should be noted that equation 6.2 provides the friction angle ($\phi = 31.6$) that is used in MC.

Table 6.2 summarizes the input parameters for each constitutive model, which have been calibrated with the use of single stress point analysis, and Figure 6.14 illustrates the results of these analyses.

Table 6.2: Plaxis input parameters of NorSand (NS), Modified Cam-Clay (MCC), and Mohr-Coulomb (MC).

NS													
G_{ref}/p_{ref}	p_{ref}	n_G	ν	Γ	λ_e	M_{tc}	N	χ_{tc}	H_0	H_ψ	R	S	ψ_0
300	100	1.0	0.15	0.875	0.03	1.27	0.35	4	100	0	1	0/1	0.03

MCC				
λ	κ	ν	M_{tc}	$e_{initial}$
0.03	0.0015	0.15	1.27	0.5

MC					
$E\ (MPa)$	ν	c_{ref}	ϕ	ψ	
69	0.15	0	31.6	0	

Figure 6.14 shows how all models match in drained conditions. Since the NorSand is unaffected by the softening flag in drained conditions, the curves with the softening flag turned off and on overlap exactly. In undrained conditions strong differences arise between all models. One can see in the q-p stress space for MCC the stress state stops evolving when it has reached its peak strength, which is explained by the hardening mechanism in MCC. The yield surface continues to harden (i.e., the shear strength increases) until it reaches the CSL. At that point, the dilatancy vector points upwards, resulting in $\dot{\varepsilon}_v^p = 0$ (section 3.2). As the hardening mechanism is tied to the plastic volumetric strain increment, hardening comes to a halt.

The stress evolution of Mohr-Coulomb in the q-p stress space in undrained conditions shows that the path goes straight up, i.e., there is no change in mean effective stress throughout the test. This is explained with the isotopic stiffness matrix of Mohr-Coulomb:

$$\begin{bmatrix} \dot{p} \\ \dot{q} \end{bmatrix} = \begin{bmatrix} K & 0 \\ 0 & G \end{bmatrix} \begin{bmatrix} \dot{\varepsilon}_v^e \\ \dot{\varepsilon}_q^e \end{bmatrix} \tag{6.4}$$

During undrained loading, the increment of the total volumetric strain $\dot{\varepsilon}_v$ $(= \dot{\varepsilon}_v^e + \dot{\varepsilon}_v^p)$ is equal to 0. As long as the stress state is in the elastic domain, there is no plastic volumetric strain increment ($\dot{\varepsilon}_v^p = 0$), meaning that the elastic volumetric strain must be zero as well to satisfy the condition of $\dot{\varepsilon}_v = 0$. The equation above shows that the mean effective stress therefore does not change. The deviatoric stress does change, however, until reaching the yield surface resulting in a plateau.

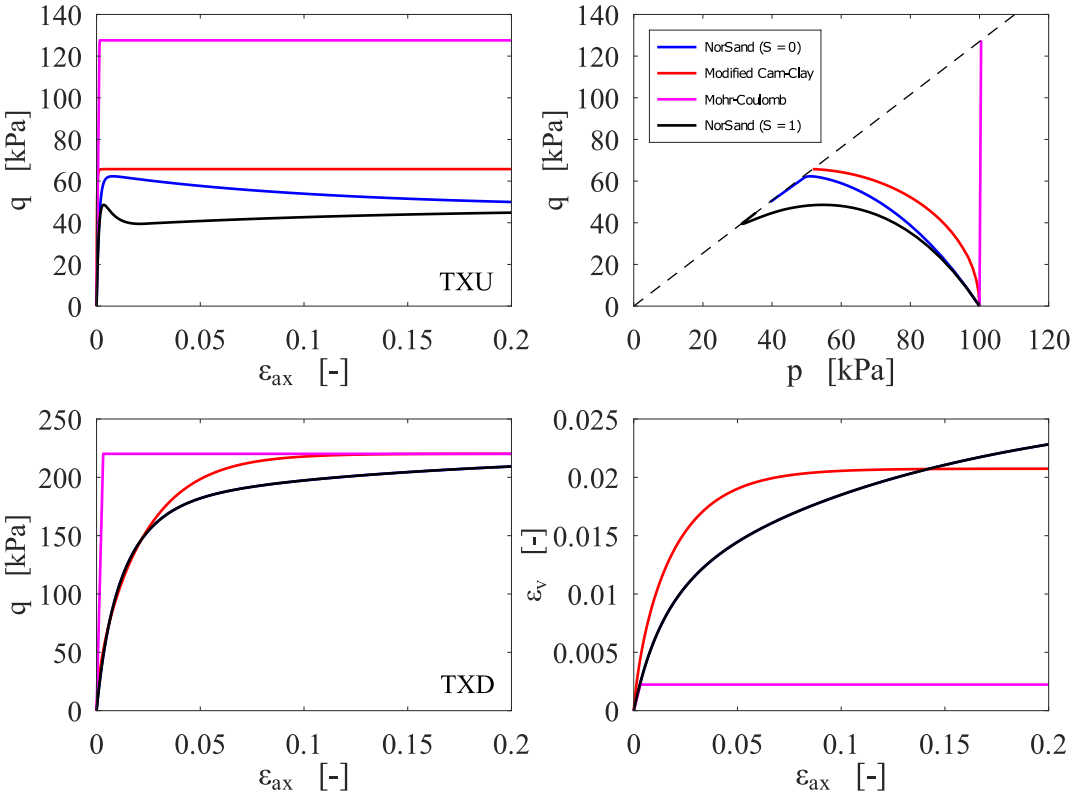

Figure 6.14: Results of the single stress point analyses of NorSand ($S = 0$ and $S = 1$), Modified Cam-Clay and Mohr-Coulomb in both undrained (top row) and drained (bottom row) triaxial conditions.

6.5.2 FEA results: different constitutive models

This section shows the various results of the underwater slope analysis for each constitutive model. Figure 6.15 shows the load-displacement response under the rigid slab and at which point the structure is unable to maintain equilibrium. Figure 6.16 illustrates the evolution of the length of total displacements at section A-A', which goes from the bottom middle point of the rigid slab vertically to the bottom of the domain (Figure 6.2). Lastly, Figures 6.17, 6.18 and 6.19 show the total displacements $|u|$, total deviatoric strain γ_s and the plastic points, respectively, throughout the domain right before the structure loses equilibrium in phase 3.

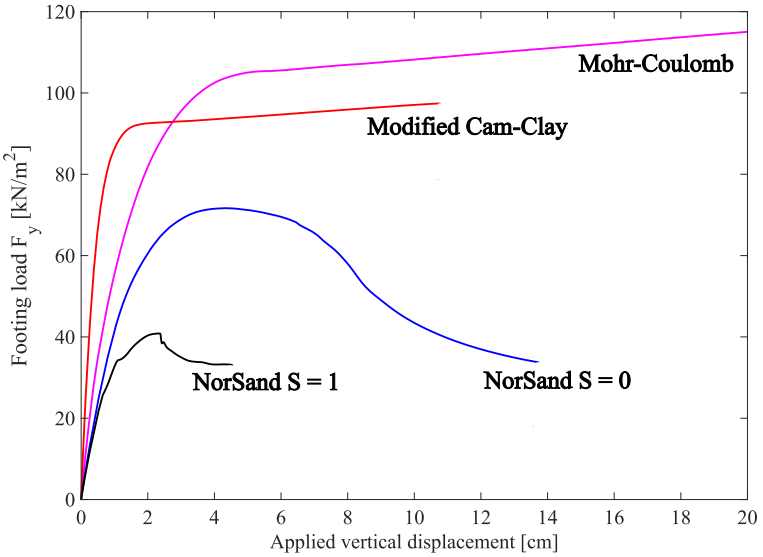

Figure 6.15: Load-displacement response under the rigid slab for each constitutive model.

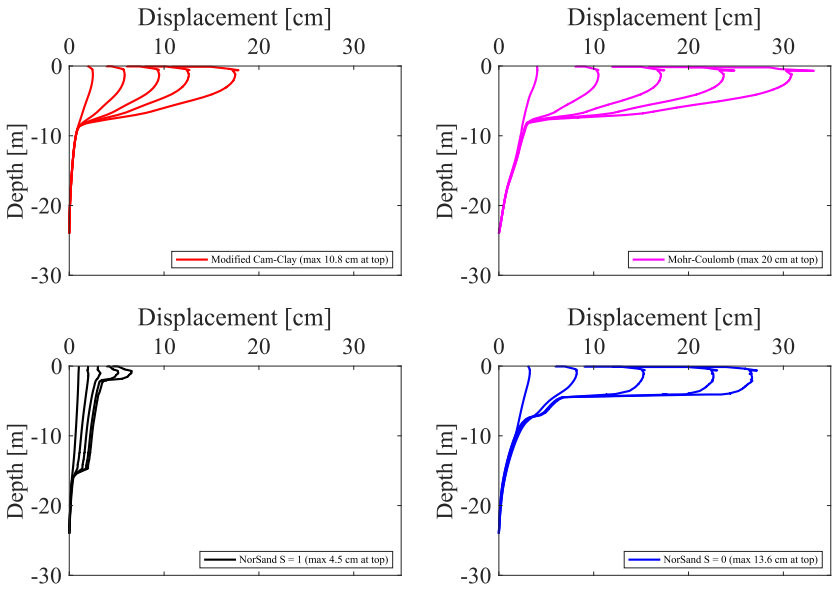

Figure 6.16: Evolution of the total displacement $|u|$ at section A-A'

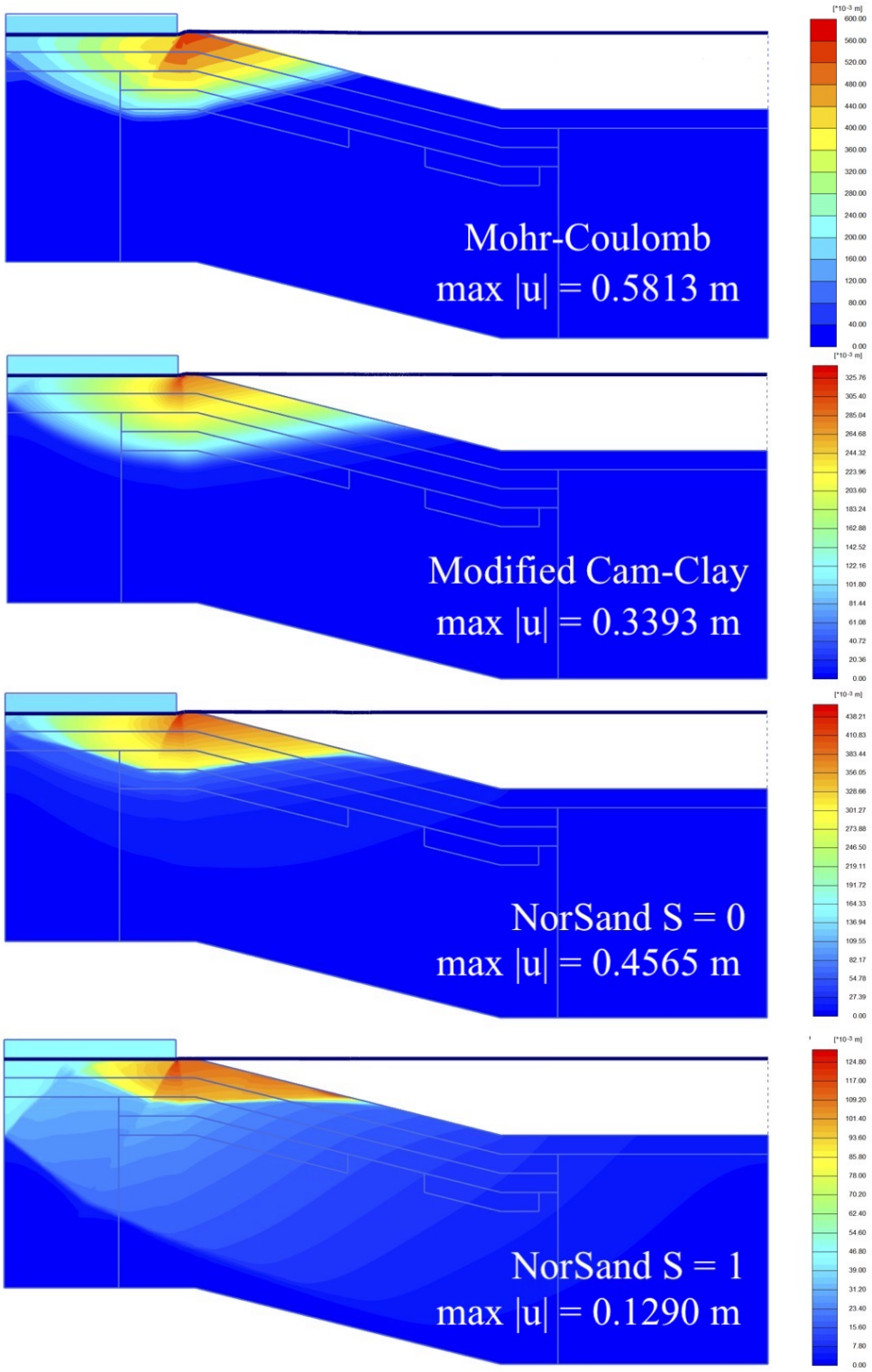

Figure 6.17: Total displacements $|u|$ at phase 3 for each constitutive model. Parameters are given in Table 6.2.

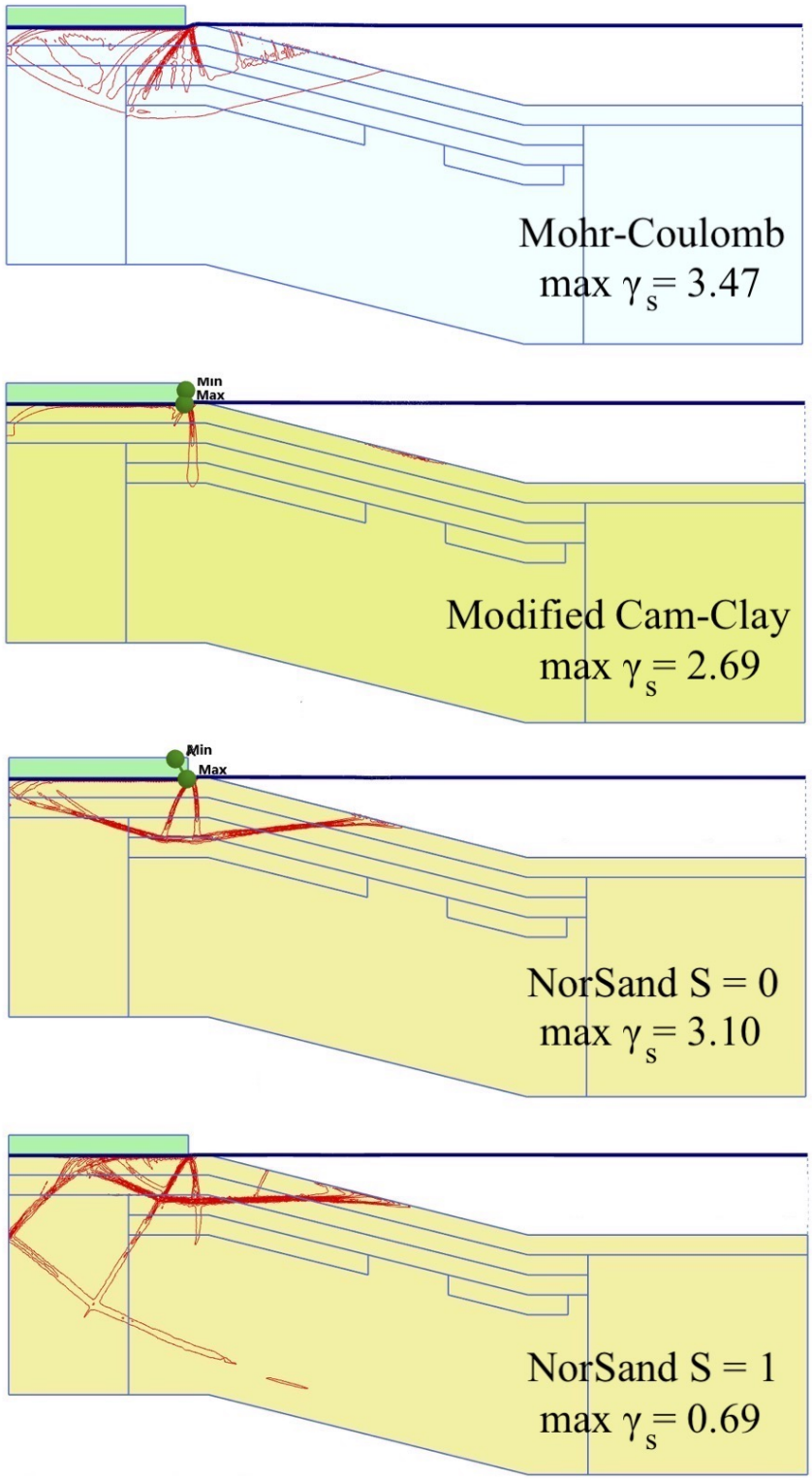

Figure 6.18: Total deviatoric strain γ at phase 3 for each constitutive model. Parameters are given in Table 6.2.

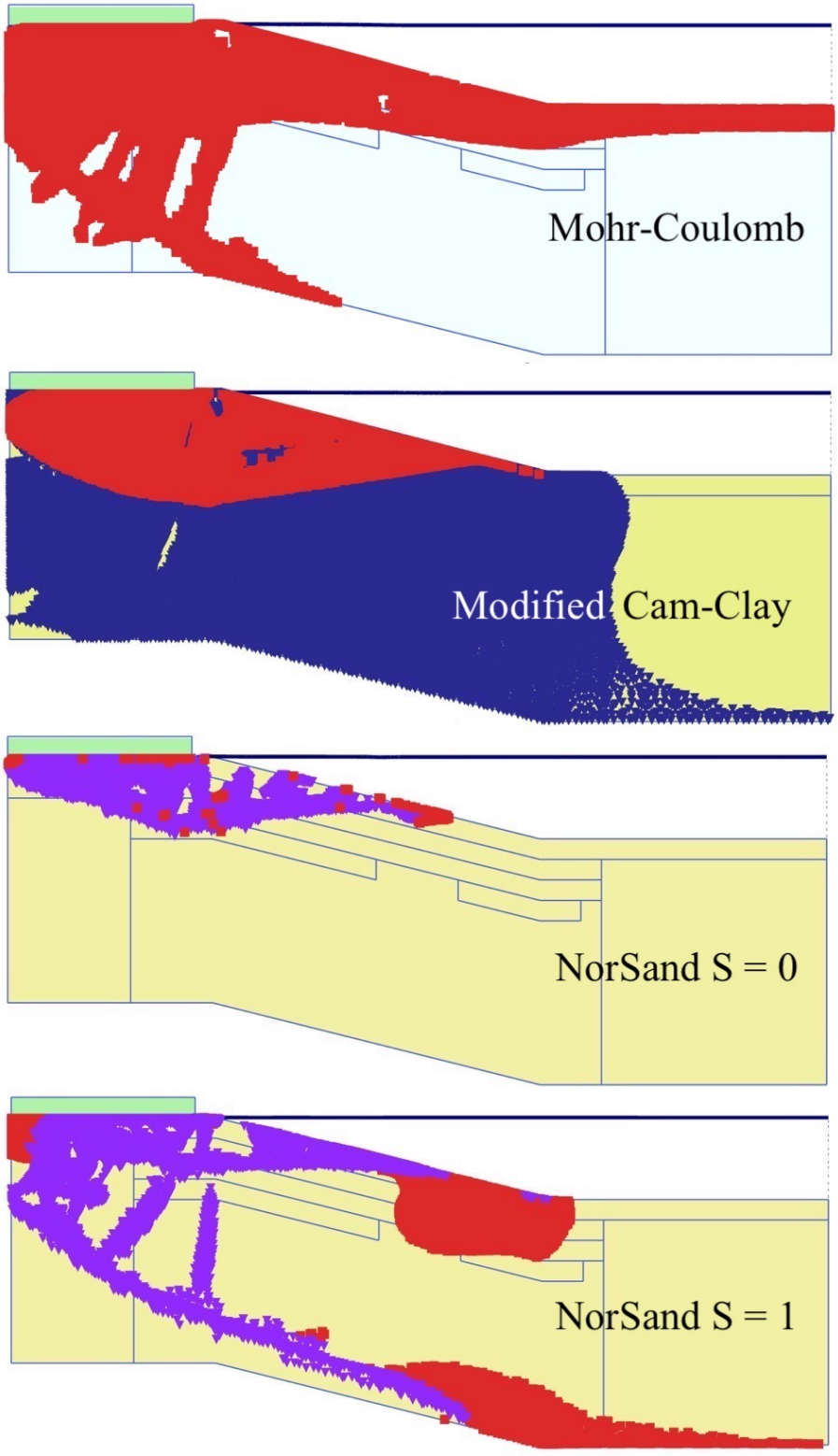

Figure 6.19: Plastic points at phase 3 for each constitutive model. Parameters are given in Table 6.2.

6.6 Discussion: FEA of the underwater slope

Arguably the first phenomenon shown in all results, that induces immediate questions, is the fact that the classic circular slip surface does not occur in the FEA results. What is found, however, is a failure surface resembling a Prandtl-type (Figure 6.20) mechanism at the moment of failure (i.e., when equilibrium cannot be maintained and the numerical solution fails to converge within an iteration limit). This is explained by both the highly unrealistic loading conditions on the structure and the employment of small strain theory within the finite element analysis. Additionally, as large strain theory is not applied, true liquefaction is not simulated as there is no fluidization and loss of structure. But, most importantly, the objective of this application is not to simulate reality, but to determine the general effects and differences of NorSand and its behaviour compared to other constitutive models.

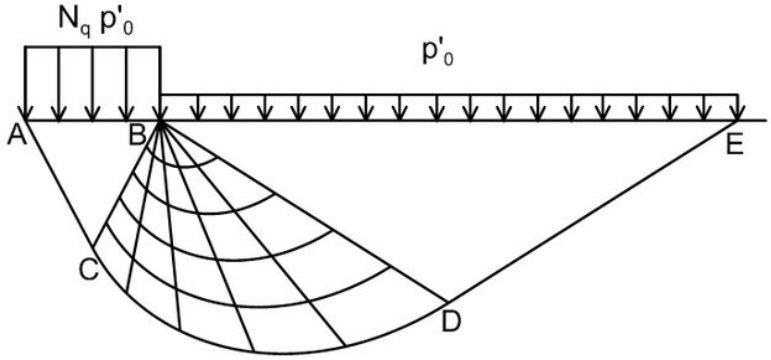

Figure 6.20: Illustration of a Prandtl failure mechanism due bearing capacity failure in a limit-equilibrium analysis where the length of the foundation is foundation is from points A to B. Taken from Mortensen, 2015.

The results shown in section 6.4.1 illustrate the expected effect of decreasing the packing density of the structure. The looser the soil (i.e., the more positive the state parameter) the quicker the structure fails under the prescribed loading. Interestingly, it can be seen in Figure 6.4 that for $\psi_0 = 0.07$ and $S = 0$ the structure has a larger bearing capacity (roughly 50 kPa/m) than for $\psi_0 = 0.03$ and $S = 1$ (roughly 40 kPa/m). This is a good indication of the strong influence of the activated softening flag on the behaviour of the loose soil. And, as the importance of the inclusion of extra softening in loose soils in undrained experimental lab tests was determined during verification and validation, this should also be kept in mind when modeling structures with loose granular soils in undrained conditions.

Another interesting effect of decreasing the initial state parameter ψ_0 is the 'shallowing' of the failure surface, where it gets closer to the surface the looser the soil becomes. This is explained by the fact that soils are a frictional material. The void ratio and friction angle of a soil are inversely proportional to each other (i.e., a larger void ratio is related to a smaller friction angle ϕ). As such, not much of the strength is mobilized in a soil when subjected to loading, resulting in a rapid and shallow failure mechanism.

Section 6.4.2 shows the effects of having a dense or a loose soil. As expected, the FEA of a submarine slope consisting of dense granular material is able to take the full 20 cm displacement. Additionally, the denser the soil, the larger the bearing capacity.

This is also illustrated in Figures 6.11 to 6.13, where more of its strength is mobilized and strains are less localized, resulting in less deformation of the structure for the same prescribed displacement.

The results in section 6.5.2 show the differences in behaviour between NorSand, Mohr-Coulomb

and Modified Cam-Clay. As explained in the parameter setup, it was expected for Mohr-Coulomb to be able to sustain the full 20 cm displacement at the top of the structure and have a large bearing capacity. This is due to its large elastic region before reaching critical state in undrained loading.

Modified Cam-Clay also shows a relatively large bearing capacity, but reaches critical state, resulting in structural failure. Another observed feature, shown in Figures 6.18 and 6.19, is the diffused compaction in the total deviatoric strain plot of the domain, whereas the other constitutive models show at least a hint of defined shear planes. However, as explained in section 3.2, this model is meant for normally consolidated clays and not particulate materials such as sands.

NorSand shows, in both cases, an overall lower bearing capacity and larger sensitivity to the applied displacement. This is especially true for the analysis with the softening flag turned on: Figures 6.17 and 6.18 show a lower maximum value for $S = 1$ compared to when $S = 0$. Additionally, the plastic point figures for NorSand clearly show liquefied points that coincide with the shear bands, indicating the liquefaction potential.

All-in-all, the FEAs of the simplified submerged landslide, which consists of granular material, indicate that NorSand, compared to the other 2 constitutive models, shows the most appropriate response to displacement in undrained conditions due to its relatively low bearing capacity, high sensitivity and propensity to failure when subjected to forced displacement. And, the model is able to clearly give liquefied points.

7 Conclusions and Recommendations

7.1 Conclusions

The objectives of this report were threefold: analyze the behaviour of the NorSand constitutive behaviour; then, to verify and validate the PLAXIS integrated NorSand; finally, to establish the capabilities of NorSand in modelling static liquefaction of underwater slopes in finite element analyses.

Two types of single stress-point analyses were performed to establish model behaviour: stress-path analyses and parametric analyses. The stress-path analyses showed the evolution of state variables for a various triaxial loading conditions. The parametric analyses showed the influence for a range of input parameters, which can then be used to help calibrate experimental lab test data.

The PLAXIS implemented NorSand (PLAXIS NorSand) was verified through two methods. First, it was compared to an implementation written in Visual Basic for Applications (VBA NorSand) by the authors of the model Jefferies and Been, which has been tested with positive results. Both models showed agreement in triaxial compression, for dense and loose soil in drained (TCD) and undrained (TCU) conditions, and in direct simple shear in undrained conditions (DSSU) for dense and loose soil.

Second, it was verified by means of an 'analytical solution'. The solution, albeit not an analytical solution in a traditional sense, was the relationship between the mobilized friction ratio M_i and state parameter ψ in its simplest form. The mobilized friction ratio and stress ratio at peak strength of PLAXIS NorSand and the 'analytical solution' were compared. The values between both showed less than 3% difference; further verifying PLAXIS NorSand.

NorSand has been validated by establishing that it is capable to approximate experimental lab tests. First, by NorSand was validated by changing the baseline soil parameters, which have been determined from TCD and TCU tests, until it was calibrated to experimental lab tests of Erksak 330/0.7 sand. Then, it was validated by comparing it to TCD and TCU lab tests for three different sands, namely Erksak 330/0.7, Nerlerk 270/1 and Ticino 530/0, but without changing the baseline soil parameters for each sand. The results showed that NorSand is able to follow lab test data decently well with one parameter set. And if one decides to take the time and calibrate individual lab test and deviate from the baseline soil parameters, they can be matched even better. Additionally, it showed a consistent need for activation of the softening flag ($S = 1$) in order to appropriately model loose soils in undrained conditions. Then, the user needs to be aware that a 'cavitation cut-off' should be enforced as the model will increase the effective stress indefinitely when simulating dense granular soil in undrained conditions.

Finally, NorSand was applied in finite element analyses of a submarine slope. On it, a 20 centimeter displacement was applied at the top through a rigid slab, to determine its behaviour in simulating static liquefaction, expecting a circular failure mechanism.

First, the difference in slope behaviour, due to a change in soil density, with NorSand was determined: dense soil resulted in the slope to bear the full 20 centimeter displacement whereas increasing the void ratio (i.e., increasing the positive value for the state parameter) gave the effect of even quicker slope collapse and a lower bearing capacity. In other words, when using NorSand, the looser soil the further the failure surface moves up and the quicker the structure fails to maintain equilibrium.

Lastly, the difference in behaviour, compared to NorSand, for various constitutive models were explored. NorSand, contrary to the other constitutive models, showed the high sensitivity to forced displacement resulting in clear shear bands resembling Prandtl-type bearing capacity failure and early onset soil body collapse - it showed the most appropriate sensitive behaviour that is expected

from submarine slopes, where a high liquefaction potential is indicated. And, even though the failure mechanism was unrealistic due to the equally unrealistic loading conditions, and the fact that small strain theory was employed, these analyses still allowed to give an indication of overall behaviour and the differences between each constitutive model.

7.2 Recommendations

Based on the results during validation, it became clear that the activation of the softening flag ($S = 1$) for loose soils during undrained loading is paramount. Furthermore, the indefinite hardening of dense soils in undrained conditions calls for the employment of a 'cavitation cut-off' when using NorSand.

NorSand has been validated to numerous triaxial compression lab tests. Even though triaxial tests belong to the industry standard to determine soil characteristic, other tests such as triaxial extension, bi-axial, and direct simple shear tests are used as well. And due to the fact that the lode angle θ is incorporated into the NorSand formulation to account for various loading conditions, it could be further validated for other types of lab tests.

The same reasoning could be applied to the stress-path analyses - they have been done in various triaxial compression conditions, but other loading paths exist as well. As such, analyses can be done for other loading conditions to determine its effects on the state variables.

In the finite element analysis, the underwater landslide was brought to liquefaction by means of monotonic loading, for instance due to sudden increase of sediment deposition, at the crest. However, there exist various causes for slope movement, which would be worth analyzing using NorSand. For instance, another cause for slope failure is due to erosion and scouring, caused by waves and marine currents. These result in gradual increase of local seabed inclination and formation of slopes around hydraulic structures and offshore foundations, monotonically increasing the stress stress in the soil body (W. Zhang and Askarinejad, 2019).

Furthermore, it must be recognized that the static liquefaction analyzed in this report was a very simplified approach: it had a uniform soil domain, had a constant water level, and it was displacement controlled. Adding phased layering, transient water conditions, weak zones and different loading conditions will introduce more intricate soil conditions to the analysis and model liquefaction more realistically.

Finally, submarine slopes are not the only structures where softening behaviour play an important role in their stability analysis. In tailings dams, for instance, weak zones of loose soil are detrimental to structure stability. Therefore, applying NorSand to various case studies where softening behaviour of particulate material has played a role can help analyze the problem.

References

Barnichon, J. (Jan. 1998). *Finite Element Modelling in Structural and Petroleum Geology (Doctoral dissertation)*. Université de Liège.

Been, K., J. Hachey, and M. Jefferies (Jan. 1991). "The critical state of sand". *Geotechnique* 41, pp. 365–381. DOI: 10.1680/geot.1991.41.3.365.

Been, K. and M. Jefferies (2015). *Soil Liquefaction: A Critical State Approach*. ISBN: 978-0419161707.

Casagrande, A. (1975). "Liquefaction and cyclic deformation of sands: A critical review". *Proceedings of Fifth Pan–American Conference on Soil, Mechanics and Foundation Engineering, Vol. 5*, pp. 79–133.

Dabeet, A. (2005). *A Practical Model for Load-unload-reload cycles on Sand (Master Thesis)*. The American University in Cairo.

Duncan, J., S. Wright, and T. Brandon (Oct. 2014). *Soil Strength and Slope Stability (2nd edition)*. Wiley. ISBN: 978-1-118-65165-0.

Elbadawy, M. (2014). *Seismic Response Analysis Considering Soil-Structure Interaction of High-Rise Buildings*. DOI: 0.13140/RG.2.1.4773.0321.

Espinoza, D. (Nov. 2019). "Lecture 20 of PGE 383". URL: https://www.youtube.com/watch?v=rMYMLorLczk.

Gao, Z. and J. Zhao (Jan. 2013). "Evaluation on Failure of Fiber-Reinforced Sand". *Journal of Geotechnical and Geoenvironmental Engineering 139(1):95-106*.

Ghafghazi, M. (2011). "Towards comprehensive interpretation of the state parameter from cone penetration testing in cohesionless soils".

Heidbach, O. et al. (2018). "The World Stress Map database release 2016: Crustal stress pattern across scales". *Tectonophysics* 744, pp. 484–498. ISSN: 0040-1951. DOI: https://doi.org/10.1016/j.tecto.2018.07.007.

Jefferies, M.G. (1993). "NorSand: a simple critical state soil model for sand". *Geotechnique* 43.1, pp. 91–103. DOI: 10.1680/geot.1993.43.1.91.

Li, X. and Y. Dafalias (Jan. 2000). "Dilatancy for Cohesionless Soils". *Geotechnique* 50, pp. 449–460. DOI: 10.1680/geot.2000.50.4.449.

Marinelli, F. (2020). "NorSand: an elasto-plastic model for soil behavior with static liquefaction".

Mitchell, J.K. and K. Soga (July 2005). *Fundamentals of Soil Behavior, 3rd Edition*. ISBN: 978-0-471-46302-3.

Mortensen, N. (May 2015). "Chain configuration in sand, theory and large scale field testing". *Frontiers in Offshore Geotechnics III - 3rd International Symposium on Frontiers in Offshore Geotechnics, ISFOG 2015*, pp. 905–912. DOI: 10.1201/b18442-130.

Schofield, A. and C. P. Wroth (Dec. 1968). *Critical State Soil Mechanics*. ISBN: 9780070940482.

Shuttle, D. and M. Jefferies (2010). "Norsand: Description, Calibration, Validation and Application".

Skempton, A. W. and A. W. Bishop (1950). "The Measurement of the Shear Strength of Soils". *Géotechnique* 2.2, pp. 90–108. DOI: 10.1680/geot.1950.2.2.90.

Tresca, H. (1864). "Sur l'écoulement des corps solides soumis á de fortes pressions". *Comptes Rendus de l'Académie des Sciences (Paris)* 59, pp. 754–758.

Van der Sloot, M. (July 2011). "Iterative settings: Influence of Arc length control". URL: https://communities.bentley.com/products/geotech-analysis/w/plaxis-soilvision-wiki/45924/iterative-settings-influence-of-arc-length-control.

Verruijt, A. (2012). "Soil Mechanics".

Wang, L., K. Shen, and S. Ye (Mar. 2008). "Undrained Shear Strength of K0 Consolidated Soils". *International Journal of Geomechanics* 8. DOI: 10.1061/(ASCE)1532-3641(2008)8:2(105).

Wanstreet, P. (2007). "Finite element analysis of slope stability (Graduate Thesis)".

Zhang, W. and A. Askarinejad (Oct. 2019). "Centrifuge modelling of submarine landslides due to static liquefaction". *Landslides* 16, pp. 1921–1938. DOI: 10.1007/s10346-019-01200-z.

Zhang, X. et al. (Jan. 2019). "A unified Lagrangian formulation for solid and fluid dynamics and its possibility for modelling submarine landslides and their consequences". *Computer Methods in Applied Mechanics and Engineering* 343, pp. 314–338. DOI: 10.1016/j.cma.2018.07.043.

A Extra information on general framework

A.1 Triaxial test

The procedure for triaxial compression consists of 3 phases:

- Phase 0 is to ensure total saturation, i.e. without any bubbles, of the soil sample by applying back-pressure.
- Phase 1 is the consolidation phase, where the valve is closed so that pore fluid of the soil cannot escape. The cell pressure is increased resulting in buildup of pore pressure within the sample. Then, the valve is opened to release the excess pressure, increasing the effective stress of the soil to that of the cell pressure. This results in isotropic consolidation where the soil contracts - i.e. its void ratio ($\frac{V_v}{V_s}$, where V_v is the volume of voids and V_s the volume of solids) reduces. If the valve is kept closed, then it does not consolidate.
- Phase 2, which is the last phase, is where the sample is brought to failure by applying deviatoric stress - it is sheared. This can be done drained, where excess pore pressure is not generated, or undrained, where excess pore pressure is generated. During the shearing stage the sample is loaded by increasing the axial load in increments for stress controlled testing or by applying displacement increments for strain controlled testing.

There are three main types of triaxial compression tests and these depend on which phases have been done drained or undrained:

- The unconsolidated undrained (UU) test is performed quickest (also known as the Q-test) since one does not have to wait for saturation in phase 0, consolidation in phase 1, and drained loading conditions during phase 2.
- Consolidated drained (CD) tests take the longest (also known as the Slow or S-Test) as the sample has to be saturated and consolidated, and drained loading conditions must occur during shearing. This takes even longer for clay samples due to their low hydraulic conductivity.
- Consolidated undrained (CU) tests are quicker than consolidated drained tests, but slower than unconsolidated undrained tests (and also known as the R-test).

A.2 Over-consolidation ratio

The over-consolidation ratio (R) is a state parameter for clays, indicating how far the current stress is from its previously maximum experienced stress. This maximum stress is also known as the pre-consolidation stress (σ'_0). The relation between the two is given as:

$$R = \frac{\sigma'_0}{\sigma'} \tag{A.1}$$

If the current stress is lower than the pre-consolidation stress, then the $R > 1$. If the current stress is equal to that of σ'_0, then the $R = 1$. When the current stress is increased further, σ'_0 increases equally. The current stress can never be larger than the pre-consolidation stress, i.e. the R is never smaller than 1.

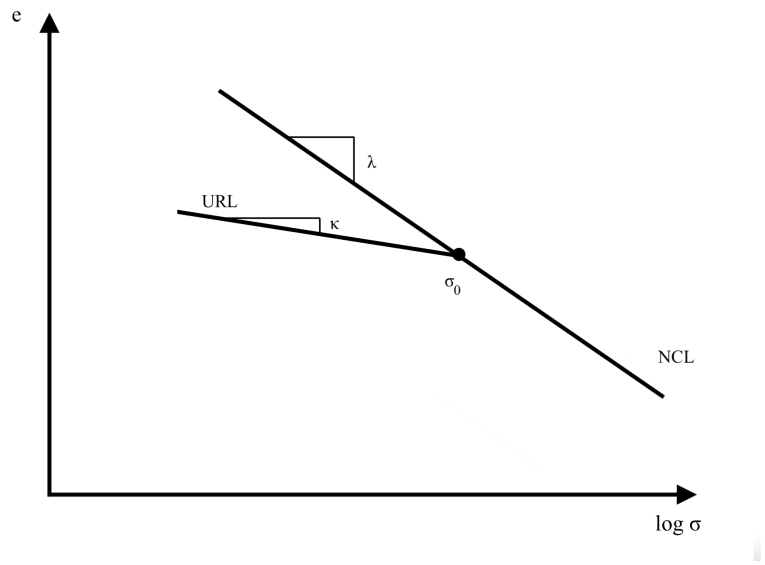

Figure A.1: Illustration of the normal consolidation line (NCL) and the unloading-reloading line (URL).

The normal consolidation line (NCL) indicates the evolution of σ_0' and is related to total strains. The unloading/reloading line (URL), also known as the swelling line, indicates the current stress when it is smaller than the pre-consolidation stress and is related to elastic strain. In other words, if the pre-consolidation stress is reached, the soil yields and total strains occur, permanently deforming the sample. If the current stress is then decreased (unloading), elastic strains occurs in the form of swelling. This deformation is not permanent and can be "reset" by reloading the soil until reaching σ_0 again.

One can appreciate that clays have a single NCL, simplifying their behaviour greatly. This is not the case with particulate materials such as sands, which is elaborated further in section 3.3.

B Basic constitutive models

Perhaps the most well-known model is the Mohr-Coulomb (MC) model, which is a simple linearly elastic perfectly plastic (LEPP) effective stress model (i.e. does not harden or soften upon yielding). When within the yield surface (which is actually a failure criteria in this case), elasticity is assumed linear. MC is an effective stress model, where its shear strength (as shear is the yield causing stress) is defined by:

$$\tau_f = c + \sigma_n tan\phi \tag{B.1}$$

where τ is the shear stress, c the effective cohesion (which would be 0 for sands), σ_n the effective normal stress, and ϕ the friction angle of the soil. It is explained in section 3.1.2 that applying principal stresses result in shear stresses on other planes. This is re-illustrated in figure B.1, but now in 2 dimensions for simplification. If the rotated unit is assumed in equilibrium, then its normal and shear stresses can be calculated using the principal stresses and trigonometry.

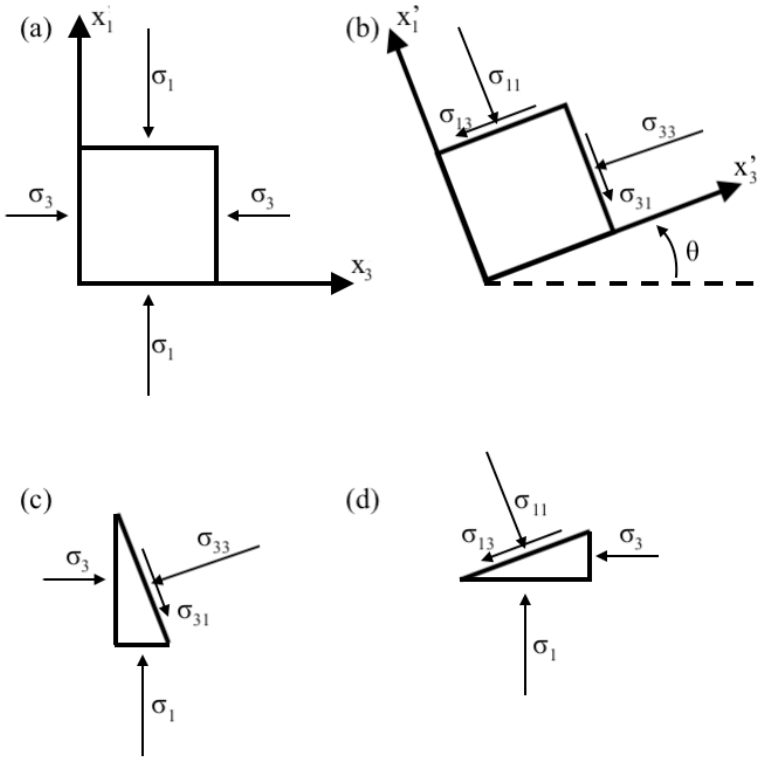

Figure B.1: Stresses on a rotated plane. The shear stresses σ_{13} and σ_{31} are equivalent to τ and the normal stresses σ_{11} and σ_{33} are equivalent to σ_n. Altered from Verruijt, 2012.

The principal stresses at failure can be plotted in the MC plane (i.e. $\tau - \sigma$ plane) with a circle between the points from which the shear and normal stress can be determined for other orientations. If one does at least 2 drained triaxial tests until failure, its failure envelope can be drawn, which has the form described in equation B.1:

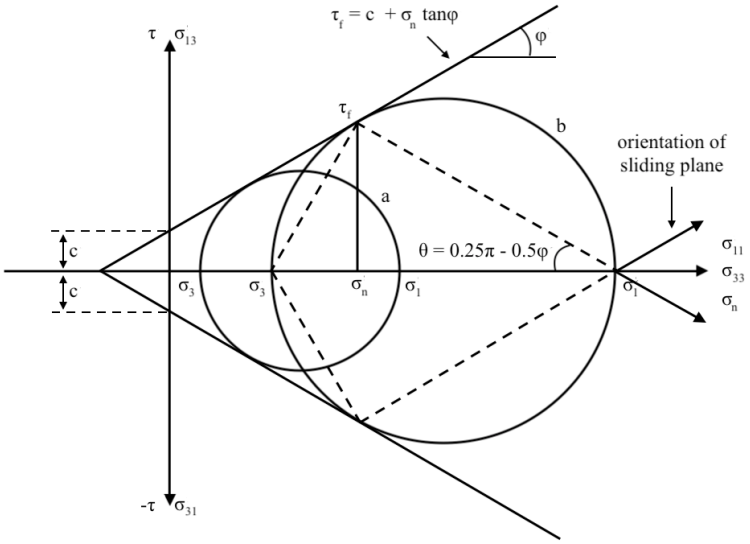

Figure B.2: Stresses plotted in the MC stress plane. Altered from Verruijt, 2012.

Alternatively, equation B.1 can be rewritten in terms of principal stresses and plotted in the 3-D stress space (figure B.3):

$$\frac{\sigma_1 + ccot\phi}{\sigma_3 + ccot\phi} = \frac{1 + sin\phi}{1 - sin\phi} \tag{B.2}$$

But just how it is preferred to have the stresses expressed in stress invariants, so too is it preferred to have the yield surface expressed in stress invariants. Hence, rewriting equation B.2 in triaxial stress invariants:

$$\frac{q}{p + ccot\phi} = \frac{-6sin\phi}{3 + sin\phi} \tag{B.3}$$

assuming $c = 0$ for sands, since they have no cohesion (unlike clays for instance), and $\eta = \frac{q}{p}$ equation B.3 turns into:

$$\eta = \frac{-6sin\phi}{3 + sin\phi} \tag{B.4}$$

As mentioned in the introduction of this subsection, MC is actually a failure surface (meaning it is the end-point for stress states, also known as the critical state) rather than a yield surface. When the friction angle at failure is known from triaxial tests, equation B.4 is rewritten finally as:

$$M_{tc} = \frac{-6sin\phi_{cv}}{3 + sin\phi_{cv}} \tag{B.5}$$

where M_{tc} is the critical stress ratio found in triaxial compression and ϕ_{cv} is the friction angle at constant volume, i.e. the critical state.

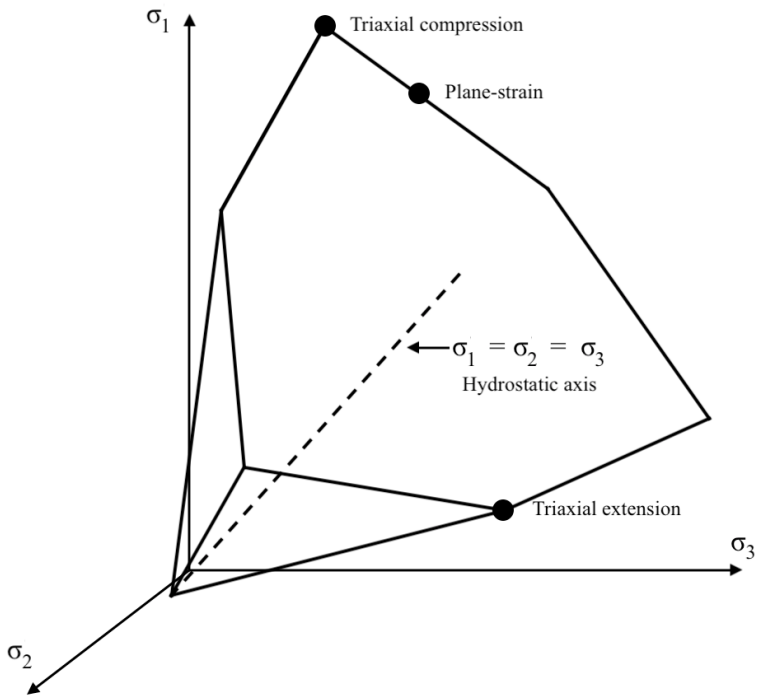

Figure B.3: Mohr-Coulomb failure criteria plotted in the 3-D principal stress space.

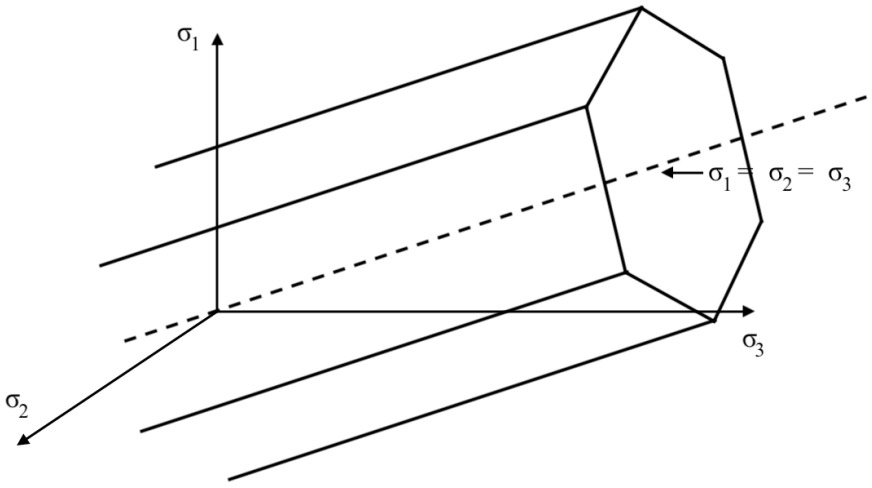

Figure B.4: Tresca failure criteria plotted in the 3-D principal stress space.

To complete the story, there exists an undrained version of the MC model, known as the Tresca model (figure B.4). It is used to model the undrained behaviour of clay in a total stress analysis. Figure B.5 shows how the maximum shear strength of the soil is independent of mean stress and depends on the undrained shear strength S_u. S_u, which in literature is also known as c_u, is the same as the parameter c in equation B.1 but specified for undrained conditions. Hence, this model is often used to model undrained uncompressed (UU) behaviour of soils. Since the yield surface is now horizontal, the friction ratio is equal to 0, simplifying equation B.1 into:

$$\tau_f = S_u \tag{B.6}$$

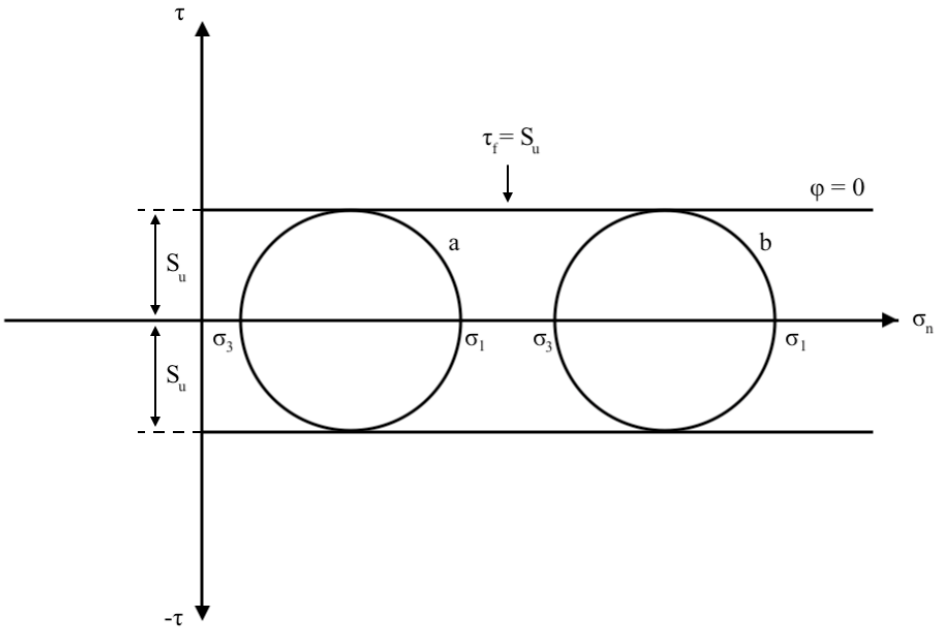

Figure B.5: Stresses plotted in the MC stress plane.

Applying normality to the MC surface implies that the dilation angle is equal to the friction angle. This results in unrealistically high volumetric strains and hence MC is typically used as a non-associated flow model with a dilation angle close to zero. MC gives reasonable predictions for strength in unconfined problems but it models volume changes poorly.

C Extra information on NorSand

C.1 Infinite NCL

The existence of infinite NCL has been proven through various experimental data, but the easiest one to follow is by comparing direct isotropic compression of Erksak 330/0.7 samples prepared at different densities with an independently determined CSL, shown in figure C.1. Each line is regarded as a true NCL because of two factors. First, the samples were prepared under low stresses (either by gentle moist tamping or pluviation) and never over-consolidated. Second, the unload–reload loops (figure C.1b to e) define a classic elastic–plastic form, even when the samples are denser than the CSL, which was previously defined as over-consolidated within the Cam-Clay framework.

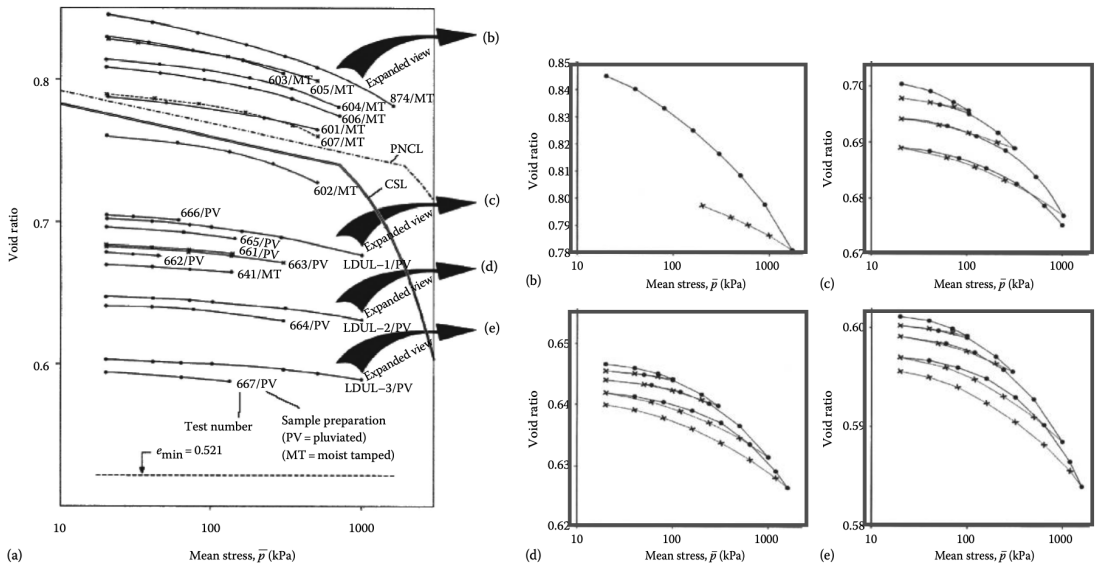

Figure C.1: Experimental evidence of an infinity of NCL. (a) All tests at same scale, (b) test 874/MT at expanded scale, (c) test LDUL-1/PV at expanded scale, (d) test LDUL-2/PV at expanded scale and (e) test LDUL-4/PV at expanded scale. Taken from Been and M. Jefferies, 2015.

Each NCL can be viewed as a hardening law for an associated yield surface. An infinity of NCL means a 'multiple infinity' of yield surfaces because any NCL can be viewed as the trace of a set of yield surfaces as they harden. Correspondingly, soil in any part of the e-p domain can plastically strain - there is no 'elastic wall' confining plastic behaviour.

Another key feature of soils, which is not captured by Cam-Clay models, is the limited maximum dilatancy dense soils exhibit for that specific soil state. There is a strong relationship between $Dmin^p$ and ψ and is explored in section 3.3.4.

With this maximum dilatancy comes an internal yield cap and is further explained in section 3.3.6. Having an internal yield cap means that soils can yield during unloading instead of simply swelling elastically.

C.2 CSL

The history behind these axioms are explored in this section. The concept that soil will eventually reach a constant stress and void ratio (density) was explored by Casagrande in 1936. He observed from shear box tests that both dense and loose sand, under same vertical effective stress, after large strain eventually reach a constant void ratio at which shear deformation continues at constant shear stress (figure C.2). This large strain void ratio distinguished which mode of behaviour the soil exhibited: sand looser than this void ratio contracts and sand that is denser dilates. Casagrande termed this void ratio as the critical void ratio.

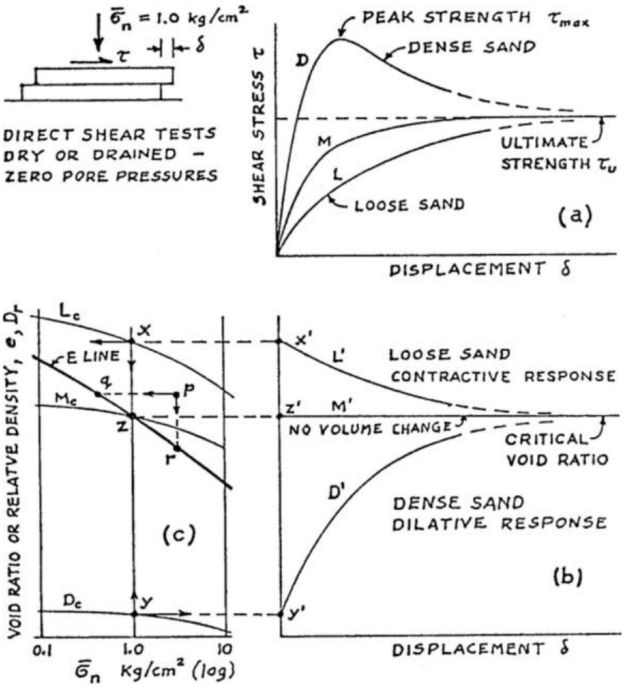

Figure C.2: Early hypothesis of critical void ratio from direct shear tests. (a) Shear stress vs. displacement, (b) Void ratio vs. displacement and (c) Void ratio vs. normal stress. Taken from Casagrande, 1975.

The first theoretical development that captured the density of soils as a state variable, rather than a soil property, and thereby accounted for volume changes during shearing, was the framework that became known as 'critical state soil mechanics' (Schofield and Wroth, 1968). The name critical state derives from anchoring the theory to Casagrande's critical void ratio. The critical state was defined by Roscoe et al. (1958) as the state at which a soil continues to deform at constant stress and constant void ratio – essentially a formalization of Casagrande's idea. In other words, the critical state is taken to be the ultimate state the soil reaches if it is continuously deformed (sheared), defined as Axiom 2. Note that there are two conditions in the definition:

- (1) The soil is at constant void ratio
- (2) It has no propensity to change from this constant void ratio condition.

Incorrect assessments and confusion arises if condition (2) is ignored, which is explored in section 3.3.5.

The question of the uniqueness of the critical state was investigated by Been et al. (1991) who provided evidence to indicate that the critical state is likely unique, being both independent of fabric, loading rate, stress path, and initial density. Figure 3.10 shows that both moist compacted and pluviated samples in undrained tests finish at the same critical state line. Drained tests were also observed to follow the same trend. The change in the slope of the critical state line at about 1000 kPa is thought to be due to grains crushing at high mean effective stress levels. The relationship between critical void ratio and mean effective stress is called the critical state locus (CSL):

$$e_c = \Gamma - \lambda ln(p_c) \tag{C.1}$$

where Γ and λ are intrinsic soil properties, meaning that they are not affected by fabric, stress history, density, etc. The subscript 'c' denotes critical state conditions. Caution is needed when looking at quoted values of λ as both log base 10 and natural logarithms are used. Natural logarithms are more convenient for constitutive modelling, whereas base 10 logarithms arise when plotting experimental data: the notations λ (or λ_e where emphasis is needed) and λ_{10} ($= 2.303\lambda$) are used, respectively. The parameter Γ also has an associated stress level, which is $p = 1$ kPa by convention.

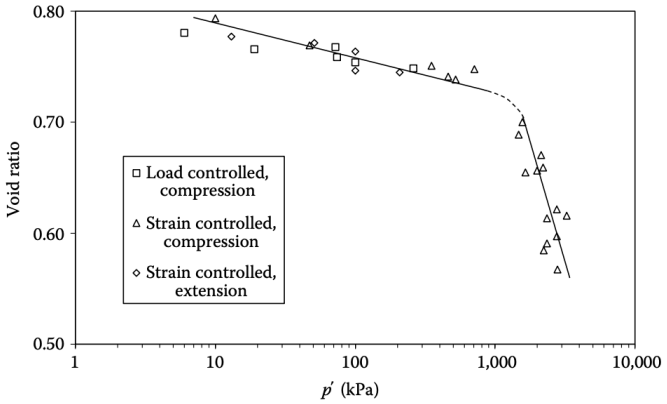

Figure C.3: Critical state line for Erksak 330/0.7 sand from undrained tests that reached a distinct critical (steady) state. Taken from Been and M. Jefferies, 2015.

Within literature, there is mention of a steady-state locus (SSL) for soils, where steady-state is defined by Poulos (1981) as: 'The steady state of deformation for any mass of particles is that state in which the mass is continuously deforming at constant volume, constant normal effective stress, constant shear stress and constant velocity'. This is a locus of steady-state void ratios is found by doing load-controlled tests, whereas the CSL is found by doing strain-controlled tests. Since strain-controlled tests result in the same steady-state conditions, the SSL and CSL can essentially be considered analogous to each other. Strain-controlled testing is actually preferable, as it requires less in the way of transducer response time and data acquisition rates, avoids inertial corrections to measured loads and provides more detailed data on the post-peak behaviour. As such, this paper will build its theory around the CSL.

Traditional geotechnical practice has approached the same soil over different densities as different materials. For instance, the same geological material may be assigned a friction angle $\phi' = 32°$ in a loose in-situ state, but given $\phi' = 36°$ for design after densification or compaction. This is an incorrect approach since intrinsic properties, such as friction angles, are not a function of soil density itself, but of state. State (section 3.3.3) relates the density of soil to its critical density. Soil is a material that exists across a range of states, with the state determining how the intrinsic properties are transformed into engineering behaviour such as strength and stiffness.

C.3 More information on stress-dilatancy

Reynolds (1885) first showed that, when sheared to failure, dense sand dilates and loose sand contracts. Taylor (1948) showed that soil strength can be broken down into a frictional component, which is a measure of the minimal strength the soil has due to inter-particle friction, and a dilational component. Loose soil lends its strength from the frictional resistance between the particles. Peak strength in dilative soils (i.e. dense sand) is caused by both the frictional resistance and the tendency of dense particles to override each other in the form of dilation. Rowe (1962) related the mobilized stress ratio to the plastic strain rates, in what has become known as stress–dilatancy theory. This relationship applied to the whole strain history, not just peak strength values. Rowe's original proposition can be stated as (for a compression positive convention):

$$\frac{\sigma'_1}{\sigma'_3} = K(1 - \frac{\dot{\varepsilon}_v}{\dot{\varepsilon}_1}) \tag{C.2}$$

After initial introduction of this theory, it was thought that K could be a constant and related to the soil mineral-mineral friction - it is now known not to be the case. This, however, does not invalidate equation C.2 entirely as it still recognizes the dilation is a work transfer mechanism between the principal stress directions and that the rates of dilation and stresses are related to each other and not their absolute values. Early on it was discovered that soil behaviour indicated that there exists an 'operating' friction ratio:

$$M_\mu < M_f < M \tag{C.3}$$

where M_μ is the mineral-mineral sliding friction ratio, M_f the 'operating' friction ratio and is related to K in equation C.2, and the critical friction ratio M. Rewriting Rowe's stress–dilatancy approach, it can be anticipated that soil behaviour will follow:

$$\eta = f(M_f, D^p) \tag{C.4}$$

where $f()$ indicates an undefined function of M_f and D^p. M_f is the mobilized critical friction ratio, varies a little with strain and rather more with state, and goes towards M as the soil goes towards critical state. D^p is the plastic components of the strain rates.

The mobilization of M_f can be illustrated experimentally with use of drained triaxial tests. First, a single test on dense Erksak 330 sand is shown in figure C.4, where its behaviour is plotted in the dimensionless stress-dilatancy space. The maximum stress ratio η_{max} and minimum dilatancy D_{min} are tagged in the top left, which is analogous to the maximum of the graph for dense sand in figure 2.6a. Due to the compression positive convention and that deviator strain is positive, dilation in dense soils correspond to negative values. Therefore, 'maximum' dilation, which corresponds to its peak strength, is actually the largest negative value (D_{min}).

It is important to note that this particular sample was not sheared to critical state, which would be indicated by the plot continuing in the downwards-right direction until reaching $D = 0$.

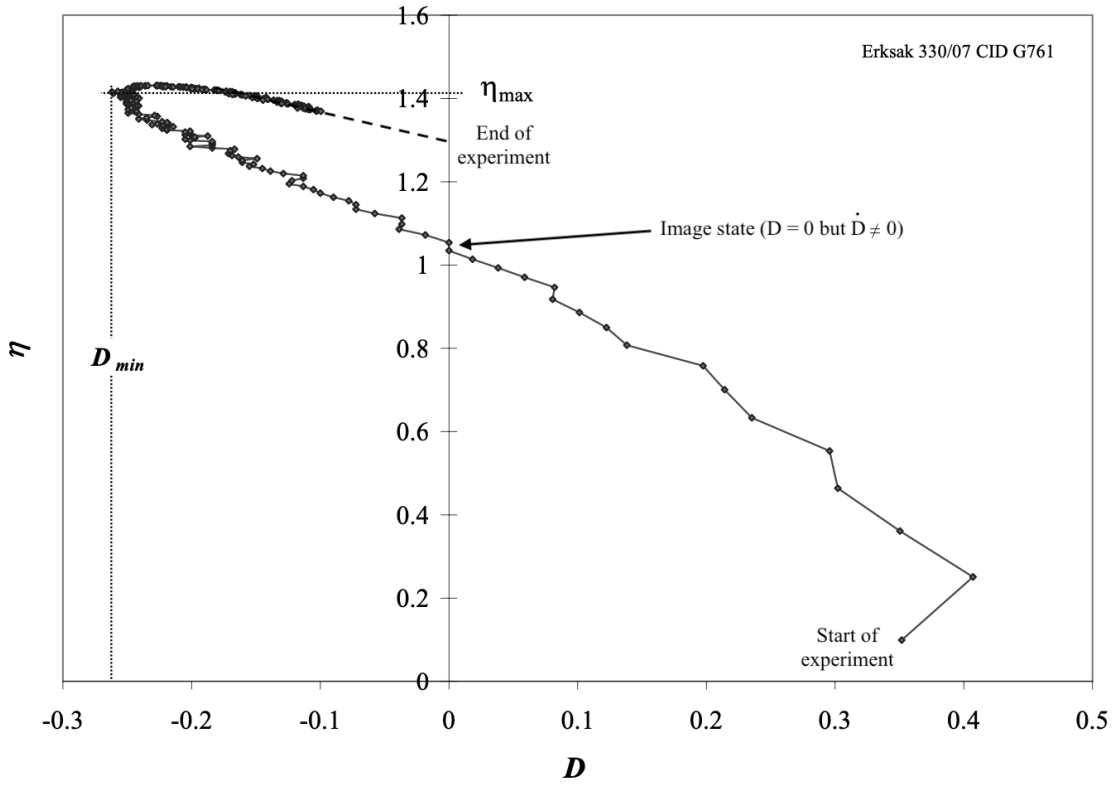

Figure C.4: Plot of single drained triaxial test on dense Erksak sand reduced to stress-dilatancy form. Altered from Shuttle and M. Jefferies, 2010

Figure C.5 shows multiple plots from which general trends can be determined. For dense samples (figure C.5a), two regression lines can be fitted. At pre-peak, there is a point where the plastic dilatancy $D^p = 0$, and turns its behaviour from contractive to dilative. This is not the critical state, however, but the image condition (also known in literature as the transient condition or pseudo-steady state) as one of two conditions of critical state is met. In mathematical terms, at the image condition $D^p = 0$ but $\dot{D}^p \neq 0$.

The regression line indicates a value less then M, which is the mobilized friction ratio M_f. After peak dilation (D^p_{min}) the second regression line, which is in the negative D^p space, goes to $D^p = 0$ where the soil does go to true critical condition and where $M_f = M_{tc}$. M_{tc} is the critical friction ratio for triaxial conditions. For loose samples (figure C.5b) the regression line indicates M rather than M_f as these samples move to critical state directly.

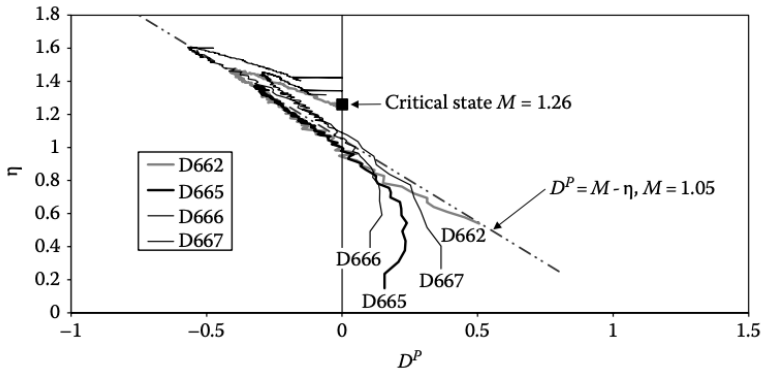

(a) Dense samples only

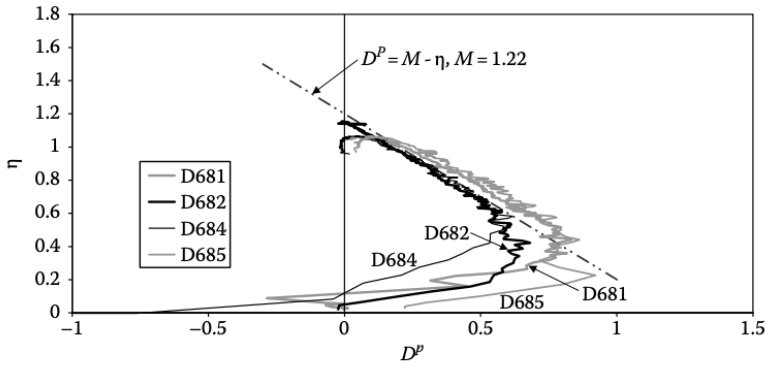

(b) Loose samples only

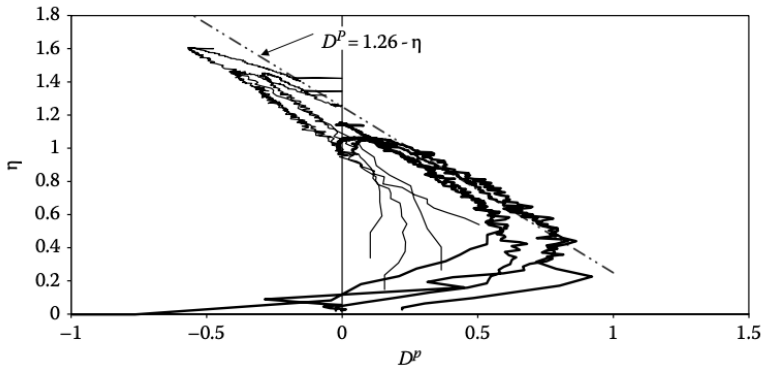

(c) All samples, with trend line for critical state M

Figure C.5: Plots of multiple drained triaxial data on dense (a), loose (b) and both (c) Erksak sand reduced to stress–dilatancy form. Taken from Been and M. Jefferies, 2015

C.4 Unloading in NorSand

Figure C.6 gives a glimpse of the dynamics of the yield surface in NorSand during unloading. Starting from 'neutral' loading, where the stress state is on the yield surface but does not push it further, the stress is decreased. In Cam-Clay the unloading path could go to the left of the yield surface, similarly as in figure C.6a, without any softening resulting in too much (i.e. unrealistic) dilation. Since NorSand employs a hardening limit resulting in an internal softening cap, the soil yields and its yield surface softens (shrinks) when the internal cap is reached, illustrated in figure C.6b. Softening continues until the appropriate size for the yield surface is reached at the end of unloading. Realistically, the internal cap has a curved shape like in figure C.6a. But, a straight internal cap, like in figure C.6b, is a simpler and adequate approximation.

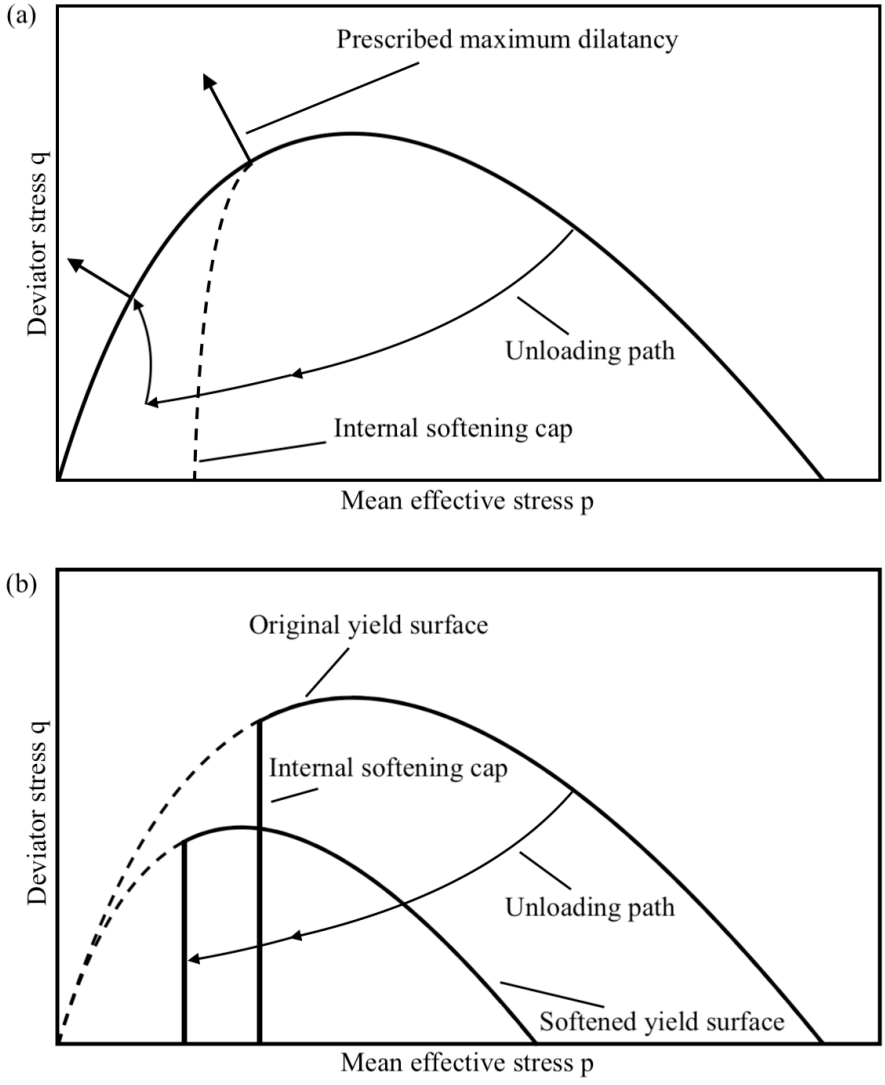

Figure C.6: NorSand yield surface softening as result of unloading. Altered from Been and M. Jefferies, 2015.

Figure C.7 shows how the critical state friction angle ϕ' decreases with the decrease of the initial void ratio of the soil (Been, Hachey, and M. Jefferies, 1991). This further shows how looser soils require a lower value for M_{tc}.

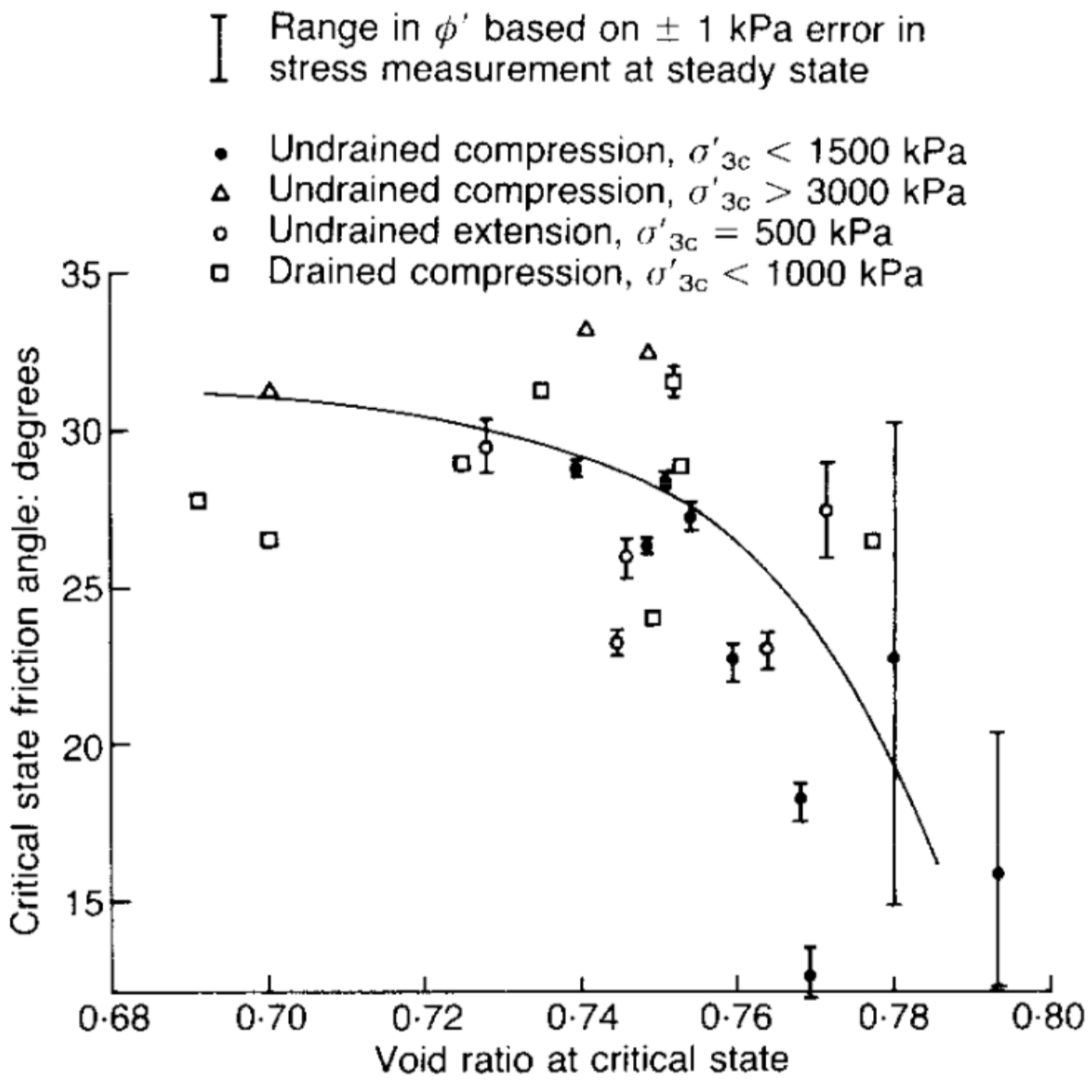

Figure C.7: Critical state friction angle for Erksak 330/O.7 sand (range in ϕ' not shown where range is less than size of symbol). Taken from Been, Hachey, and M. Jefferies, 1991.

D Extra information on Application

D.1 Boundary conditions

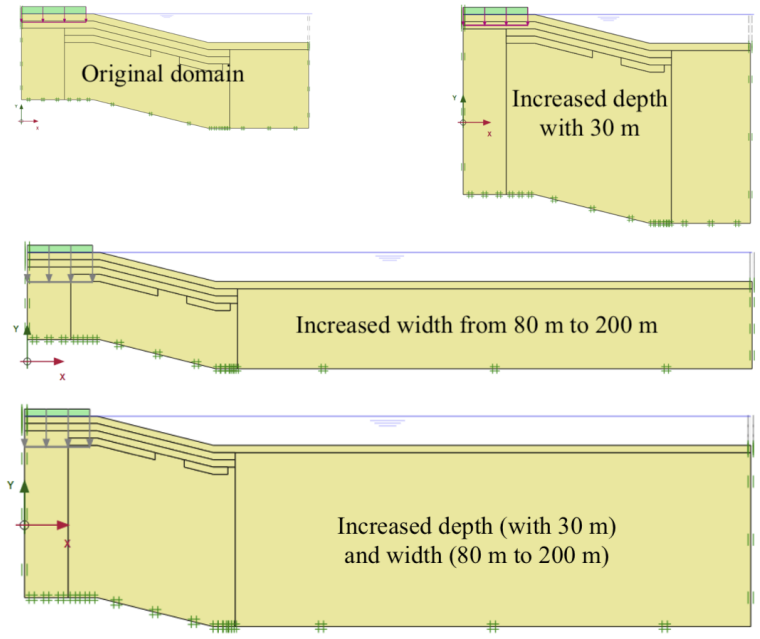

Figure D.1: Domains with different boundary conditions.

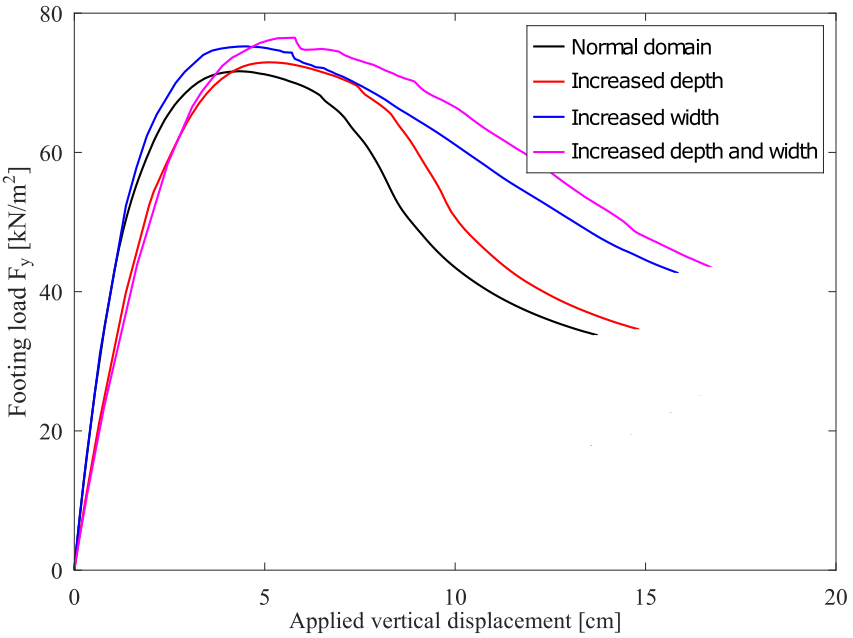

Figure D.2: Load-displacement response under the rigid slab for different boundary conditions.

D.2 Arc-length control

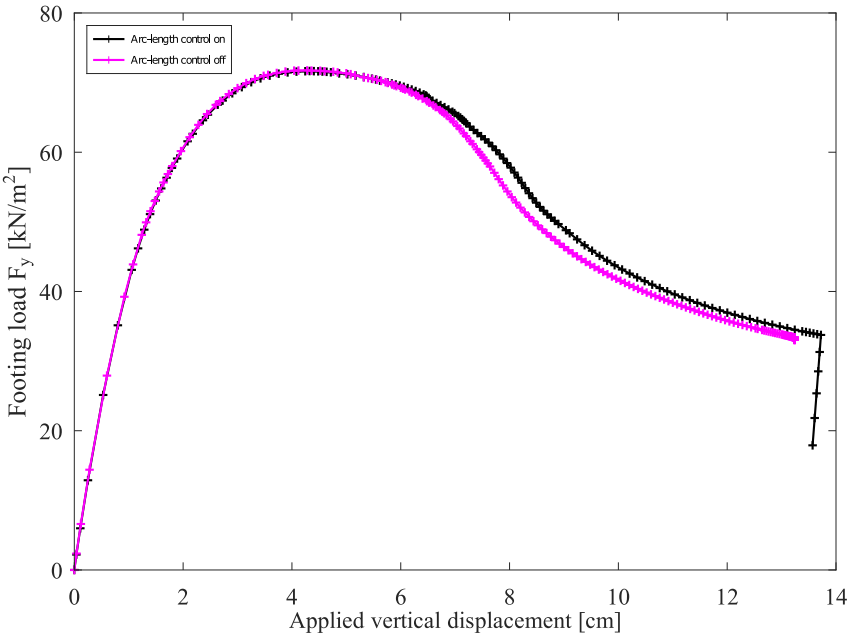

Figure D.3: Load-displacement response under the rigid slab for NorSand where the arc-length control is turned off (pink) and on (black).

D.3 Mesh size dependency

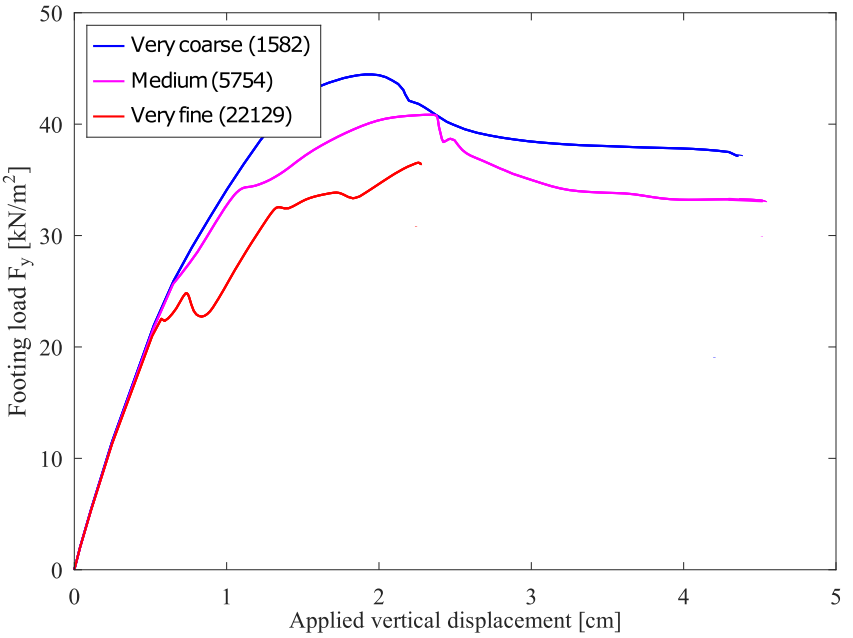

Figure D.4: Vertical force F_y at the pre-described displaced nodes versus the displacement for different mesh size densities

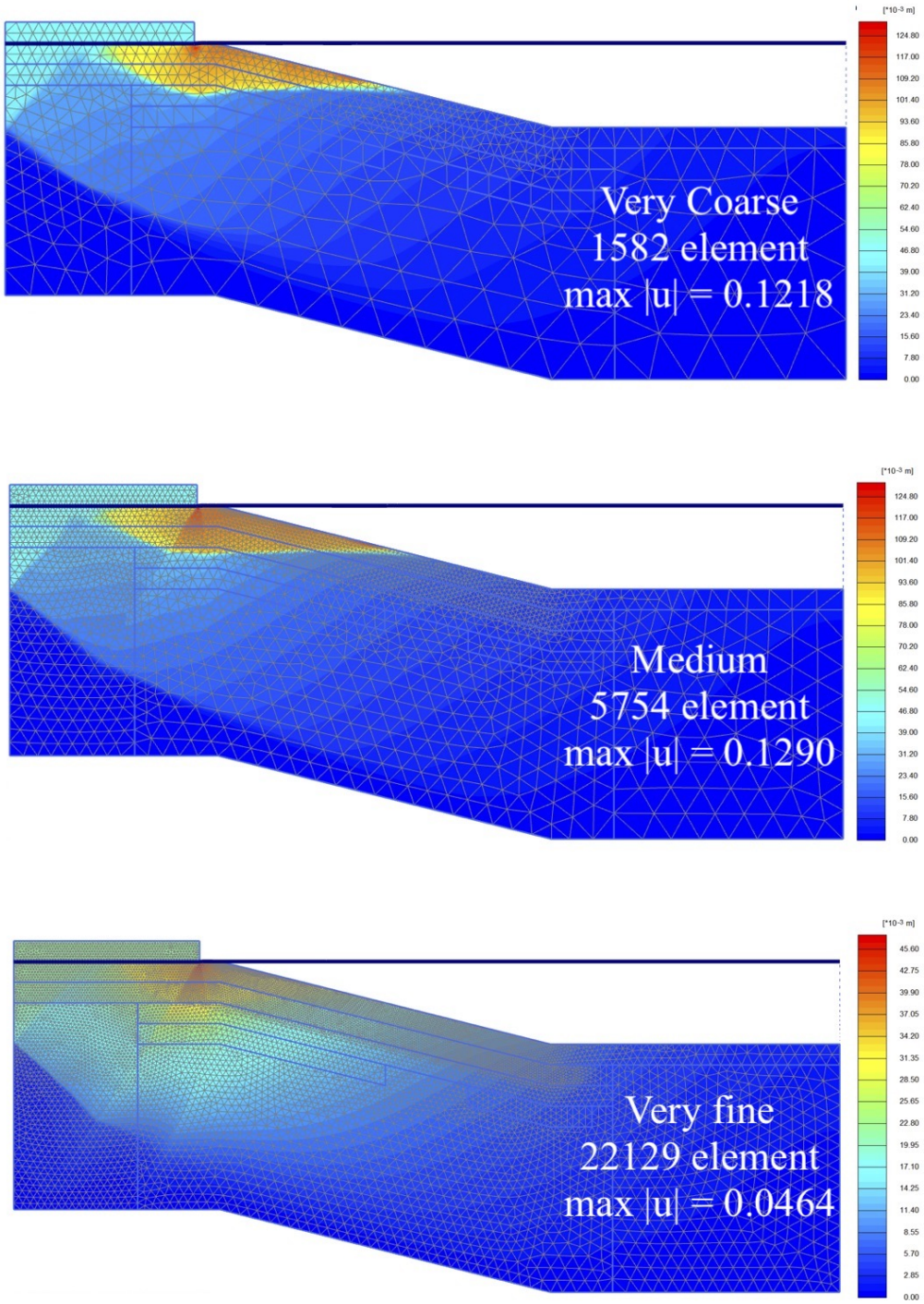

Figure D.5: Total displacements $|u|$ at phase 3 for three different mesh sizes with NorSand (S = 1). Parameters are given in Table 6.2.

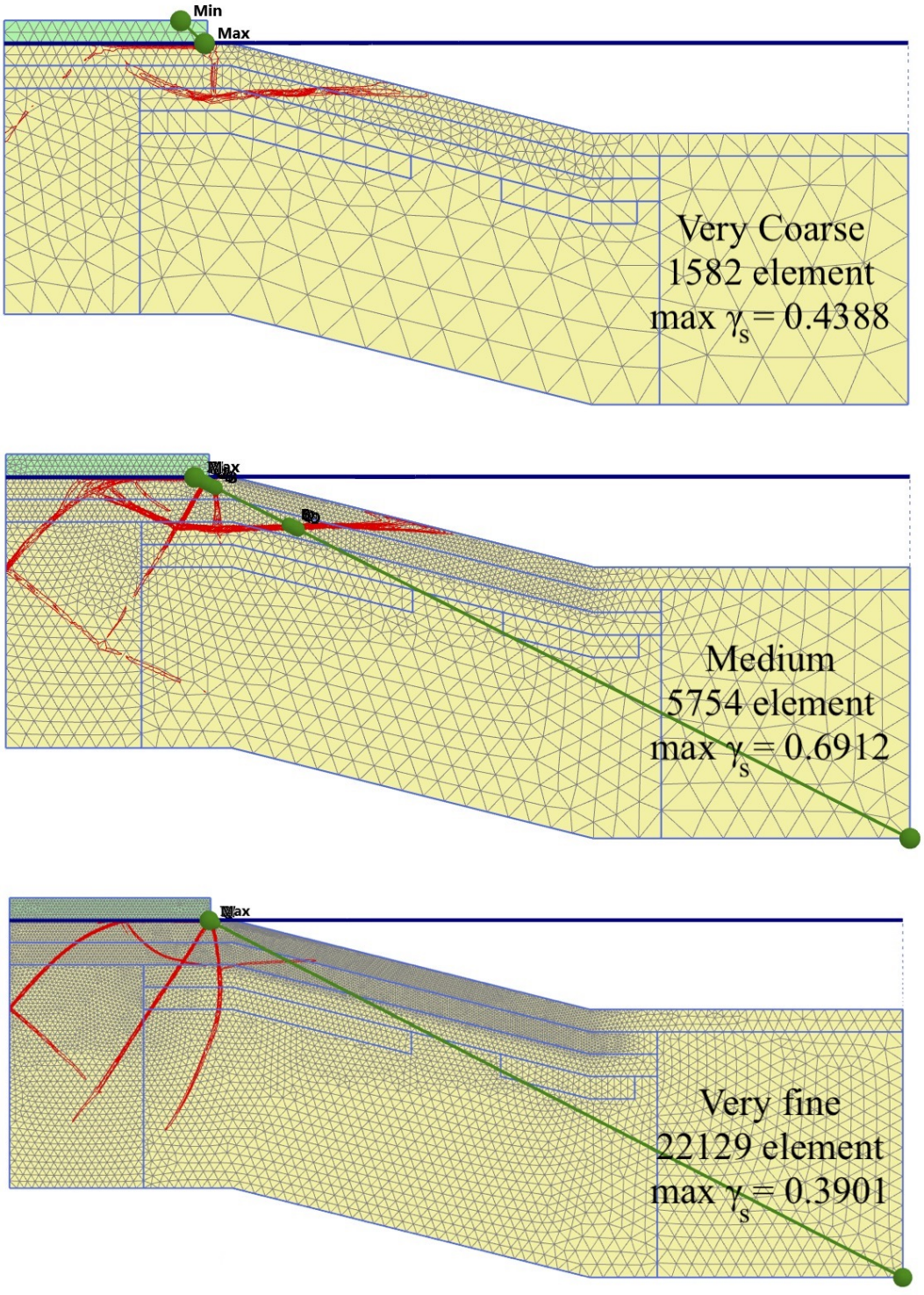

Figure D.6: Total deviatoric strain γ_s at phase 3 for three different mesh sizes with NorSand (S = 1). Parameters are given in Table 6.2.

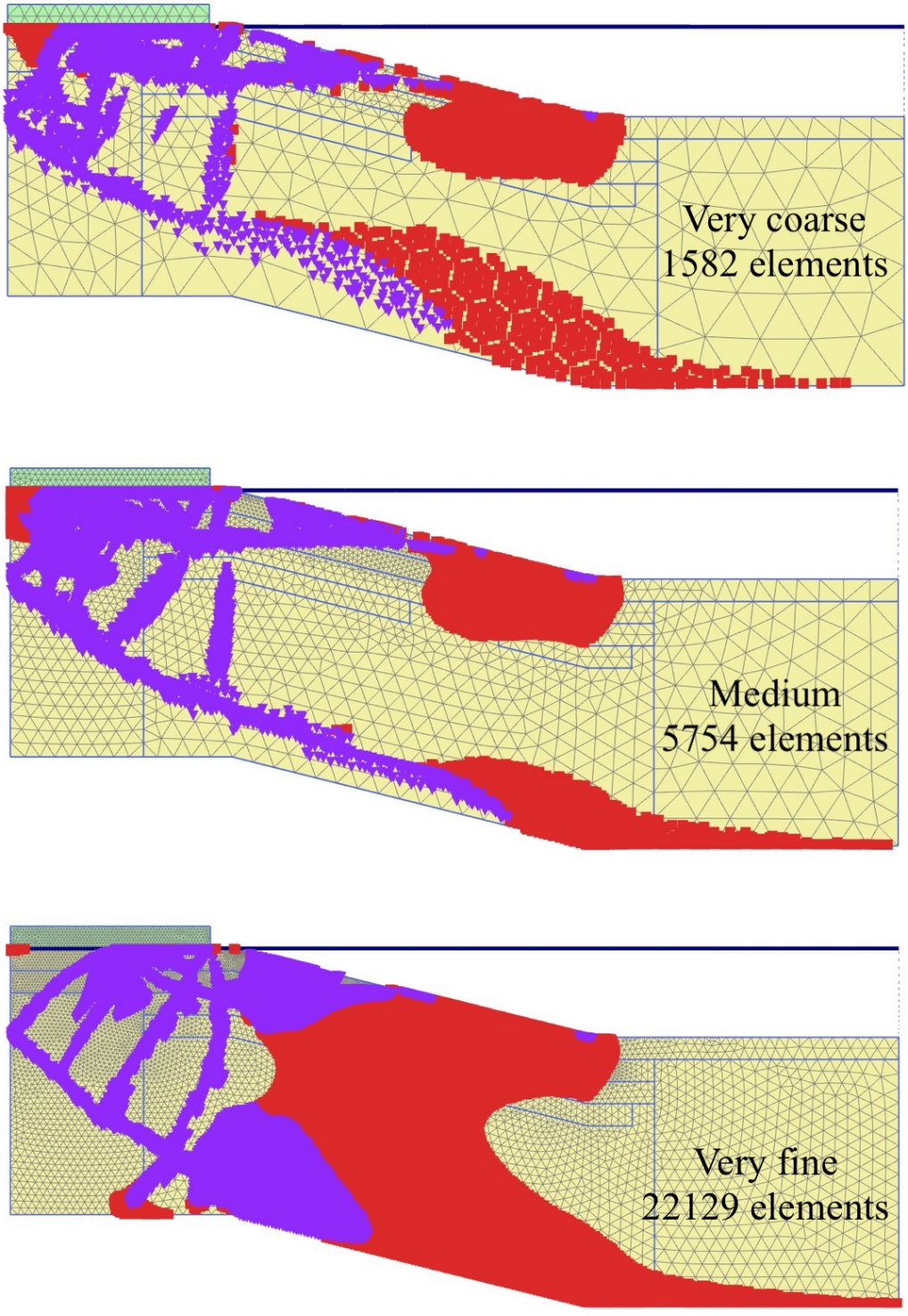

Figure D.7: Plastic points at phase 3 for three different mesh sizes with NorSand (S = 1). Parameters are given in Table 6.2.